PANK2's Role in Controlling Cellular Coenzyme A Dynamics

by

Sandra Maria Nordlie

A Dissertation Presented in Partial Fulfillment
of the Requirements for the Degree
Doctor of Philosophy

Approved April 2022 by the
Graduate Supervisory Committee:

Michael Kruer, Co-Chair
Janet Neisewander, Co-Chair
Sergio Padilla Lopez
Christos Katsanos

ARIZONA STATE UNIVERSITY

May 2022

ABSTRACT

Free coenzyme A (CoASH) carries acyl groups for the tricarboxylic acid (TCA) cycle and fatty acid metabolism, and donates acyl groups for protein posttranslational modifications. Cellular de novo CoASH synthesis starts with a pantothenate kinase (PANK1-3) phosphorylating pantothenate (vitamin B5). Mutations in PANK2 cause a subtype of neurodegeneration with brain iron accumulation (NBIA). The PANKs have differential subcellular distribution and regulatory properties. However, the purpose of each PANK has remained obscure, with knockout mouse models presenting with mild phenotypes unless challenged with a high-fat diet. Based on PANK2's known activation by palmitoylcarnitine, the PANK2-deficient cells were challenged with palmitic acid (PAL) added to glucose-containing media. The high nutrient mixture generated a surprising "starvation" profile of reduced proliferation, low ATP, AMPK activation, and autophagy upregulation in PANK2-deficient PAL-challenged cells. Further experiments showed that fatty acids accumulated and that PANK2-deficient cells had reduced respiration when provided with palmitoylcarnitine as a substrate, seemingly due to an impaired ability to oxidize fatty acids during PAL-induced Randle Cycle activation. Intriguingly, whole-cell CoASH levels remained stable despite the PAL-induced starvation phenotype, and increasing CoASH via PANK1β overexpression did not rescue the phenotype, demonstrating a unique role for PANK2 in fatty acid metabolism. Even though a direct CoASH deficiency was not detected, there were changes in short chain CoA-derivatives, including acetyl-CoA, succinyl-CoA, and butyryl-CoA, as well as evidence of impaired TCA cycle function. These impairments in both the TCA cycle and

i

fatty acid oxidation implicate a role for PANK2 in regulating mitochondria CoA dynamics.

DEDICATION

Till mamma, Ann-Charlotte, och pappa, Udo, detta var bara möjligt med ert stöd,

uppmuntran, och kärlek. Till Adrian och Marc, mina skyddsänglar. Jag älskar er alla.

To John, min kanin. Thank you for making my dreams ours, for the best lunches and all

the cat memes. For your principles, for your support and love, thank you.

Let us make the rest of our dreams come true. I love you.

ACKNOWLEDGMENTS

First, I would like to thank my advisor, Dr. Michael Kruer, for giving me the opportunity to pursue a meaningful and perplexing scientific question. Thank you for your guidance and support, for pushing and challenging my scientific thinking. Thank you for your kindness, for providing a wonderful example of great leadership.

Next, I would like to thank Dr. Sergio Padilla Lopez for being my mentor, always excited to discuss the latest findings and encouraging through setbacks. I appreciate all the time that you have spent teaching and providing me guidance. Thank you for all the discussions questioning dogma, in science and elsewhere, for making a difficult time more bearable. Your support has been invaluable.

A special thank you to Dr. Janet Neisewander and Dr. Christos Katsanos for your feedback and time, serving on my committee.

To all current and past Kruer Lab members, thank you all for your help and contribution to this work. Thank you to Dr. Sara Lewis for offering and providing your assistance and valuable feedback. Helen Magee, thank you for keeping me sane and for being my friend.

I interviewed with Dr. Kruer and Dr. Padilla Lopez in what seemed like a broom closet, a wonderful Harry Potteresque start to a Ph.D. journey, full of challenges and accomplishments, summarized here with this dissertation.

TABLE OF CONTENTS

LIST OF FIGURES

Figure   Page

CHAPTER 1

INTRODUCTION

Inborn errors in free coenzyme A (CoASH) synthesis and transport cause

Neurodegeneration with Brain Iron Accumulation (NBIA) and Recurrent Metabolic

Crises with variable Encephalomyopathic Features and Neurologic Regression

(MECREN) respectively. NBIA is a progressive neurodegenerative disorder

accompanied with dystonia and parkinsonism leading to early death (Arber et al., 2016).

The globus pallidus is particularly affected and iron deposits show up on T_2-weighted

MRI called "the eye of the tiger" (Kruer et al., 2011).

Other disorders linked to dysfunctional CoASH and CoA-derivative homeostasis

include diabetes, cancer, cardiovascular disease and additional neurological disorders

including Reye's syndrome (Gout, 2018). Two NBIA subtypes, pantothenate kinase

associated neurodegeneration (PKAN) and COASY Protein-Associated

Neurodegeneration (COPAN), highlight the complexity of CoASH homeostasis,

especially as data to date is lacking showing a clear molecular mechanism connecting

CoASH and neurodegeneration in PKAN and COPAN (Mignani et al., 2021). This thesis

focuses on the cellular role of pantothenate kinase 2 (PANK2), the protein impaired in

PKAN, and how loss of PANK2 affect all CoA (CoASH & CoA derivative) levels and

dependent cellular processes.

CoASH synthesis and compartmentalization

CoASH is an acyl-carrying cofactor. Oxidation of fatty acids, glucose, and some

amino acids depend on CoASH to enter the TCA cycle as acetyl-CoA or succinyl-CoA,

the two most abundant short chain CoA-derivatives in the cell (Trefely et al., 2022).

Biosynthesis of several complex molecules; lipids, bile, neurotransmitters, heme, and more, are also dependent on CoA-derivatives. Increasingly, the role of CoA-species in regulating cellular processes i.e. gene expression and autophagy is recognized (Mariño et al., 2014; Trefely et al., 2020; Yu et al., 2021)

Historically, the regulation of cellular processes have focused on acetyl-CoA levels due to the acetyl-group link between catabolism and post translational modifications (PTMs) (Trefely et al., 2020), but more studies on the ratio of CoASH to acetyl-CoA (and acyl-CoA) could provide additional nuance to the regulation of these cellular processes. Several lysine acetyltransferases (KATs) bind both acetyl-CoA and CoASH with similar K_d i.e. the KATs: Gcn5, picNuA4, and PCAF (Albaugh et al., 2011). Therefore, as the CoASH to acetyl-CoA ratio fluctuate in the cell with starvation to fed state; the KATs switch from off to on. As such, localized or compartment specific CoASH/CoA-derivative synthesis may have an effect on the KATs microenvironment (Albaugh et al., 2011).

In addition to CoASH influence on acetylation, CoASH is also a source of CoAlation and 4′-phosphopantetheinylation (Yu et al., 2021). CoAlation is a recently coined term for the direct binding of CoASH to protein cysteines (Tsuchiya et al., 2017). The amount of cellular protein CoAlation depend on the cells CoASH concentration, induced by oxidative and metabolic stress. 65-80% percent of CoAlated proteins in rat heart and liver are metabolic enzymes (Tsuchiya et al., 2017). For 4′-phosphopantetheinylation, phosphopantetheinyl transferases (PPTases) use CoASH to attach 4′-phosphopantethein to proteins such as the mitochondria acyl carrier protein (mACP) (Beld et al., 2014).

Compartmentalization allow the cell to increase efficiency and add spatial

regulation to metabolism. CoASH and acyl-CoAs exists in discrete intracellular pools,

only able to enter or exit mitochondria, peroxisomes and the endoplasmic reticulum via

transporters and shuttle systems (Naquet et al., 2020; Trefely et al., 2020). This creates

unique CoASH and acyl-CoA profiles in each compartment. For example, succinyl-CoA

is the major CoASH species in the mitochondria while CoASH and acetyl-CoA are more

abundant in cytosol (or non-mitochondria) fractions (Trefely et al., 2022). However, on a

concentration basis, mitochondria CoASH is estimated to be in the range of 2-5mM

compared to the estimated cytosolic CoASH concentration at around 0.02 to 0.14mM

depending on the cell type and metabolic state (Leonardi et al., 2005).

How the mitochondria CoASH concentration is established and maintained in

mammalian cells is a topic of debate. Canonically, mammalian CoASH synthesis

proceeds in a five-step process, depicted in figure 1.1, in the cytosol catalyzed by four

different proteins: pantothenate kinase (PANK), phosphopantothenoylcysteine synthetase

(PPCS), phosphopantothenoylcysteine decarboxylase (PPCDC), and the bifunctional

coenzyme A synthase protein (COASY) that together turn pantothenate (Vitamin B_5) into

CoASH (Fig 1.1) (Leonardi et al., 2005). Mutations in the *COASY* gene cause another

subtype of NBIA, COASY Protein-Associated Neurodegeneration (COPAN) (Dusi et al.,

2014).
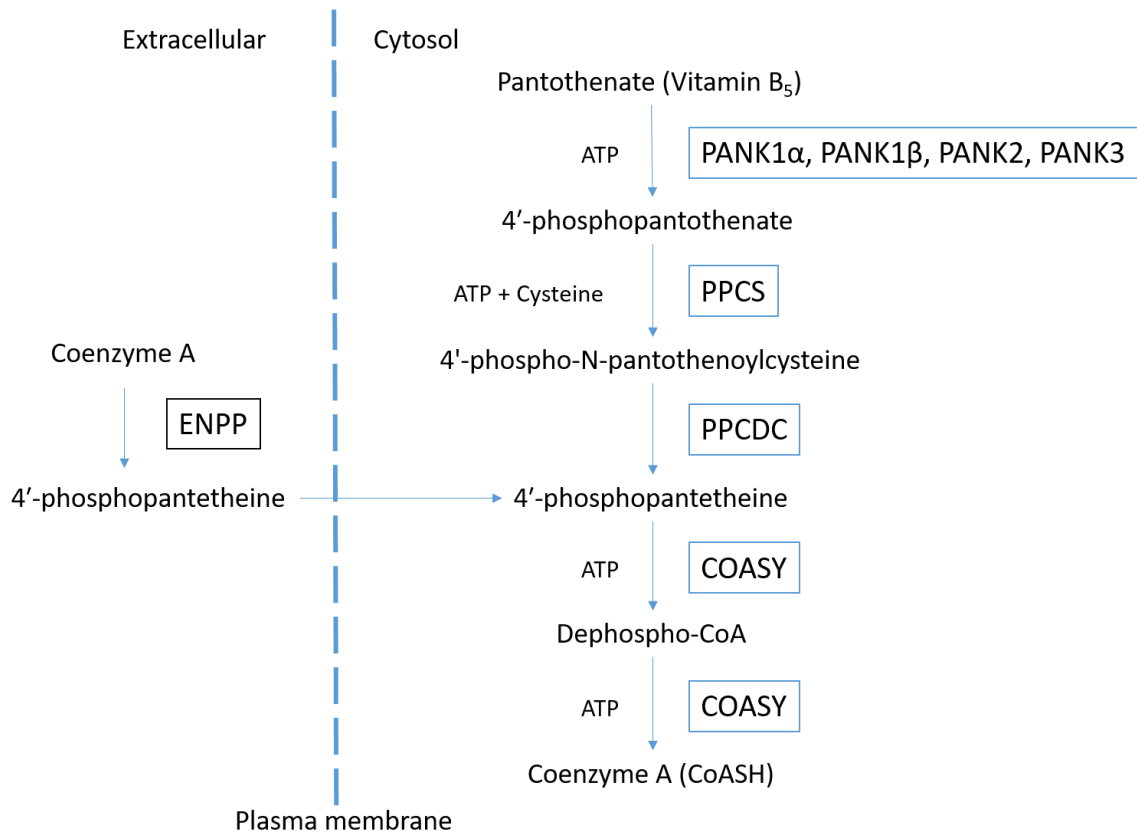
Figure 1.1. Coenzyme A Biosynthesis. Free coenzyme A biosynthesis starts with a pantothenate kinase (PANK1-3) phosphorylating pantothenate (Vitamin B_5). In the next step, phosphopantothenoylcysteine synthetase (PPCS) adds cysteine. Phosphopantothenoylcysteine decarboxylase (PPCDC) decarboxylates to generate 4′-phosphopantetheine. 4′-phosphopantetheine is the precursor for coenzyme A synthase (COASY), which first add AMP to generate dephospho-CoA and then finish with phosphorylation to generate free coenzyme A (CoASH). Coenzyme A cannot pass through the plasma membrane, but ectonucleotide pyrophosphatases can breakdown coenzyme A to 4′-phosphopantetheine. COASY use 4′-phosphopantetheine as a precursor for coenzyme synthesis.

In addition to the canonical pathway, recent experiments show evidence for the ability of cells to take up 4′-phosphopantetheine, which COASY can convert to CoASH (Fig 1.1) (Srinivasan et al., 2015). Extracellular CoASH in serum can be broken down to 4′-phosphopantetheine by an ectonucleotide pyrophosphatases (ENPP) and pass through

the plasma membrane via passive diffusion (Srinivasan et al., 2015). If 4′-phosphopantetheine can pass through the plasma membrane, it is plausible that 4′-phosphopantetheine can pass through mitochondria membranes to supply a mitochondria localized COASY (Dusi et al., 2014; Rhee et al., 2013; Skrede & Halvorsen, 1979).

Once synthesized in the cytosol, experimental evidence show that CoASH can be imported into the mitochondria matrix (Fiermonte et al., 2009; Tahiliani, 1991). In early biochemical experiments isolated mitochondria incubated with [^{14}C]-CoASH accumulated CoASH and the CoASH import was dependent on the mitochondria membrane electrical gradient (Tahiliani, 1991). SLC25A42 is a mitochondria inner membrane protein that can rescue a mitochondria CoASH deficient yeast strain. When reconstituted into proteoliposomes SLC25A42 transports dephospho-CoA, CoASH, ADP and adenosine 3′,5′-diphosphate (Fiermonte et al., 2009). Mutations in *SLC25A42* cause MECREN and some individuals present with brain iron accumulation suggesting an overlapping etiology with NBIA (Almannai et al., 2018).

In addition to the cytosolic CoASH synthesis and mitochondria transport model, one hypothesis is that mitochondria contains its own CoASH biosynthesis pathway. Early biochemical experiments found that isolated rat mitochondria contained enzymatic activity corresponding to the last two steps in CoASH synthesis, but it is unclear if this activity was within the mitochondria (Skrede & Halvorsen, 1979; Tahiliani & Beinlich, 1991). Newer experiments has focused on localizing the canonical CoASH synthesis enzymes to subcellular compartments with fractionation, microscopy, and APEX tagging. Besides PPCDC, these studies have shown that one isoform for each step in CoASH biosynthesis localize to the mitochondria including PANK2 and COASY (Alfonso-

Pecchio et al., 2012; Dusi et al., 2014; Jeong et al., 2019; Kotzbauer et al., 2005; Rhee et al., 2013; Thul et al., 2017). Localization studies have also found PANK isoforms and COASY in the nucleus (Alfonso-Pecchio et al., 2012; Lin et al., 2018). However, concrete evidence for subcellular CoASH synthesis is still missing.

Three different *PANK* genes (*PANK1*, *PANK2*, and *PANK3*) give rise to functional PANK proteins with different subcellular localization and regulatory properties. The *PANK1* gene give rise to two different transcripts generating two protein isoforms PANK1α and PANK1β (Rock et al., 2002). PANK1α localize to the nucleus while PANK1β is cytosolic and associated with vesicles (Alfonso-Pecchio et al., 2012). CoASH does not inhibit PANK1β, while PANK1α is feedback inhibited ($IC_{50} = 80\mu M$). Both are regulated by acetyl-CoA at ($IC_{50} = 5\mu M$) and ($IC_{50} = 10\mu M$) for PANK1α and PANK1β respectively (Zhang et al., 2005). PANK3 is a cytosolic protein with greater inhibition by CoA-derivatives (acetyl-CoA $IC_{50} = 1\mu M$) then by CoASH itself ($IC_{50} > 80\mu M$) (Alfonso-Pecchio et al., 2012; Zhang et al., 2005).

PANK2 on the other hand is the only PANK that localizes to the mitochondria in addition to the cytosol and the nucleus (Alfonso-Pecchio et al., 2012; Hortnagel, 2003; Johnson et al., 2004; Kotzbauer et al., 2005). Convincing evidence of PANK2 localizing to the mitochondria include immunoelectron microscopy showing endogenous PANK2 staining in neuronal mitochondria (Kotzbauer et al., 2005). The PANK2 sequence contain both a mitochondria and nuclear localizing signal. PANK2 is transcribed as a pre-peptide that can move from the nucleus to the mitochondria and once PANK2 is imported into the mitochondria the pre-peptide is cleaved twice to generate a mature PANK2 (Alfonso-Pecchio et al., 2012; Kotzbauer et al., 2005). Proteins with two cleavable mitochondria

6

targeting sequences are often associated with the mitochondria inner membrane space (IMS), but there is no other evidence pinpointing PANK2's submitochondria localization (Roberta Leonardi et al., 2007).

PANK2 is inhibited by CoASH and acetyl-CoA at $IC_{50} < 1\mu M$ *in vitro*, which might make PANK2 inactive in the mitochondria matrix where CoASH concentrations are 2-5mM. However, palmitoylcarnitine can activate PANK2 allowing it to overcome acetyl-CoA inhibition (Roberta Leonardi et al., 2007; Zhang et al., 2006). If PANK2 localize to IMS, palmitoylcarnitine, generated by outer mitochondria membrane (OMM) transmembrane protein carnitine palmitoyltransferase I (CPT1), would be readily available to activate PANK2 when fatty acids are imported to the mitochondria for fatty acid oxidation (Roberta Leonardi et al., 2007). PANK2 could at this intersection sense a reduction in CoASH because of fatty acid oxidation, which relieves inhibition, and at the same time PANK2 activated by palmitoylcarnitine, could generate CoASH for mitochondria fatty acid oxidation.

PPCS and PPCDC are cytosolic proteins, but no focused studies looking at their subcellular localization exists in human cells. One mouse fractionation study showed a portion of PPCS protein co-fractionating with mitochondria and the Protein Atlas database show PPCS as localizing to the mitochondria (HumanProteinAtlas, 2022b; Jeong et al., 2019; Thul et al., 2017). The Protein Atlas database show PPCDC as a cytosolic protein (HumanProteinAtlas, 2022a; Thul et al., 2017). Large mitochondria proteomics studies do not detect PPCS and PPCDC in the mitochondria (Rath et al., 2021; Rhee et al., 2013).

COASY was the first enzyme purified from mitochondria fractions. Follow up microscopy experiments and APEX tagging have placed COASY in the matrix, in association with the mitochondria outer membranes as well as the cytosol and nucleus (Dusi et al., 2014; Rhee et al., 2013; Skrede & Halvorsen, 1979; Zhyvoloup et al., 2003). Reasons for COASYs matrix localization while all other proteins appear to be located outside of the mitochondria matrix include: matrix CoASH synthesis from dephospho-CoA, which could be imported by SLC25A42 (Fiermonte et al., 2009), sequestering COASY for spatial regulation, or a mitochondria import and processing mechanism, which transiently place COASY in the mitochondria matrix.

Mitochondria CoASH deficiency is a major hypothesis for why mutations in *PANK2*, *COASY*, and *SLC25A42* cause neurodegeneration. Understanding mitochondrial CoASH homeostasis, and how it affects the whole cell, would be an important step forward in understanding the link between CoASH and neurodegeneration.

Metabolic regulation by CoASH and CoA-derivatives

CoA-species can act as a regulator of cellular processes. CoASH and the short chain CoA-derivatives have well defined roles in regulating protein activity via feedback regulation and acyl-group donation. CoASH can directly regulate protein activity via CoAlation and by 4-phosphopantetheinylation (Beld et al., 2014; Yu et al., 2021). Acyl-group donation by acyl-CoAs i.e. acetylation and propionylation link metabolism with the regulation of protein activity and gene expression via PTMs (McDonnell et al., 2016; Trefely et al., 2022; Wellen et al., 2009). An emerging regulatory mechanism involves the idea of local production of acyl-CoAs in the nucleus from carbon substrates to coordinate the link between metabolism and gene expression (Madiraju et al., 2009;

8

McDonnell et al., 2016; Sutendra et al., 2014). These regulatory properties of CoASH and CoA-derivatives are described in more detail below.

The regulatory role served by CoA-species is evident in the homeostatic processes called the Randle Cycle. The Randle Cycle describes how an influx in fatty acids will cause the cell to preferentially oxidize fatty acids while inhibiting glucose oxidation (Hue & Taegtmeyer, 2009). The Randle Cycle work by inhibiting multiple steps in glucose oxidation, but also via the inhibition of the pyruvate dehydrogenase complex (PDH). PDH converts pyruvate to acetyl-CoA in the mitochondria. Both acetyl-CoA and CoASH regulate PDH activity via the pyruvate dehydrogenase kinases by mechanisms explained below.

Pyruvate dehydrogenase kinases (PDK1-4) inhibit PDH activity via phosphorylation. Fatty acid oxidation increase acetyl-CoA levels, stimulates PDK2 via allosteric regulation to phosphorylate and block PDH activity (Hue & Taegtmeyer, 2009; Woolbright & Harris, 2021). A recent study found that PDK2 is CoAlated and that CoAlation inactivated PDK2 *in vitro* (Tsuchiya et al., 2017). If confirmed in future studies, these findings suggests a possible reciprocal mechanism whereby acetyl-CoA stimulates PDK2 activity (blocking PDH) while CoASH inhibits PDK2 (allowing PDH activity). In two mice studies, researchers showed that high CoASH levels marked PDK4 for Lon protease degradation in heart mitochondria and that high fat feeding prevented this mechanism, putatively by decreasing mitochondria CoASH levels (Crewe et al., 2017; Schafer et al., 2018). More experiments will determine the contribution of CoASH synthesis and compartmentalization to the PDK-PDH regulatory axis, and CoAlation is a developing regulatory property that needs more study.

Besides CoAlation, CoASH can affect proteins via another PTM called 4-phosphopantetheinylation. Two 4-phosphopantetheinylated proteins are involved in fatty acid synthesis: the cytosolic acyl carrier protein in the fatty acid biosynthesis type I system (FASI) and the mitochondrial acyl carrier protein (mACP) in the fatty acid biosynthesis type II system (FASII) (Beld et al., 2014). The cytosolic FASI system synthesize palmitic acid and the mitochondrial FASII system is required for lipoic acid synthesis. Lipoic acid is essential for protein lipoylation, a PTM required for the proper functioning of PDH, α-ketoglutarate (KDH), branched-chain a-keto acid dehydrogenase (BCKDH), and the glycine cleavage system (GCS) (Rowland et al., 2018).

The connection between CoASH, 4-phosphopantetheinylation, mACP, lipoic acid, and four different neurodegenerative disorders (PKAN and CoPAN included) led researchers to investigate mACP, lipoylation and PDH function in PKAN models (Jeong et al., 2019; Lambrechts et al., 2019). These studies found reduced PDH activity in PANK2 KO mice in the globus pallidus (area affected in PKAN) and reduced PDH activity and lipoylation in drosophila with disrupted CoASH synthesis. In human SHSY5Y cells, they found reduced mACP levels. Most intriguingly in drosophila dPANK/fbl RNAi, stimulation of PDH activity with dichloroacetate dramatically increased drosophila viability (Jeong et al., 2019; Lambrechts et al., 2019). It would be interesting to know what the CoASH levels are in the drosophila dPANK/fbl RNAi model, since the dichloroacetate results suggest that PDH activity is the main cause of death in this model.

Acetyl-CoA exerts a powerful influence on the cell via histone acetylation. Remarkably, metabolic programming reflects the acetyl-CoA carbon source i.e. lipid-

derived acetyl-CoA favors transcription of the fatty acid oxidation network, while glucose-derived acetyl-CoA promotes glycolytic gene expression (McDonnell et al., 2016; Wellen et al., 2009). In the case of fatty acid oxidation, the upregulation of both *CPT1* and *PDK4* gene expression reflect changes in the cellular transcriptome to facilitate fatty acid oxidations (McDonnell et al., 2016; Pettersen et al., 2019). How the cell can differentiate between glucose and lipid derived acetyl-CoA for histone acetylation remains to be determined, but one hypothesis suggests that local nuclear production of acetyl-CoA from acyl-carnitines regulate the process (McDonnell et al., 2016).

If not oxidized in the TCA cycle, mitochondrial acetyl-CoA can acetylate mitochondria proteins or the mitochondria may export acetyl-CoA in the form of citrate. In the cytosol, ACLY converts citrate back to acetyl-CoA and oxcaloacetate. Nucleocytosolic acetyl-CoA become a source for either PTMs or malonyl-CoA. Malonyl-CoA is another important example of how a CoASH derivative regulate a metabolic junction. Malonyl-CoA is the precursor for fatty acid synthesis and an allosteric inhibitor of carnitine palmitoyltransferase 1 (CPT1), the protein responsible for shuttling long chain fatty acids into the mitochondria for β-oxidation (Hue & Taegtmeyer, 2009).

The contribution of compartmentalized CoA-derivative production to cell regulation is increasingly recognized as a possible regulatory mechanism (McDonnell et al., 2016). Two surprising means for the cell to generate nuclear acyl-CoAs for histone PTMs include the conversion of acylcarnitine to acetyl-CoA by a nuclear carnitine acetyltransferase (CRAT) and the conversion of pyruvate to acetyl-CoA by a nuclear localized pyruvate dehydrogenase complex (Madiraju et al., 2009; Sutendra et al., 2014). Interestingly, PANK1α, PANK2, and COASY all localize to the nucleus and CoASH can

alter the activity of KAT enzymes, making it feasible that if local nuclear production of CoASH exists, it would have an effect on gene expression (Albaugh et al., 2011; Alfonso-Pecchio et al., 2012; Lin et al., 2018).

Studies on the effect of CoA-derivative compartmentalization on cell regulation has focused on how carbon source availability alter the acyl-CoA pool. Considering the compartmentalization of the CoASH biosynthetic enzymes and CoASH, it would be reasonable to hypothesize that the availability of CoASH in addition to nutrient availability, regulate acyl-CoA production. Thereby CoASH synthesis would also regulate histone and protein PTMs. Changes to CoASH levels themselves alter the ratio of CoASH to acyl-CoA, which regulate proteins and perhaps even histone acetylation (Albaugh et al., 2011; Yu et al., 2021). CoASH biosynthetic enzymes localize to the cytosol, nucleus, and the mitochondria, where they could provide a carbon source independent mode of regulation to acyl-CoA levels.

CoASH synthesis and β-oxidation

The mitochondria is the location of several CoASH dependent cellular processes, both oxidative and synthetic. β-oxidation of fatty acids is one such process highly dependent on CoASH. The full oxidation of palmitic acid, a 16-carbon fatty acid, would require eight molecules of CoASH to generate eight molecules of acetyl-CoA in the mitochondrial matrix. Isolated rat mitochondria provided palmitoylcarnitine instead of pyruvate as a substrate, significantly decrease its CoASH content within 2 minutes (Schafer et al., 2018). During high fat feeding or starvation in rats and mice, total cellular CoASH content increase in their livers and kidney (Dansie et al., 2014; HORIE et al., 1986; Leonardi et al., 2010; Leonardi et al., 2005). The high fat diet increases CoASH,

acetyl-CoA, and long chain acyl-CoA levels in mitochondria, peroxisome, and cytosolic fractions (HORIE et al., 1986). Altogether, this indicate that new CoASH synthesis is required to support β-oxidation.

The next step is to understand how the CoASH biosynthesis machinery coordinate to increase CoASH levels in order to support β-oxidation. The PANK enzymes regulate the first and rate-limiting step in CoASH synthesis, but we do not know the contribution of each isoform to the different CoASH pools and under what circumstances each PANK contributes. Both PANK1 and PANK2 are the most researched PANK isoforms and both are strong candidates for the regulation of CoASH during β-oxidation.

Knocking out PANK1 in mice prevents an increase in liver CoASH in response to fasting (Leonardi et al., 2010). Liver homogenates without PANK1 show a 40% reduction in PANK activity. The *PANK1* knockout (KO) mice also accumulate long chain acyl-CoAs, acyl-carnitines, and lipid droplets, while fatty acid oxidation measured in liver extracts decrease slightly, but significantly. Overall, the PANK1 KO mice are healthy, but this study showed that PANK1 is important for CoASH levels during fasting and for fatty acid oxidation (Leonardi et al., 2010). However, it is unknown if the decrease in fatty acid oxidation is due to an alteration in peroxisome or mitochondria fatty acid oxidation, and a substantial amount of fatty acid oxidation capability remains even without PANK1.

PANK2 KO mice, made to model human PKAN disease, are relatively healthy besides a smaller size, retinal degeneration, and azoospermia, and do not show signs of neurological or movement impairment (Kuo et al., 2005). However, when the *PANK2* KO mice eat a ketogenic diet, high fat with low carbohydrates, the mice develop a

13

movement impairment (Brunetti et al., 2014). The levels of the ketone body β-hydroxybutarate was comparable to wild type (Brunetti et al., 2014). Mechanistically it is unclear if the impairment induced by the ketogenic diet was due to an inability to oxidize fatty acids, use ketone bodies, or another factor.

It is hypothesized that human PANK2 acts as an acyl-carnitine sensor in the mitochondria IMS (Roberta Leonardi et al., 2007). In their study, Leonardi et al found that palmitoylcarnitine activates PANK2 *in vitro*, allowing the protein to overcome acetyl-CoA feedback inhibition. Palmitoylcarnitine generation would be high in the IMS where PANK2 is located when CPT1 converts palmitoyl-CoA to palmitoylcarnitine for β-oxidation (R. Leonardi et al., 2007). There has not been any follow up studies performed to test this model and PANK2's role during β-oxidation is still unknown.

The cells stress response and CoA

When the cell encounters stressors and ATP levels fall, it can override the Randle Cycle to allow the use of both glucose and lipids for ATP generation (Hue & Taegtmeyer, 2009). The cellular ATP/AMP and calcium sensor, AMP-activated protein kinase (AMPK), has widespread substrate reach with the general result of increasing autophagy, fatty acid and glucose oxidation, while blocking energy demanding process i.e. non-essential synthesis. AMPK achieve this override in part by adjusting malonyl-CoA levels, increasing glucose uptake by upregulating GLUT4, and by relieving inhibition of glucose oxidation (Hue & Taegtmeyer, 2009).

Autophagy is the recycling and degradation of cellular components in response to cellular stress, as a means of quality control, and for tissue remodeling (Mariño et al., 2014). Starvation is a potent autophagy inducer. Interestingly, during starvation acetyl-

CoA levels are the first metabolite reduced (not ATP nor NADH) and this causes a potent activation of cellular autophagy (Mariño et al., 2014). Injecting acetyl-CoA, but not CoASH into the cell, prevents starvation-induced autophagy and mechanistically acetyl-CoA appear to partly achieve this by altering the acetylation status of EP300 (Mariño et al., 2014).

These experiments show the incredible role of acetyl-CoA in regulating autophagy. However, the role of CoASH require more consideration. In their experiment, they also inject CoASH and do not see inhibition of autophagy and therefore conclude that acetyl-CoA alone regulates autophagy. However, high CoASH levels might actually signal starvation and reduced CoASH levels are more likely to act as a signal to block autophagy. It is clear that CoASH levels increase in response to starvation (HORIE et al., 1986; Leonardi et al., 2005) and therefore it would be unexpected that increasing CoASH would inhibit autophagy as in the experiments performed by Mariño et al (Mariño et al., 2014). This leaves the possibility open that reduction in CoASH and that changes to CoASH/acetyl-CoA ratio is another important autophagy regulator not fully considered.

The role of CoASH in autophagy is not broadly studied. However, COASY interact with important autophagy regulators including PI3K and S6K, which are part of the mTOR signaling pathway, but the consequence of this interaction is unknown (Nemazanyy et al., 2004; Theodoulou et al., 2014). CoASH itself can activate CAMKII, a calcium sensor that can activate AMPK (Theodoulou et al., 2014). CoAlation, which increase in response to oxidative and metabolic stress, could present another regulator of autophagy and stress responses in general (Tsuchiya et al., 2017).

Summary of hypothesis for PKAN disease

15

From the bird's eye view, PANK2 is a CoASH synthesizing enzyme and the major hypothesis is that a deficiency in CoASH synthesis cause PKAN. Intriguingly, CoASH levels in PKAN mouse and cellular models have CoASH levels comparable to controls i.e. there is no discernible whole-cell CoASH deficiency (Lambrechts et al., 2019; Mignani et al., 2021). I*n vitro* experiments, show that some PKAN associated PANK2 mutants have no synthesis activity while other have increased catalytic activity (Zhang et al., 2006). Catalytically active PANK2 mutants might have dysfunctional localization and or regulatory properties, which might explain how catalytically functional PANKs still cause PKAN. The discovery of mutations in the *COASY* gene, the last CoASH biosynthetic enzyme, causing another subtype of NBIA, reinforces the hypothesis that defective CoASH synthesis cause PKAN and CoPAN (Dusi et al., 2014). However, in fibroblasts derived from individuals with CoPAN, there was also no significant difference in whole-cell CoASH levels (Dusi et al., 2014).

A CoASH deficiency might be restricted to the brain, a subcellular compartment, a specific metabolic or stress condition, or masked by the compensation of the other PANKs. Owing to the association between PANK2, COASY, and the mitochondria, a more specific hypothesis is that a deficiency in mitochondria CoASH or the regulation of mitochondria CoASH causes PKAN/CoPAN. PKAN muscle biopsies have shown the presence of altered and giant mitochondria (Brunetti et al., 2014). In model systems including neuronal cells, several studies have found deformed mitochondria and reduced mitochondrial respiratory activity (Brunetti et al., 2014; Orellana et al., 2016). One study, found significantly lower CoASH levels in the mitochondria of PKAN derived fibroblasts (Álvarez-Córdoba et al., 2019). Although, a mitochondria CoASH deficiency is likely,

more studies are required to confirm mitochondria CoASH levels in PKAN model systems with a homogenous genetic background.

Mitochondria dysfunction have led some to speculate that dysregulated mitophagy, the specific autophagic degradation of mitochondria, is behind NBIA (Arber et al., 2016). Two additional NBIA subtype, BPAN and Kufor-Rakeb syndrome, is caused by mutations in *WDR45* needed for autophagy and mutations in *ATP13A3* a lysosomal protein respectively, implicate dysfunctional autophagy in NBIA. Parkinsonism is a common symptom in PKAN and PINK1, a mitophagy protein, cause a familial form of Parkinson (Morais et al., 2009). Currently, how dysfunctional CoASH synthesis would cause dysregulated autophagy is unknown, but mitochondria dysfunction or decreased acetyl-CoA production, could both be mechanisms causing increased autophagy.

The role of PANK2 might also be context dependent. As seen in the *PANK2* KO mice, a ketogenic diet cause the mice to develop a movement disorder (Brunetti et al., 2014). One such hypothesis is that PANK2 is required for maintaining adequate mitochondria CoASH levels during β-oxidation. The high acetyl-CoA levels in the mitochondria IMS is enough to inactivate the PANK2 protein (Roberta Leonardi et al., 2007). Palmitoylcarnitine, abundant in mitochondria during β-oxidation, is able to displace inhibitory acetyl-CoA and activate PANK2 (Roberta Leonardi et al., 2007). Understanding the cellular role of the PANKs, and specifically when PANK2 is required, is another area that needs more research.

Lastly, a recent hypothesis postulate that PANK2 is required to supply enough mitochondria CoASH for 4-phosphopantetheinylation (Jeong et al., 2019; Lambrechts et

al., 2019). A reduction in 4-phosphopantetheinylation could impair iron-sulfur cluster synthesis explaining brain iron accumulation and 4-phosphopantetheinylation is needed for lipoic acid synthesis. This hypothesis also depend on a specific mitochondria CoASH deficiency caused by defective PANK2.

Considering the many roles of mitochondria CoASH, it would be surprising if reduced mitochondria CoASH only affected one CoA-dependent pathway. Therapeutics aimed at restoring CoASH levels with CoASH synthesis intermediates or small molecule alternatives, as well as iron chelation therapy, have so far not shown clinical benefit (Iankova et al., 2021). Therapies might have to be combinatorial i.e. increase CoASH production, stimulate PDH with dichloroacetate, and use an iron chelator. Alternatively, early intervention or targeting mitochondria CoASH is necessary for successful therapy. The many hypothesis, PKAN models, and attempted therapeutics for PKAN (and CoPAN) disease show the complexity of cellular CoASH dynamics.

CHAPTER 2

PANK2 IS REQUIRED FOR CELLULAR FATTY ACID UTILIZATION

Abstract

An influx of fatty acids increase the mitochondrial demand for free coenzyme A (CoASH) to generate acetyl-CoA. In pantothenate kinase associated neurodegeneration (PKAN), one CoASH biosynthetic enzyme, PANK2 is impaired. The existence of several PANK isoform obscure investigations into PANK2s non-redundant functions that cause PKAN. Here we report that the cell is dependent on PANK2 for effective fatty acid utilization. Supplementing PANK2-deficient cells with palmitic acid cause reduced cell viability, fatty acid accumulation, reduced ATP levels, and autophagy upregulation. Oxygen consumption measurements show that cells lacking PANK2 have a reduced ability to respire palmitoylcarnitine. Overexpression of cytosolic PANK1β elevate CoASH levels, but this does not rescue palmitic acid induced PANK2 phenotypes, providing evidence for PANK2s unique role in supporting cellular fatty acid metabolism.

Introduction

Long chain fatty acid oxidation preferentially take place in the mitochondria matrix. The complete oxidation of the long chain fatty acid, palmitic acid, requires eight molecules of CoASH to generate eight molecules of acetyl-CoA. Experiments in rats and mice suggest that mitochondria β-oxidation is dependent on *de novo* CoASH synthesis. In isolated mouse mitochondria provided palmitoylcarnitine as a substrate, CoASH reserves are quickly depleted (Schafer et al., 2018). High fat feeding and starvation, which activate β-oxidation, increase total coenzyme A (CoA) and free coenzyme A (CoASH) levels in whole tissue and rat liver mitochondria (Berge et al., 1984; HORIE et al., 1986).

These studies suggest that *de novo* CoASH synthesis is necessary to meet the increased CoASH demand during β-oxidation.

Mammalian CoASH synthesis is a five-step process with the first and rate-limiting step catalyzed by a pantothenate kinase (PANK) (Robishaw et al., 1982). The subsequent steps in CoASH synthesis are catalyzed by PPCS, PPCDC, and the final two steps by COASY (Daugherty et al., 2002). In mammalian cells, three genes encode functional PANKs: *PANK1*, *PANK2*, and *PANK3*. The PANK proteins exhibit differential tissue expression, subcellular localization, and regulatory properties, which suggests that the PANKs contribution to CoASH synthesis is context dependent (Alfonso-Pecchio et al., 2012; Dansie et al., 2014; Leonardi et al., 2005). In what context the different PANKs are required is unknown.

The *PANK1* gene encode two protein isoforms PANK1α and PANK1β localizing to the nucleus and cytosol respectively (Alfonso-Pecchio et al., 2012). PANK2 is the only PANK that localize to the mitochondria in addition to the cytosol and the nucleus (Alfonso-Pecchio et al., 2012; Hortnagel, 2003; Kotzbauer et al., 2005). The sub-mitochondria localization of PANK2 is unknown. PANK2 is strongly feedback inhibited by acetyl-CoA IC_{50} <1μM compared to PANK1β IC_{50} = 10 μM, which is enough for PANK2 to be inactive in the mitochondria matrix (Roberta Leonardi et al., 2007; Zhang et al., 2005, 2006). Interestingly, palmitoylcarnitine, abundant in mitochondria during fatty acid influx, activates PANK2 removing the inhibitory effect of acetyl-CoA (Roberta Leonardi et al., 2007). Palmitoylcarnitine activation in combination with PANK2s mitochondrial localization suggest that PANK2 could be important for CoASH synthesis during mitochondrial fatty acid oxidation (Roberta Leonardi et al., 2007).

20

Inborn errors in CoASH synthesis cause two subtypes of neurodegeneration with brain iron accumulation (NBIA), pantothenate kinase associate neurodegeneration (PKAN) and COASY protein associated neurodegeneration (CoPAN), by mutations in PANK2 and COASY respectively (Dusi et al., 2014; Zhou et al., 2001). Mutations in PPCS cause autosomal-recessive dilated cardiomyopathy (Iuso et al., 2018). A whole-cell CoASH deficiency is present in fibroblasts from individuals affected with PPCS-cardiomyopathy (Iuso et al., 2018). However, the link between the NBIA disorders and CoASH is not clear, since whole-cell CoASH levels are comparable to healthy controls (Dusi et al., 2014; Lambrechts et al., 2019; Mignani et al., 2021). One recent study show a mitochondria specific CoASH deficiency in fibroblasts from individuals affected with PKAN (Álvarez-Córdoba et al., 2019). If this holds true the role of PANK2 could be to regulate mitochondria CoASH levels, where the oxidation of long chain fatty acids take place.

All three CoASH biosynthetic disease-causing proteins have varying degrees of experimental evidence for mitochondrial localization. Microscopy, fractionation experiments, and large-scale proteomics involving APEX-tagging localize COASY to the mitochondrial matrix, but microscopy and fractionation studies also place COASY on the outer mitochondria membrane (OMM) (Dusi et al., 2014; Rhee et al., 2013; Skrede & Halvorsen, 1979; Zhyvoloup et al., 2003). PPCS has not been studied extensively, but it is an active cytosolic protein (Skrede & Halvorsen, 1979). However, one mouse fractionation study and a microscopy study done by the Human Protein Atlas localize PPCS to the mitochondria (HumanProteinAtlas, 2022b; Jeong et al., 2019; Thul et al., 2017).

Evidence for cytosolic CoASH synthesis exists and the mitochondria protein SLC25A42 is responsible for transporting CoASH into the mitochondria (Fiermonte et al., 2009; Tahiliani, 1991; Tahiliani & Beinlich, 1991). However, the subcellular distribution of PANK2, PPCS, and COASY opens up the possibility of a mitochondria CoASH synthetic pathway. Early biochemical experiments only detected COASY activity in mitochondria and no activity from the four upstream enzymes (Skrede & Halvorsen, 1979). Following PANK2 overexpression, one group detected PANK2 activity in isolated mitochondria (after subtracting background PANK activity), but it is not clear if the PANK2 activity is associated with the mitochondria or inside the mitochondria (Kotzbauer et al., 2005).

Irrespective of complete mitochondria CoASH biosynthesis, PANK2 in the mitochondria could sense a drop in CoASH and become activated by the influx of palmitoylcarnitine, resulting in increased CoASH synthesis (Roberta Leonardi et al., 2007). PANK2 KO mice, which are generally healthy except for azoospermia and retinal degeneration, develop a movement disorder when provided with a ketogenic, high fat diet (Brunetti et al., 2014). There are no direct studies investigating the requirement for PANK2 in cellular fatty acid homeostasis including fatty acid oxidation. In this study, we report the effect of palmitic acid supplementation on cells lacking PANK2.

Results

Palmitic acid supplementation is toxic for PANK2, but not PANK1 knockdown cells.

Studies on PANK1 and PANK2 suggest that both could have a role in fatty acid homeostasis. PANK1 KO mice do not increase liver CoASH levels in response to fasting and display reduced liver fatty acid oxidation (Leonardi et al., 2010). On the other hand,

22

palmitoylcarnitine activate PANK2 and PANK2 KO mice fed a high fat diet develop a movement disorder (Brunetti et al., 2014; Roberta Leonardi et al., 2007). Human embryonic kidney cells (HEK293T), are an easy cell model to manipulate that is non-cancerous with higher RNA expression of PANK2 then PANK1 (Dansie et al., 2014). To investigate the role of PANK1 and PANK2 in the cellular response to long chain fatty acids we exposed HEK293T cells treated with scrambled control (SR), PANK1 siRNA (siPANK1), or PANK2 siRNA (siPANK2) to 250µM palmitic acid-conjugated BSA (PAL) or BSA vehicle control (BSA) for 24 hours in complete growth media.

The siRNA treatment successfully reduced PANK1 or PANK2 expression, respectively (Appendix A, SFig 5.1A-C) without general toxicity in the BSA control conditions (Fig 2.1). During the 24-hour PAL treatment, there was a significant decrease in cell confluence for the siPANK2, but not for siPANK1 cells (Fig 2.1A). Based on a trypan blue cell-counting assay PAL-challenged siPANK2 cells had reduced viability and total number of live siPANK2, but not siPANK1 cells (Fig 2.1B-C). The siPANK2, but not siPANK1 cells, accumulated fatty acids in the PAL-condition (Fig 2.1D). Based on these findings we concluded that PANK2, but not PANK1, is required to support cellular palmitic acid handling in HEK293T cells.
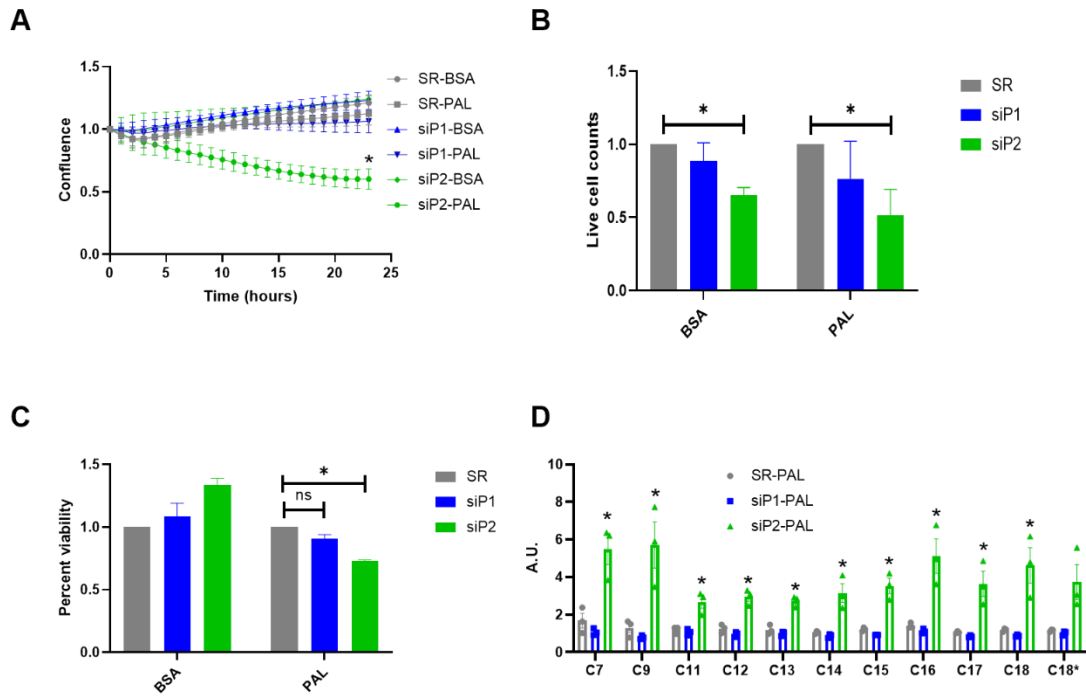
Figure 2.1. Effects of 24-hour BSA or PAL supplementation. Evaluating the effects of 24-hour BSA or PAL supplementation on PANK1 or PANK2 KD added to complete media to scrambled (SR) (n=3), PANK1 (siP1) (n=3), or PANK2 (siP2) (n=3) knockdown in HEK293T assessed via: A) a change in cell confluence for each condition normalized to its own starting point. Statistical significance determined via two-tailed unpaired t-test. B-C) Number of live cells and percent viable cells normalized to SR BSA or SR PAL and expressed as fold change. Statistical significance determined by two-way ANOVA with Tukey's multiple comparisons test. D) Cellular saturated fatty acid profile (except C18* linoleic acid, polyunsaturated) fold change expressed in arbitrary units (A.U) statistical significance determined via multiple t-test corrected for multiple comparison with Holm-Sidak. Data for the BSA condition not shown (no significant change). The * indicates statistically significant at $P < 0.05$ for all conditions error bars are SD for A and SEM for B-C.

PAL activate energy compensatory mechanisms in siPANK2 cells.

Next, we sought to understand why the PAL-challenge caused increased cell death in cells lacking PANK2. When both palmitic acid and glucose is provided in the media, fatty acids are preferentially oxidized over glucose in accordance with the Randle cycle (Hue & Taegtmeyer, 2009; Randle et al., 1963) (Fig 2.2). A cellular influx of fatty

24

acids would activate a fatty acid oxidation program, including increasing the mRNA and

protein expression of carnitine palmitoyltransferase 1 (CPT1) and pyruvate

dehydrogenase kinase 4 (PDK4) (McDonnell et al., 2016; Pettersen et al., 2019). CPT1 is

the rate-limiting step in long chain fatty acid oxidation and PDK4 inhibit pyruvate

dehydrogenase (PDH) to spare pyruvate oxidation in favor of fatty acid oxidation (Hue &

Taegtmeyer, 2009). The siPANK2 cells upregulated *CPT1* and *PDK4* mRNA expression

in the PAL condition, but failed to increase CPT1 and PDK4 protein content (Fig 2.3A-

F). Low CPT1 could cause impaired transport of fatty acids into the mitochondria for β-

oxidation and low PDK4 indicate that pyruvate oxidation is still active, possibly as a

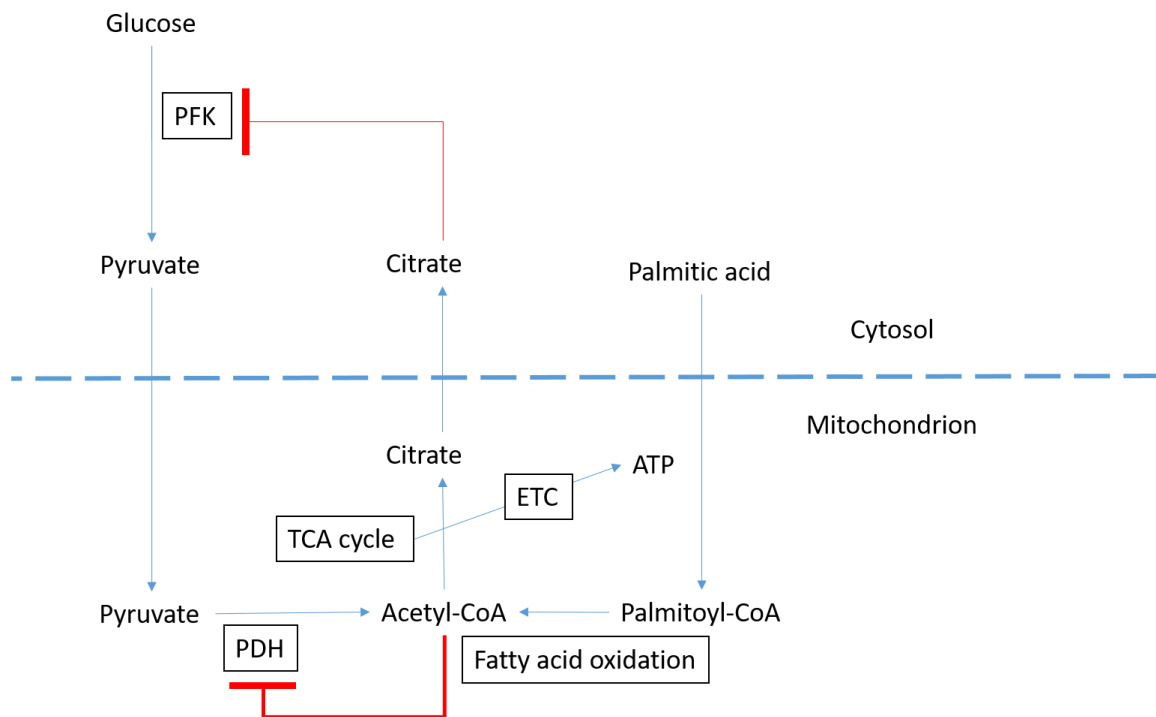compensation for impaired energy generation from palmitic acid.

Figure 2.2. Diagram of the Randle effect. The Randle effect explains how the cell favor fatty acid oxidation while sparing glucose and pyruvate oxidation. Abbreviations: PDH, pyruvate dehydrogenase; TCA cycle, tricarboxylic acid cycle; ETC, electron transport chain, PFK, phosphofructokinase-1.
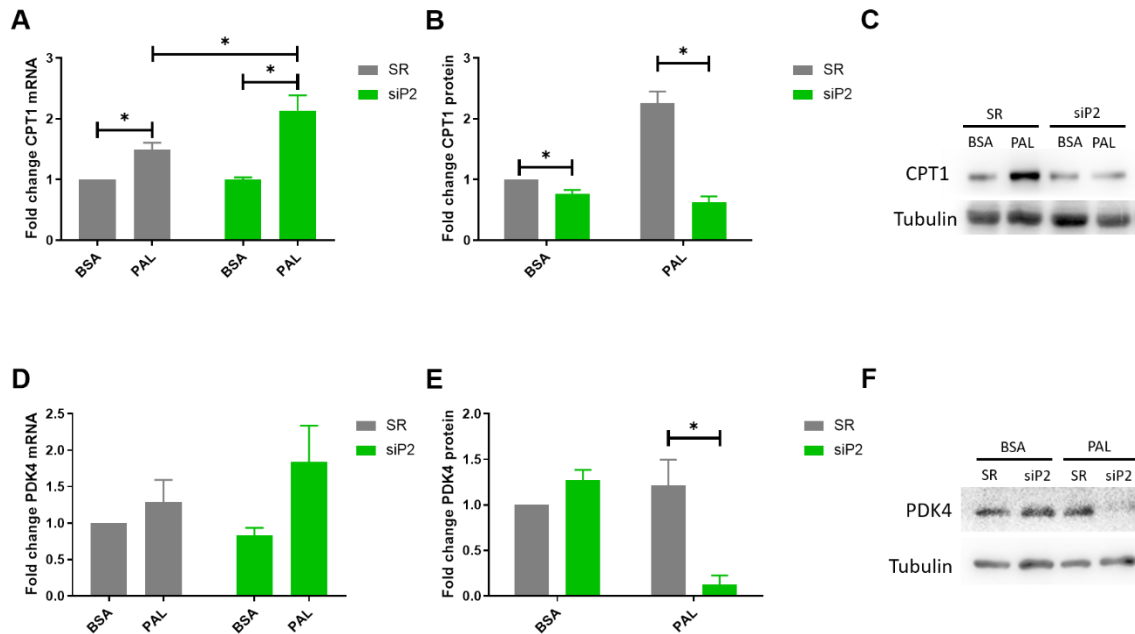
Figure 2.3. PANK2 KD cells fail to increase CPT1 and PDK4 protein expression. A) Quantification of *CPT1* mRNA expression (n=3). B) Quantification of CPT1 protein expression (n>10) normalized to tubulin. C) Representative western blot of CPT1 and tubulin loading control. D) Quantification of *PDK4* mRNA expression (n=3). B) Quantification of PDK4 protein expression (n=3) normalized to tubulin. C) Representative western blot of PDK4 and tubulin loading control. All data expressed as fold-change from SR BSA. The * indicates statistically significant at P < 0.05 determined with two-way ANOVA with Tukey's multiple comparisons test. All error bars are SEM.

AMP activated protein kinase (AMPK) is a cellular energy sensor, active when phosphorylated at Thr-172 because of low ATP and high AMP (Hue & Taegtmeyer, 2009). AMPK activation can override the PAL induced Randle cycle block of glucose oxidation, allowing for the simultaneous oxidation of both carbon sources for ATP generation (Hue & Taegtmeyer, 2009). In siPANK2 cells, ATP was decreased (p=0.04) and AMPK phosphorylation was increased 15-fold (p=0.014) in the PAL condition signaling energy impairment in siPANK2 PAL-challenged cells (Fig 2.4A-B, F).

In addition to allowing multiple catabolic pathways for energy generation, AMPK activates autophagy by inhibiting mTORC1 and activating ULK1 (Herzig & Shaw,

2018). To evaluate the extent of energy distress and compensation occurring in siPANK2 PAL-challenged cells, we decided to measure autophagy in the siPANK2 cells. One type of autophagic flux measurement track the conversion of LC3I to LC3II in the absence and presence of the lysosome inhibitor chloroquine. Chloroquine prevents degradation of autophagic cargo by changing the lysosomal pH (Redmann et al., 2017). The LC3II to LC3I ratio during chloroquine treatment was significantly increased 10-fold ($p<0.0001$) in the PAL condition in siPANK2 cells (Fig 2.4C, F).

Chloroquine also blocks the degradation of the adaptor protein p62, which bring ubiquitinated cargo for autophagy degradation. Hence increased p62 accumulation is also a common measurement of autophagy (Bjørkøy et al., 2009). The phosphorylation of p62 at Ser-349 occur in response to both oxidative and proteomic inhibition (Tanji et al., 2014). P62 accumulated in siPANK2 cells in the PAL condition ($p<0.0001$) (Fig 2.4D, F). Phosphorylation at Ser-349 was significantly increased ($p=0.007$) in the PAL condition (Fig 2.4E-F). In a high nutrient media, containing both palmitic acid and glucose, the siPANK2 cells activate AMPK and autophagy. In order to understand why

the PANK2-deficient cells fail to thrive in the PAL condition we decided to assess
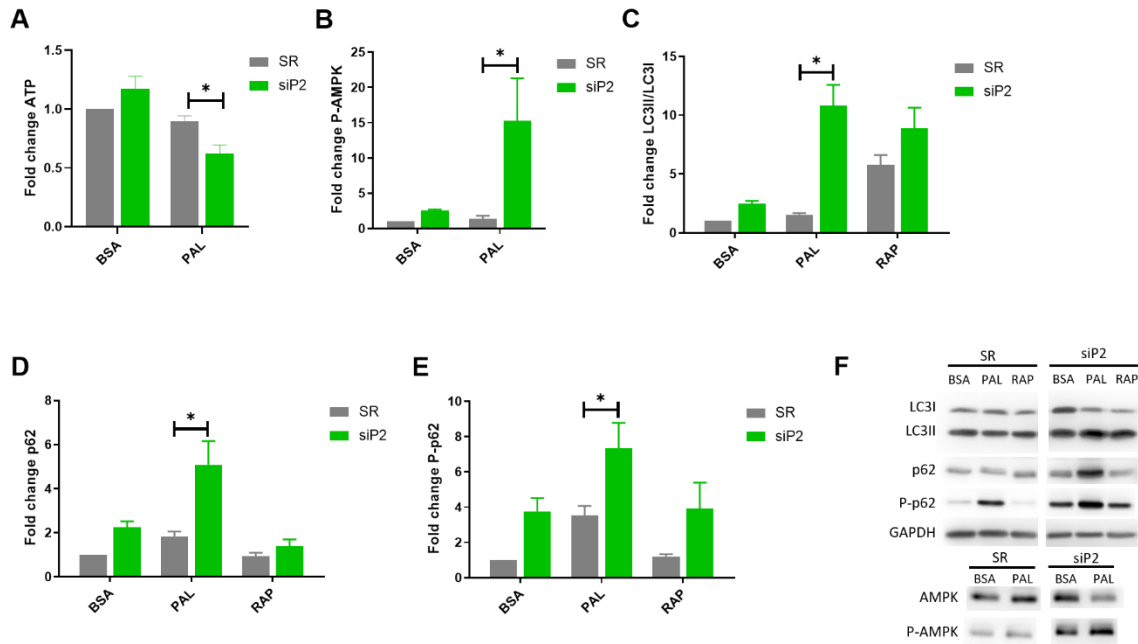
mitochondrial respiration and β-oxidation.

Figure 2.4. PAL-challenge cause decreased ATP and upregulation of compensatory homeostatic processes in PANK2 KD cells. A) ATP levels determined via luminescence assay (n=3). B) Quantification of Thr-172 phosphorylated-AMPK normalized to cellular AMPK levels (n=3). C) Quantification of LC3II/LC3I ratio during chloroquine inhibition with rapamycin as a positive control (n=15). D) Quantification of p62 levels normalized to GAPDH (n=15) E) Quantification of Ser-349 phosphorylated-p62 normalized to p62 levels (n=8). F) Representative western blots for LC3I, LC3II, p62, p-p62, GAPDH, AMPK, and p-AMPK. The * indicates statistically significant at P < 0.05 determined with two-way ANOVA with Tukey's multiple comparisons test. All error bars are SEM.

PANK2 is required for fatty acid oxidation.

To examine the respiratory capabilities of PANK2-deficient cells, we transitioned

to two models of permanent PANK2 loss: HEK293T CRISPR-Cas9 edited PANK2

knockout (PANK2 KO) cells and fibroblasts from three individuals affected with PKAN,

one individual with compound heterozygote mutations (p. R286C) (PKAN1) and two

individuals with early stop codon (p. Y190*) (PKAN2 and PKAN3).

The Seahorse XF96/XF24 Analyzers (Agilent) measure oxygen consumption rate (OCR) and assess mitochondrial respiration and substrate oxidation. First, we measured OCR in HEK293T and PANK2 KO cells with the mitochondria stress test assay using glucose as a substrate and the XF96 analyzer (Agilent). As shown in the combined OCR traces of three different experimental runs and the derived respiratory parameters, PANK2 KO cells had a mild impairment of maximal respiration, coupled respiration, and spare respiratory capacity (Fig 2.5A-B).

Next, we performed the mitochondrial stress test assay on the PKAN derived fibroblasts. The stress test for PKAN1 was analyzed on the XF96 analyzer, while the stress test for PKAN2 and PKAN3 was analyzed on the XF24 analyzer. The data collected on the XF24 Seahorse analyzer was done in collaboration with Dr. Carlos Santos Ocaña's lab. The stress test revealed mild mitochondria respiratory impairment including decreased maximal respiration, coupled respiration and spare respiratory capacity in PKAN2 and PKAN3. Discernable impairment was absent from PKAN1, which behaved as the combined results of the two healthy fibroblast controls (Fig 2.5C-F).

The mitochondrial stress test experiments show that PANK2-deficient cells are generally capable of oxidizing glucose. In light of the reduced viability, activated AMPK and autophagy, which PAL induce in the PANK2 KD cells, we next wanted to investigate fatty acid oxidation in PANK2-deficient cells. One method to measure palmitoylcarnitine substrate utilization with the Seahorse Analyzer is to first inject digitonin to permeabilize the cell membrane followed by a subsequent injection of palmitoylcarnitine. Palmitoylcarnitine will efficiently reach the mitochondria in the permeabilized cells to

29

fuel the mitochondria. In the PKAN affected cells tested, PKAN2 and PKAN3, we saw

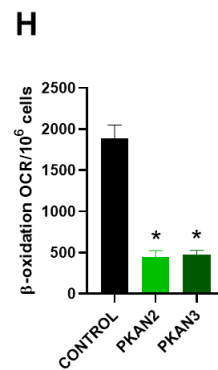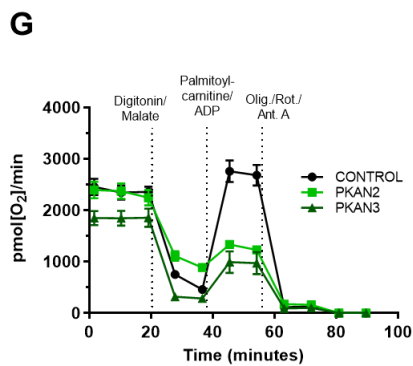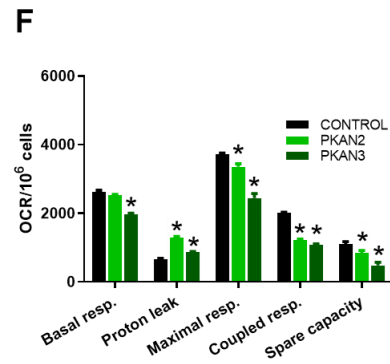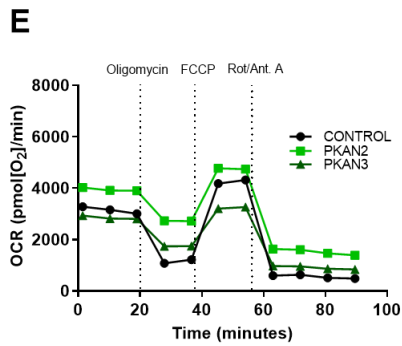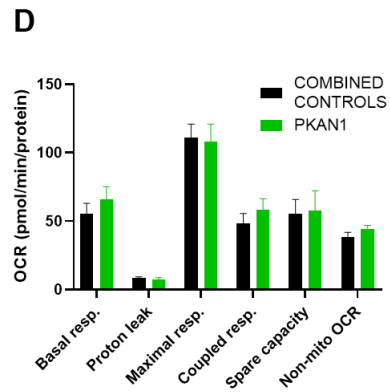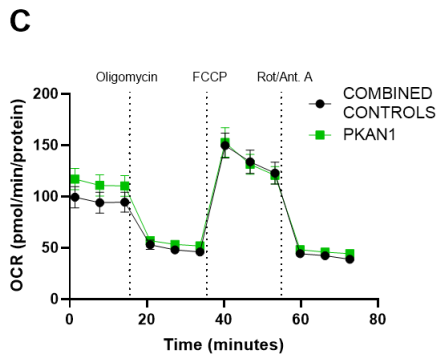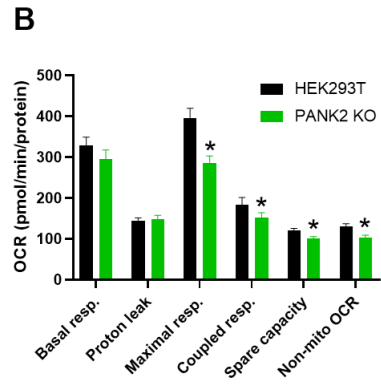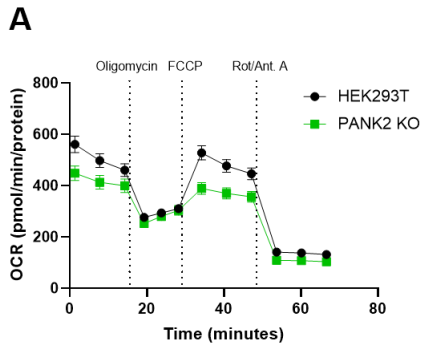severe β-oxidation impairment ($p < 0.0001$) (Fig 2.5G-H).

Figure 2.5. Assessment of mitochondrial respiration and β-oxidation in PANK2-deficient cells. Mitochondria respiration combined OCR traces and derived respiratory parameters for: A-B) WT HEK293T and PANK2 KO (n=3 with 5-10 replicates for each run) measured with XF96 and normalized to protein measured with the BCA assay. C-D) Combined data for two healthy controls (GMO8399 and GMO8398) and PKAN1 (n=3 with 3 replicates for each run) normalized to protein measured with the BCA assay. E-F) health fibroblast control (HDFneo) (n=6), PKAN2 (n=7), and PKAN3 (n=7) (p. Y190*) measured with XF24 analyzer and normalized to cell counts. G-H) β-oxidation OCR trace (n=4) and derived measurement for β-oxidation for control (n=6), PKAN1 (n=10), PKAN2 (n=10), measured with XF24 analyzer and normalized to cell counts. The * indicates statistically significant at $P < 0.05$ determined via two-tailed unpaired t-test. All error bars are SEM. Data generated in collaboration with Dr. Carlos Santos Ocaña's lab.

Whole-cell CoASH is unaffected in PANK2-deficient cells.

PANK2 can catalyze the first step in CoASH biosynthesis and fatty acid oxidation require CoASH (Kotzbauer et al., 2005). Considering the fatty acid oxidation impairment in PANK2-deficient cells and the reduced viability, fatty acid accumulation, and autophagy in siPANK2 cells, we wanted to understand if CoASH deficiency was the cause. Whole-cell CoASH and acetyl-CoA levels were unaffected in the PANK2 KO cells and the PKAN cells (Fig 2.6A-B) (Data for PKAN fibroblasts generated in collaboration with Dr. Carlos Santos Ocaña's lab). Similarly, whole-cell CoASH and acetyl-CoA levels were unaffected in the siPANK2 cells in both the BSA and PAL condition (Fig 2.6C-D). One explanation for the unchanged whole-cell CoASH levels could be due to compensation from the other PANKs. PANK1 and PANK3 mRNA expression was significantly increased in the PAL condition in siPANK2 cells (p = 0.0005 and p=0.001 for PANK1 and PANK3 respectively) (Fig 2.6E-F).

Following the reasoning that high CoASH produced by the other PANKs could compensate for the loss of PANK2 we decided to knockdown PANK2 in stably overexpressing PANK1β cells (PIβ O/E). PANK1β cells have more than 10-fold higher CoASH and acetyl-CoA then wild type HEK293T cells (Fig 2.6C-D). When PANK2 was

32

knocked down, CoASH and acetyl-CoA levels remained unaffected in PIβ siPANK2

cells (Fig 2.6C-D). Interestingly, knocking down PANK2 in PIβ cells also caused an

increase in PANK1 and PANK3 mRNA expression (only 2 experiments), which was

significant in the PAL condition (p=0.0005 and p=0.02 for PANK1 and PANK3

respectively) (Fig 2.6E-F). The increased PANK1/PANK3 mRNA expression in

siPANK2 cells is therefore unlikely in response to reduced whole-cell CoASH levels, but

possibly a drop in CoASH levels that our 24-hour period did not detect.
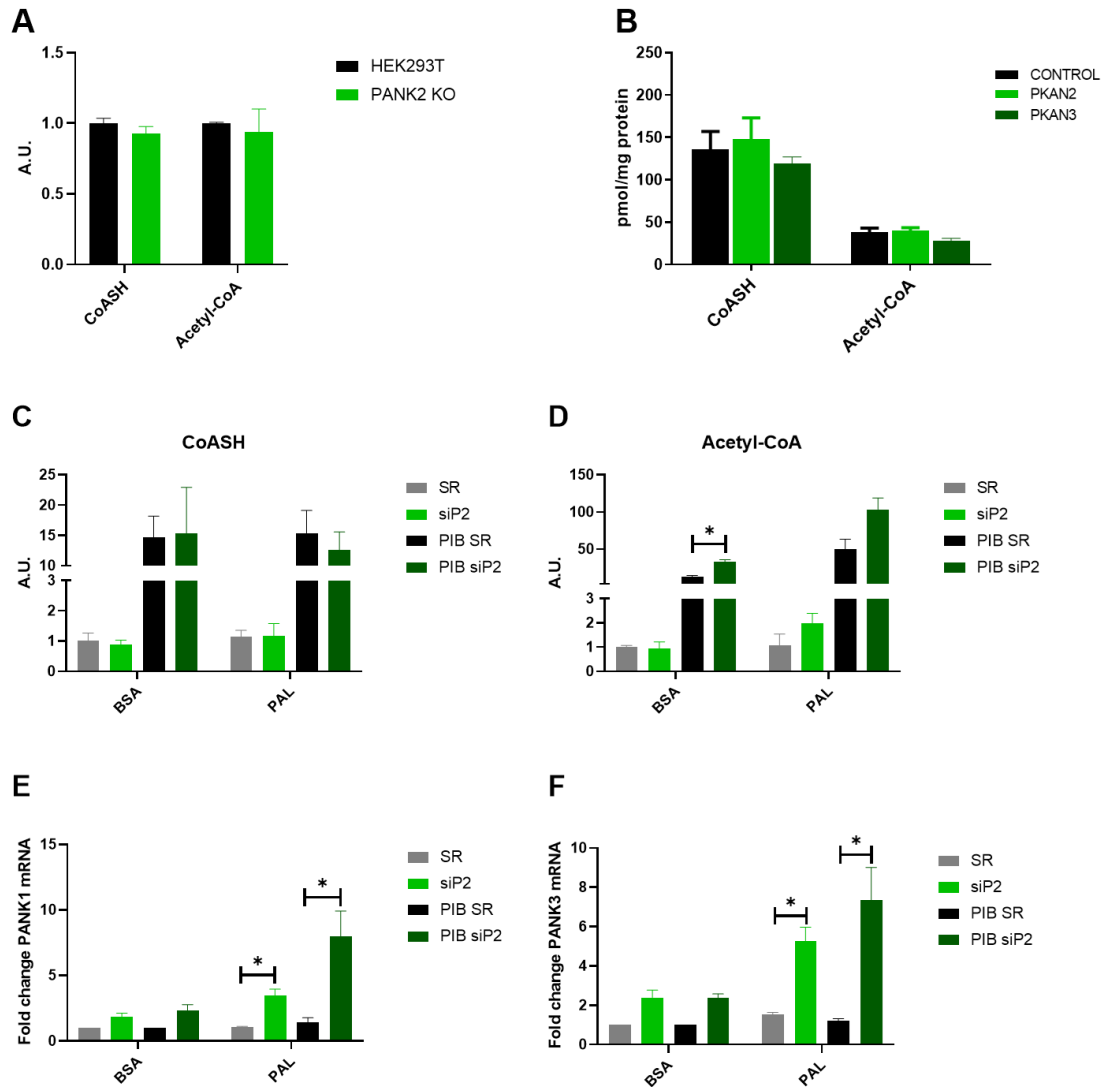
**Figure 2.6. Whole-cell CoASH and acetyl-CoA is unaffected in PANK2-deficient
cells.** A) Whole-cell CoASH and acetyl-CoA levels in WT HEK293T (n=3) and PANK2
KO cells (n=6) expressed as fold-change to SR BSA. B) Whole-cell CoASH and acetyl-
CoA in healthy fibroblast control (HDFneo) (n=4), PKAN2 (n=4), PKAN3 (n=4)
absolute quantification expressed in pmol/mg. C) Whole-cell CoASH and acetyl-CoA
measurements in scrambled (SR) and PANK2 (siP2) knockdown in HEK293T (n=3) and
in scrambled (PIβ SR) and PANK2 (PIβ siP2) knockdown in PANK1β (PIβ)
overexpressing cells (n=3). A, C-D metabolite data are expressed as a fold change from
HEK293T SR in arbitrary units (A.U). E-F) PANK1 and PANK3 mRNA expression in
HEK293T and PANK1β cell lines, in all conditions tested. The mRNA expression for
each cell line is normalized to its own SR BSA and expressed as a fold change, SR and
siP2 (n=3), PIβ and PIβ siP2 (n=2). The * indicates statistically significant at $P < 0.05$
determined via C-D) multiple t-test corrected for multiple comparison with Holm-Sidak

E-F) two-way ANOVA with Tukey's multiple comparisons test. All error bars are SEM. Data for healthy fibroblast control (HDFneo), PKAN2, PKAN3 generated in collaboration with Dr. Carlos Santos Ocaña's lab.

Elevated CoASH from PANK1β does not rescue PAL-induced toxicity, AMPK, and

autophagy activation in PANK2 KD cells.

To test if elevating intracellular CoASH levels via PANK1β rescued the siPANK2 PAL-induced toxicity we performed the same PAL toxicity experiments as in figure 2.1 and the CPT1/PDK4/AMPK/autophagy experiments in figure 2.2-2.3 in PIβ O/E cells. PANK1β overexpression did not rescue the siPANK2 PAL-induced decrease in confluence, viability, and live cells, nor the fatty acid accumulation (Fig 2.7A-D).

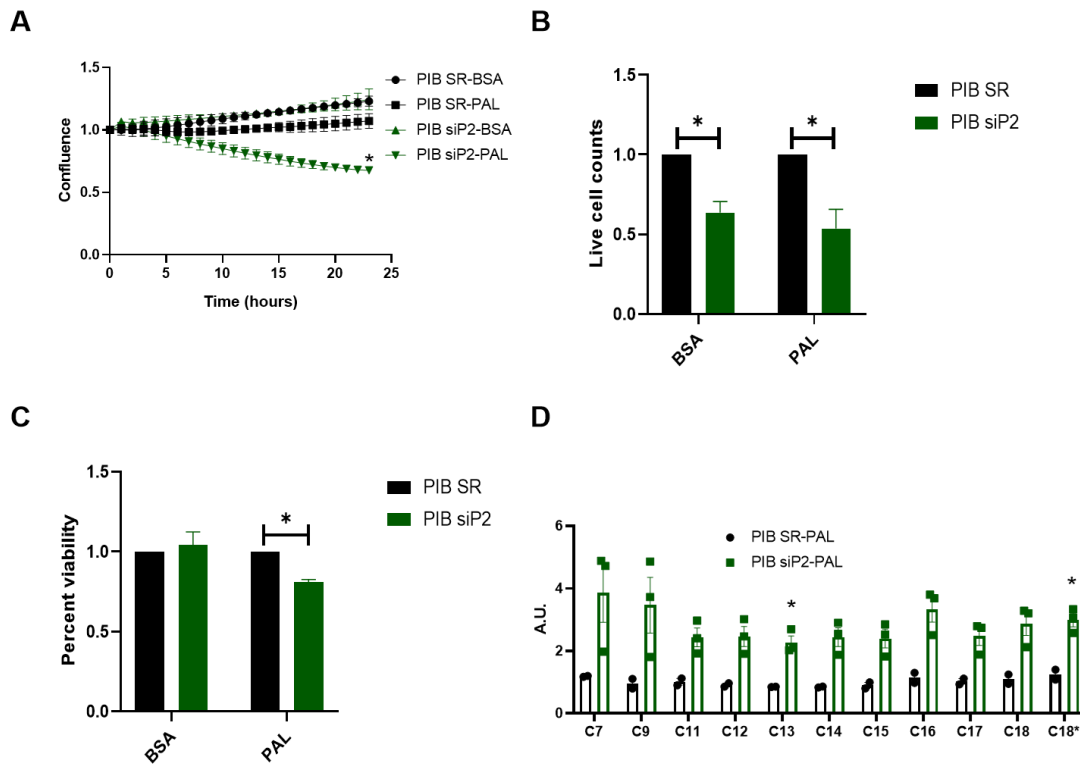**Figure 2.7. Cells overexpressing PANK1β with elevated whole-cell CoASH and acetyl-CoA levels are not able to compensate for PANK2 KD.** Compensation was assessed via: A) change in cell confluence for each condition normalized to its own starting point (n=3, PIβ SR-PAL n=2). B-C) Number of live cells and percent viable cells normalized to PIβ SR BSA control or PIβ SR PAL control (n=3). D) Cellular saturated

35

fatty acid profile (except C18* linoleic acid, polyunsaturated) (PIβ SR-PAL n=2, PIβ siP2-PAL n=3) fold change expressed in arbitrary units (A.U). The * indicates statistically significant at P<0.05 determined by (A-C) two-tailed unpaired t-test, (D) multiple t-test with corrected for multiple comparison with Holm-Sidak. Error bars are SD for (A) and SEM for (B-D).

The siPANK2 PIβ could increase mRNA expression of *CPT1* and *PDK4*, but similar to PANK2 knockdown in WT HEK293T, CPT1 and PDK4 protein expression was significantly lower in the PAL-condition (p<0.0001 for CPT1, p=0.01 for PDK4) (Fig 2.8A-F). High CoASH is linked to PDK4 degradation in mice, but it is counterintuitive to expect that knocking down PANK2 would have the same effect and mechanism on PDK4 (Schafer et al., 2018). We could not rescue CPT1 or PDK4 with the proteasomal inhibitor MG132 or the lysosomal inhibitor bafilomyacin (data not shown), but degradation of PDK4 could be mediated by a mitochondria Lon protease (not tested) (Schafer et al., 2018).
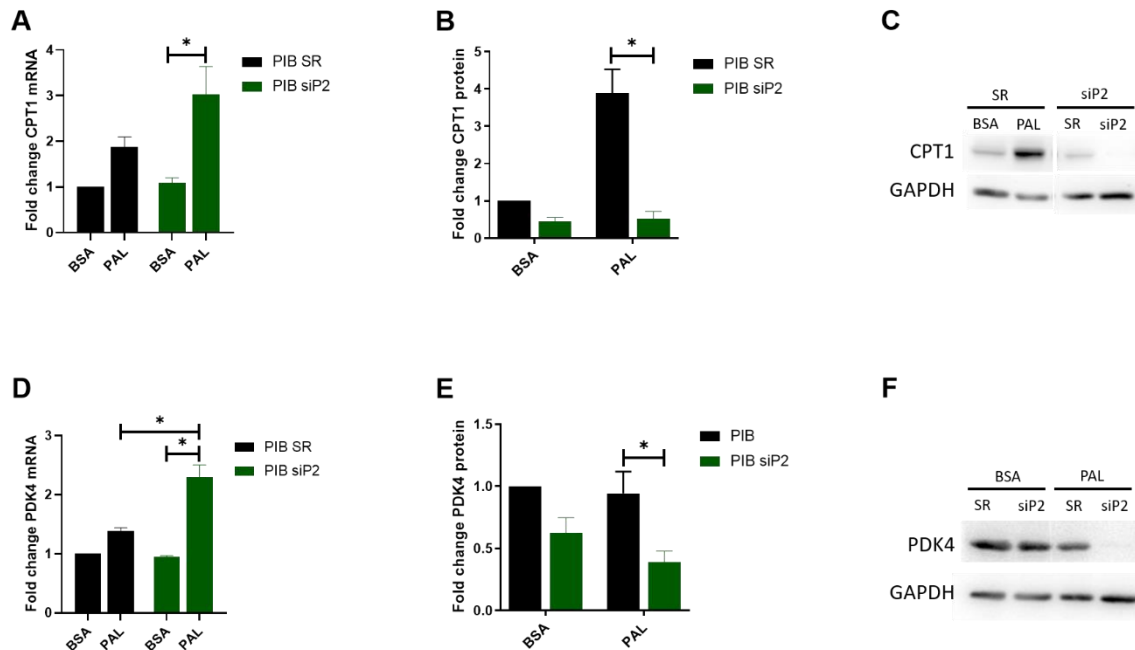

Figure 2.8. PANK1β PANK2 KD cells with high CoASH fail to increase CPT1 and PDK4 protein expression. A) Quantification of *CPT1* mRNA expression (n=2). B)

36

Quantification of CPT1 protein expression (n>10) normalized to GAPDH. C) Representative western blot of CPT1 and GAPDH loading control. D) Quantification of *PDK4* mRNA expression (n=2). E) Quantification of PDK4 protein expression (n=3) normalized to GAPDH. F) Representative western blot of PDK4 and GAPDH loading control. All data expressed as fold-change from SR BSA. The * indicates statistically significant at $P < 0.05$ determined with two-way ANOVA with Tukey's multiple comparisons test. All error bars are SEM.

AMPK phosphorylation was elevated, but not significantly in PIβ siPANK2 (Fig 2.9A, E). Knocking down PANK2 in PANK1β cells increased autophagic flux in the PAL condition. The PAL-challenge significantly increased the LC3II/LC3I ratio ($p < 0.0001$), caused p62 accumulation (0.012), and increased phosphorylated p62 (p=0.0005) (Fig 2.9B-E). Interestingly, the increased acetyl-CoA levels in the PIβ cells, a potent inhibitor of autophagy under physiological conditions, did not prevent autophagy during PANK2 knockdown, indicating cellular activation of autophagy likely represents an attempted compensation rather than a pathological response with loss of PANK2. These experiments demonstrate that high CoASH and acetyl-CoA levels supplied by PANK1β could not rescue the loss of PANK2 during palmitic acid supplementation.
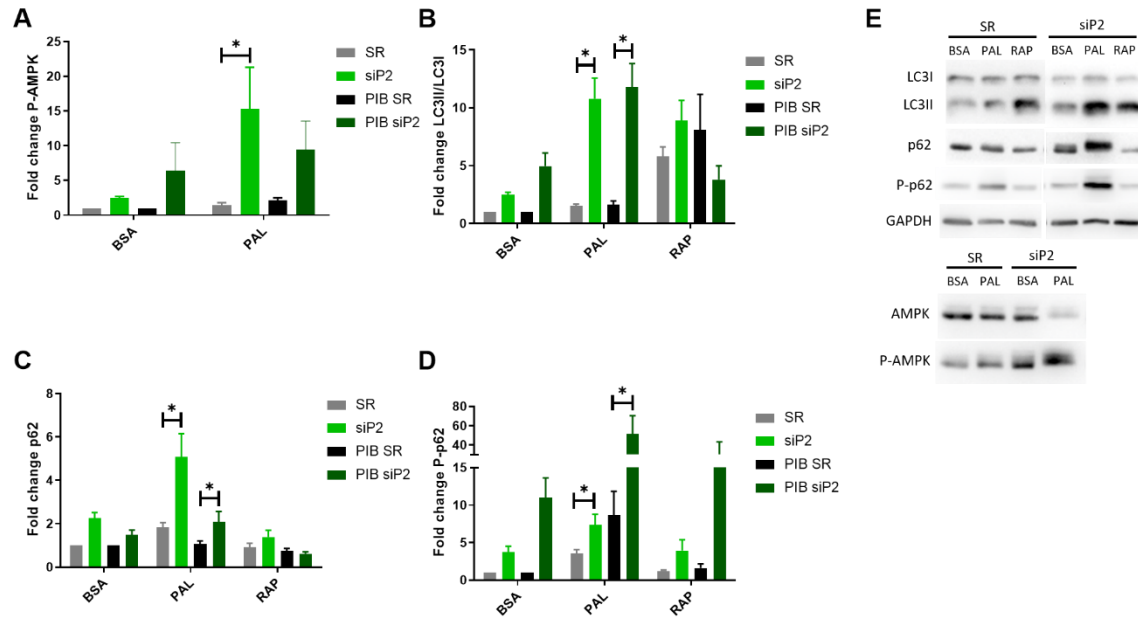
Figure 2.9. PANK1β elevated intracellular CoASH cannot rescue PANK2 KD PAL-induced energy impairment. Data for siPANK2 in WT HEK293T included for comparison refer to figure 2.3 for description of data. A) Quantification of Thr-172 phosphorylated-AMPK normalized to cellular AMPK levels (n=8). B) Quantification of LC3II/LC3I ratio during chloroquine inhibition with rapamycin as a positive control (n=10). C) Quantification of p62 levels normalized to GAPDH (n=10) D) Quantification of Ser-349 phosphorylated-p62 normalized to p62 levels (n=8). E) Representative western blots for LC3I, LC3II, p62, p-p62, GAPDH, AMPK, and p-AMPK. The * indicates statistically significant at $P<0.05$ determined with two-way ANOVA with Tukey's multiple comparisons test. All error bars are SEM.

Discussion

This study show a novel function of PANK2 in supporting cellular fatty acid usage that the other PANKs cannot compensate for. In the mouse model of PKAN, PANK2 loss does not cause a severe phenotype until challenged with a ketogenic, high fat diet (Brunetti et al., 2014). We similarly observe only mild phenotypes in PANK2-deficient cells, possibly because the other PANKs can compensate for each other to some extent. However, palmitic acid supplementation induce severe toxicity including cell

death and fatty acid accumulation in PANK2-deficient cells, but not in the PANK1 knockdown model.

We also show that PANK2-deficient cells have an impaired ability to respite on palmitoylcarnitine. CPT1 regulates a rate-limiting step in fatty acid oxidation, the entry of long chain fatty acids into the mitochondria. PANK2 cells were not able to increase CPT1 levels in response to palmitic acid. Diminished fatty acid oxidation may cause fatty acid overloaded mitochondria and perhaps maintaining low CPT1 levels is a protective mechanism in response to reduced fatty acid oxidation. Inability to utilize fatty acids combined with the Randle cycle's effect of blocking glucose oxidation could explain the need for the cell to activate AMPK and maintaining low PDK4 levels. PDK4 inhibits PDH activity, as such maintaining low PDK4 would allow for pyruvate oxidation. AMPK activation would override any glucose blockage and upregulate autophagy as a compensatory mechanism for reduced ATP production.

Next, we wanted to understand if the palmitic acid induced phenotype was due to low cellular CoASH. This we reasoned would be evident in low cellular CoASH or in the rescue by increasing intracellular CoASH. There was not a whole-cell CoASH deficiency in cells lacking PANK2 with or without palmitic acid supplementation. This is in agreement with what other studies have found (Lambrechts et al., 2019; Mignani et al., 2021).

Cells overexpressing PANK1β have a 10-fold increase in intracellular CoASH compared to WT HEK293Ts. Interestingly, knocking down PANK2 in PANK1β cells followed by the same palmitic acid challenge reproduces the impaired fatty acid utilization phenotype observed in PANK2 HEK293T knockdown cells. This demonstrate

39

that more intracellular CoASH do not compensate for the loss of PANK2 during palmitic acid supplementation. Seemingly, CoASH produced by PANK2 is different from CoASH produced by PANK1β unless PANK2s role in fatty acid metabolism is separate from its role in CoASH synthesis. There is no published work describing an alternate function of PANK2.

PANK1β is a cytosolic protein, while PANK2 localize to the mitochondria, cytosol, and the nucleus (Alfonso-Pecchio et al., 2012; Hortnagel, 2003). We propose that the palmitic acid induced phenotype observed in cells lacking PANK2 is because PANK2 control mitochondria CoASH. One study report a specific mitochondria deficiency in fibroblast from individuals affected with PKAN (Álvarez-Córdoba et al., 2019). Follow up studies should include mitochondria CoASH measurements during palmitic acid treatment, including if PANK1β overexpression can elevate mitochondria CoASH via SLC25A42 CoASH transport. Understanding how CoASH distribution depend on the different PANKs will be important in developing effective treatments for PKAN and other CoASH-related disorders.

Methods

Cell culture.

All cell lines were maintained in complete growth media containing DMEM (Life Technologies) supplemented with 10% FBS and 1mM GlutaMAX (Gibco) and 1mM

sodium pyruvate (Sigma) at 37°C under 5% carbon dioxide with a humidified atmosphere.

siRNA knockdown.

Cells were seeded at $0.3x10^6$ in 6-wells the day before transfection. Two transfections were performed on sequential days in fresh Opti-MEM (Gibco) supplemented with 6.5% FBS. Transfections followed the Lipofectamine RNAiMAX (ThermoFisher) protocol with control scramble siRNA (Origene, SR30004), or human siRNA oligo duplex against either PANK2 (Origene, SR325087) or PANK1 (Origene, SR309983). On the fourth day, cells were provided with fresh complete growth media supplemented with either vehicle BSA or palmitic acid conjugated to BSA at a 250µM final concentration. Cells were harvested after the 24-hour palmitic acid-bsa exposure.

Autophagic flux measurements.

Autophagy was assessed by tracking the conversion of LC3I to LC3II, p62, and phospho-p62 with and without the lysosomal inhibitor chloroquine (CQ) (Sigma) at 100nM final concentration for 4-hours. Rapamyacin was used at 200nM to induce autophagy.

RIPA buffer protein extraction and western blotting.

Cellular proteins were extracted with RIPA buffer (Thermo Fisher) supplemented with protease cocktail (Thermo Fisher) and phosphaptase inhibitor cocktail (Sigma) on ice, centrifuged at 13,000g and supernatant collected. Protein concentration were measured with the BCA assay and an equal amount of protein separated on SDS-page and transferred to nitrocellulose membrane 0.2µm (BIO-RAD). Membranes were blocked with 5% BSA. The membranes were incubated with antibodies against anti-LC3B

41

(Abcam; ab51520), anti-AMPK (Cell signaling; 2532), anti-phospho-AMPK (Cell signaling; 2531), anti-p62 (Abcam; ab109012), anti-phosphop-p62 (Abcam; ab211324), anti-CPT1A (Abcam; ab128568), anti-PANK2 (Origene; TA501419), anti-PANK1 (Abcam; ab96173), anti-tubulin (Abcam; ab4074), and anti-gapdh (Abcam; ab9485). Detected with anti-rabbit or anti-mouse HRP (GE Health Sciences) 1:5,000.

Confluence measurements and trypan blue counts.

Growth of siRNA treated cells with vehicle BSA or palmitic-bsa were monitored with the Incucyte S3 (Sartorius) at 10X and analyzed with the confluence setting for the 24-hour treatment. Percent live cells and cell numbers were trypan blue stained and counted with Countess II FL cell counter (Life technologies).

q-PCR measurements.

RNA was extracted using a Direct-zol RNA MiniPrep kit (Zymo Research) according to the manufacturer's instructions, with DNase I (Zymo Research) treatment. Reverse transcription was done with iScript™ Reverse Transcription Supermix for RT-qPCR (BIO-RAD) following manufacturers protocol. The qPCR was performed with SsoAdvanced Universal SYBR Green Supermix (BIO-RAD) following manufacturer's protocol. Primers for GAPDH (IDT; Hs.PT.39a.22214836), CPT1 (IDT; Hs.PT.58.2799026), PDK4 (IDT; Hs.PT.58.28212793), PANK1 (IDT; Hs.PT.58.2284965), PANK3 (IDT; Hs.PT.58.2201075).

ATP quantification.

ATP from 10^6 cells was quantified via luminescence using an ATP quantification kit (Abcam; ab113849).

Oxygen consumption measurements with 96XFe analyzer.

Oxygen consumption rate (OCR) was measured with the Seahorse extracellular flux 96XFe analyzer (Agilent). Cells were seeded at 50,000 cells/well on a matrigel coated 96-well cell culture microplate (Agilent) 24-hours before measurement. An hour before OCR measurements the media was replaced with serum free DMEM supplemented with 1mM pyruvate, 1mM glutamine and 4mM glucose and incubated at 37C° without CO2. Baseline OCR was measured before injecting inhibitory compounds and then followed by OCR measurements after the sequential addition of oligomycin (1μM), FCCP (1.5 μM), and antimycin (1μM)/rotenone (1μM) respectively. The OCR measurements were normalized to the amount of protein as measured by the BCA protein assay.

Oxygen consumption measurements with 24XFe analyzer.

Oxygen consumption rate (OCR) was measured with the Seahorse extracellular flux 24XFe analyzer (Agilent). Cells were seeded at 50,000 cells/well on 24-well culture plates (Agilent) 24-hours prior to measurements. An hour before measurements the media was replaced with seahorse XF media supplemented with 1mM glucose, 1mM glutamine, and 1mM sodium pyruvate incubated at 37 without CO2. Baseline OCR was measured before injecting inhibitory compounds and then followed by OCR measurements after the sequential addition of oligomycin (1μM), FCCP (2μM), and antimycin (2.5μM)/rotenone (1μM) respectively. The OCR measurements were normalized to cell numbers counted with the Scepter™ 2.0 cell counter.

Palmitoylcarnitine oxygen consumption measurements.

Cellular respiration of palmitoylcarnitine was measured with the Seahorse extracellular flux 24XFe analyzer (Agilent). Cells were seeded at 50,000 cells/well on 24-

well culture plates (Agilent) 24-hours prior to measurements. An hour before measurements the media was replaced with a mitochondrial assay solution (MAS) containing HEPES, $MgCl_2$, KH_2PO_4, mannitol, sucrose and EGTA (pH 7.2) and BSA was added fresh the same day. The first injection contained digitonin (5µg/ul) and malate (250mM). Next, injection contained the palmitoylcarnitine (50µM) and ADP (1mM). Finally, antimyacin A (2.5µM) and rotenone (1µM) was injected to inhibit mitochondrial respiration. The OCR measurements were normalized to cell numbers counted with the Scepter™ 2.0 cell counter.

CoASH and acetyl-CoA HPLC measurements of fibroblasts.

Healthy control fibroblasts and fibroblasts from individuals affected with PKAN were washed with PBS and pelleted. Cell pellets were thawed metabolites extracted with 100mM KH_2PO_4 and 10 volumes of methanol. The extracts were centrifuged for 5 minutes at 17,000g and dried in the SpeedVac™ (Thermo Fisher). The pellets were resuspended in 200 µL of 100 mM KH_2PO_4 and filtered using 0.22 µm nylon filters. CoA and acetyl-CoA were quantified in the sample by HPLC with an Ultrabase C-18 column with dimensions of 100 x 4 mm and a particle size of 2.5 µm. The column was thermostated at 30ºC and was coupled to an ultraviolet detector (Transgenomic) that detected a wavelength of 260 nm. The mobile phase was composed of two phases: (A) 100 mM KH_2PO_4 and (B) HPLC-grade methanol. A linear gradient from 100% to 80% of mobile phase A was used from 5 to 30 minutes. The constant flow was 0.7 mL/min and the run time was 40 minutes. As external standard, the same analyte was used to determine the retention time. The areas of the peaks corresponding to CoA and acetyl-

CoA were quantified and the nmol or pmol of CoA and acetyl-CoA was determined and normalized to protein measured with the Bradford method.

CoASH, Acetyl-CoA, and fatty acid measurements for PANK2 KO and PANK2 KD.

Cells were grown in 6-wells, confluence tracked with the Incucyte for normalization for 24-hours, washed with ice cold PBS followed by H_2O. The plates were snap frozen in liquid nitrogen. GC-MS and LC-MS measurements performed by the University of Iowa's metabolomics core. Cell culture plates were lyophilized overnight and then scraped into 1 ml of ice-cold 2:2:1 methanol:acetonitrile:water containing a mixture of internal standards (D4-citric acid, D4-succinic acid, D8-valine, and U13C-labeled glutamine, glutamic acid, lysine, methionine, serine, and tryptophan; Cambridge Isotope Laboratories) to extract metabolites. The cell extraction mixtures were transferred to a microcentrifuge tube and flash frozen in liquid nitrogen. Frozen extracts were thawed for 10 minutes in a water bath sonicator and then incubated for 1 hour at –20°C. Metabolite extracts were centrifuged for 10 minutes at 21,000 x g and supernatants were transferred to autosampler vials (GC) or microcentrifuge tubes (LC) and dried using a SpeedVac vacuum concentrator (Thermo).

GC-derivatization. Dried metabolite extracts were derivatized using methoxyamine hydrochloride (MOX) and N,O-Bis(trimethylsilyl)trifluoroacetamide (TMS). Briefly, dried extracts were reconstituted in 30 μl of 11.4 mg/ml MOX in anhydrous pyridine, vortexed for 5 minutes, and heated for 1 hour at 60°C. Next, 20 μl of TMS was added to each sample, samples were vortexed for 1 minute, and heated for 30 minutes at 60°C.

GC-MS method for fatty acid quantification. Derivatized samples were analyzed using GC-MS. GC was conducted using a Trace 1300 GC (Thermo) fitted with a TraceGold TG-5SilMS column (Thermo). 1 µl of derivatized sample was injected into the GC operating under the following conditions: split ratio = 20-1, split flow = 24 µl/minute, purge flow = 5 ml/minute, carrier mode = Constant Flow, and carrier flow rate = 1.2 ml/minute. The GC oven temperature gradient was as follows: 80°C for 3 minutes, increasing at a rate of 20°C/minute to 280°C, and holding at a temperature at 280°C for 8 minutes. Ion detection was performed by an ISQ 7000 mass spectrometer (Thermo) operated from 3.90 to 21.00 minutes in EI mode (-70eV) using select ion monitoring (SIM).

LC-sample preparation CoASH and acetyl-CoA measurements. Dried metabolite extracts were reconstituted in a 1/10th volume of 1:1 acetonitrile:water and vortexed for 10 minutes (200 µl of metabolite extract was resuspended in 20 µl). Reconstituted extracts were maintained at -20°C overnight and centrifuged at 21,000 x g for 10 minutes. Supernatants were transferred to autosampler vials for LC-MS analysis. LC-MS method. 2 µL of the prepared samples were separated using a Millipore SeQuant ZIC-pHILIC (2.1 X 150 mm, 5 µm particle size) column with a ZIC-pHILIC guard column (20 x 2.1 mm) attached to a Thermo Vanquish Flex UHPLC. Mobile phase was comprised of Buffer A [20 mM $(NH_4)_2CO_3$, 0.1% NH_4OH (v/v)] and Buffer B [acetonitrile]. The chromatographic gradient was run at a flow rate of 0.150 mL/min as follows: 0–21 min-linear gradient from 80 to 20% Buffer B; 20-20.5 min-linear gradient from 20 to 80% Buffer B; and 20.5–28 min-hold at 80% Buffer B. Data was acquired using a Thermo Q Exactive MS operated in polarity-switching fullscan mode from 70-

1000 m/z with a spray voltage set to 3.0 kV, the heated capillary held at 275°C, and the HESI probe held at 350°C. The sheath gas flow was set to 40 units, the auxiliary gas flow was set to 15 units, and the sweep gas flow was set to 1 unit. MS data resolution was set at 70,000, the AGC target at 10e6, and the maximum injection time at 200 ms.

Data analysis. Raw data were analyzed using TraceFinder 4.1 (Thermo). For GC-MS data, metabolite identification and annotation required at least two ions (target + confirming) and a unique retention time per metabolite that corresponded to the ions and retention times of reference standards previously determined in-house. For LC-MS data, metabolite identification and annotation required ion accurate mass ± 5 mmu and retention time per metabolite to correspond to the ions and retentions times of reference standards previously determined in-house. A pooled-sample generated from metabolite extracts was analyzed before, at a set interval, and after the analytical run to correct peak intensities using the NOREVA tool (Li et al., 2017).

CHAPTER 3

CELLULAR METABOLIC PROFILING HIGHLIGHT COASH COMPENSATION

AND IMBALANCED METABOLITES IN PANK2-DEFICIENT CELLS.

Abstract

Pantothenate kinase 2 (PANK2) catalyze the first step in free coenzyme A

(CoASH) synthesis. Defective PANK2 cause pantothenate kinase associated

neurodegeneration (PKAN), a lethal brain iron accumulation disorder. The molecular link

between PANK2 and PKAN is obscured by the existence of three other catalytically

active pantothenate kinase isoforms (PANKs) capable of catalyzing the same reaction

stabilizing whole-cell CoASH levels. Due to CoASH central role in cellular metabolism,

we performed metabolic profiling on three separate PANK2-deficiency cell models. We

treated cells with and without palmitic acid supplementation, to create a CoASH

challenge unique for PANK2 to reveal the impact that loss of PANK2 have on metabolic

pathways. PANK2-deficient cells show disrupted succinyl-CoA and acetyl-CoA

metabolism with accompanying alterations in the TCA cycle. We propose that fatty acid

oxidation compete with a disrupted TCA cycle for CoASH explaining the failure of

PANK2-deficient cells to thrive during a palmitic acid challenge. Additionally, we

observe an increase in metabolites that indicate a compensatory attempt at maintaining

CoASH levels and an imbalance in purine metabolites. Our results show the benefit of

cellular metabolic profiling to generate new hypothesis for further mechanistic study.

Introduction

Coenzyme A is cofactor carrying acyl-groups, required for the TCA cycle, fatty

acid metabolism, and protein posttranslational modifications. Cells convert pantothenic

48

acid (vitamin B$_5$) to free coenzyme A (CoASH) in five steps. A pantothenate kinase

(PANK) catalyze the first step, phosphorylating pantothenic acid to 4′-

phosphopantothenate. Three genes encode catalytically active PANKs (*PANK1-3*). The

PANK1 gene give rise to two PANK1 isoforms, PANK1α localize to the nucleus and

PANK1β localize to the cytosol (Alfonso-Pecchio et al., 2012). PANK3 localize to the

cytosol (Alfonso-Pecchio et al., 2012). The PANK2 protein is unique among the PANKs,

localizing to the mitochondria as well as the cytosol and nucleus (Alfonso-Pecchio et al.,

2012; Hortnagel, 2003; Johnson et al., 2004).

Mutations in *PANK2* cause pantothenate kinase associated neurodegeneration

(PKAN) (Zhou et al., 2001). PKAN is a subtype of neurodegeneration with brain iron

accumulation (NBIA), a lethal disease manifesting with dystonia and iron accumulation

in the basal ganglia (Kruer et al., 2011). The cellular mechanism linking PANK2 to

PKAN disease is unclear. A general hypothesis is that reduced mitochondria CoASH

levels due to impaired PANK2 activity disrupt cellular metabolism. Recently a study

found a slight mitochondria CoASH deficiency in isolated mitochondria in fibroblasts

from individuals affected with PKAN (Álvarez-Córdoba et al., 2019). Additional data

supporting a CoASH involvement in PKAN include the finding that mutations in *COASY*,

encoding the last enzyme in CoASH biosynthesis, cause a second subtype of NBIA (Dusi

et al., 2014). Individuals with mutations in the CoASH transporter SLC25A42 can also

present with brain iron accumulation (Almannai et al., 2018). It would be useful to link

PANK2 synthesized CoASH to specific metabolic pathways to separate the function of

PANK2 from the other PANKs.

If a mitochondria CoASH specific deficiency exists in PKAN cells, it would be reasonable to expect an overall impact on cellular metabolism without PANK2. The mitochondria house two prominent CoASH dependent pathways: the TCA cycle and fatty acid oxidation. Fatty acid metabolism is dependent on CoASH and the carnitine derivative, palmitoylcarnitine, activate PANK2, allowing the protein to overcome acetyl-CoA inhibition (Roberta Leonardi et al., 2007). Fatty acid oxidation cause increased mitochondria acetyl-CoA generation, which inhibit pyruvate oxidation by blocking pyruvate dehydrogenase (PDH) and leads to mitochondria export of citrate, which inhibit phosphofructosekinase 1 (PFK1) blocking glycolysis (Hue & Taegtmeyer, 2009; Randle et al., 1963). Glucose and pyruvate sparing in favor of fatty acid oxidation is part of the concept called the Randle cycle and it occurs during both starvation and high fat feeding in non-neuronal tissue (Randle et al., 1963).

In our previous study, we noted a novel role of PANK2 in fatty acid metabolism. Loss of PANK2 had a detrimental effect on fatty acid utilization causing fatty acids to accumulate and low ATP levels. Reduced ATP levels due to a decreased ability to respire palmitoylcarnitine caused an activation of AMPK and autophagy, we argued (Chapter 2). AMPK activation can override the Randle effect, allowing glycolysis to proceed to respond to unmet energetic needs and upregulate autophagy (Hue & Taegtmeyer, 2009).

Metabolite profiling performed on plasma, fibroblasts, and urine from individuals affected with PKAN found relatively mild metabolite disruptions (Leoni et al., 2012; Williams et al., 2013). In plasma from individuals with PKAN, the metabolites lactate, (a mitochondria dysfunction marker), pantothenic acid (vitamin B_5), and inosine (a purine nucleoside) were elevated. The reason for elevated inosine was unknown. A limited

analysis of fibroblast metabolism showed dysfunctional bile acid synthesis and low levels

of four fatty acids (Leoni et al., 2012). In contrast, fatty acid profiling on red blood cells

found slightly elevated polyunsaturated fatty acids and normal saturated fatty acids. In

the same study, urinary mevalonate was slightly elevated and the organic acids measured

were not reported, presumably because the organic acid profile was normal (Williams et

al., 2013).

There is no reported data on short chain CoA levels, besides acetyl-CoA, due to

the loss of PANK2. CoASH, acetyl-CoA, and succinyl-CoA are the major short chain

CoA derivatives in the cell (Trefely et al., 2022). Other short chain CoA derivatives

include propionyl-CoA, butyryl-CoA, and malonyl-CoA, which are important in fatty

acid metabolism. Mitochondria produce acetyl-CoA via pyruvate, fatty acid, and amino

acid oxidation. The mitochondria export excessive acetyl-CoA to the cytosol as citrate

where it is re-converted to acetyl-CoA by ATP-citrate lyase (Wellen et al., 2009). Acetyl-

CoA is used for acetylation and fatty acid synthesis in both the mitochondria and cytosol

(Trefely et al., 2020). Cellular acetylation is in part dependent on the concentration of

acetyl-CoA and CoASH; cells with artificially high CoASH have increased acetylation

(Shi & Tu, 2015; Wagner & Payne, 2013; Yu et al., 2021).

Succinyl-CoA is the most abundant short chain CoA derivative in the

mitochondria in cells (Trefely et al., 2022). Two metabolic pathways converge to

generate mitochondria succinyl-CoA; the TCA cycle and propionyl-CoA catabolism

(Trefely et al., 2020). In the TCA cycle α-ketoglutarate dehydrogenase use CoASH and

α-ketoglutarate to produce succinyl-CoA. Next, succinyl-CoA synthase (SCS) removes

CoASH to generate succinate. Oxidation of amino acids, odd-chain fatty acids, and

51

cholesterol side chains produce propionyl-CoA, which is converted to succinyl-CoA via propionyl-CoA carboxylase (PPC), methylmalonyl CoA epimerase (MCEE), methylmalonyl-CoA mutase (MCM) (Figure 3.3). Defects in PPC and MCM can cause propionic and methylmalonic academia as a result of increased production of 3-hydroxypropionate, methylcitrate, and methylmalonate (Baumgartner et al., 2014). Individuals with defective SCS, which cause an accumulation of succinyl-CoA, can also present with a slight elevation of methylmalonate (Van Hove et al., 2010). In addition to its role in the TCA cycle, the cell use succinyl-CoA for heme synthesis, ketone body production, and succinylation.

PKAN individuals have stable periods with limited disease progression, followed by rapid decline caused by unknown factors (Leoni et al., 2012). Detectable plasma and urine metabolic perturbations may be limited to periods of rapid decline. The PKAN mouse model is relatively healthy, but when challenged with a ketogenic diet the mice develop a movement disorder (Brunetti et al., 2014). The mouse model shows that modeling PKAN disease depend on finding a context where PANK2 is required. We have identified palmitic acid as such a challenge that cause an upregulation of autophagy, decreased ATP generation, and reduced cell viability in PANK2-deficient cells (Chapter 2). Cell models are convenient for follow up studies to investigate mechanisms behind pathways identified as disrupted in a metabolic profile. Additionally, there is no extensive profile of CoA derivatives and metabolites in PANK2-deficient cells. Therefore, we decided to perform metabolic profiling in PANK2 knockdown and knockout cell models to detect pathways that may be dependent on PANK2. We followed up on some of these

findings with some additional mechanistic studies reported here in addition to generating some new hypothesis for future follow up.

Results

Study rational and cell models.

We performed metabolic profiling of three different cell models of PANK2 loss. PANK2 knockdown (KD) was done in HEK293T cells and in PANK1β (PIβ) overexpressing cells with either siRNA against PANK2 (siPANK2/PIβ siPANK2) or with a scrambled control (SR/PIβ SR) (Appendix A, SFig 5.1A-C). These two models allow for a comparison between the effect of PANK2 loss in a low and a high CoASH cell line (Chapter 2). Lastly, we generated a Crisper-CAS9 PANK2 KO in HEK293T (PANK2 KO) as a model for the permanent loss of PANK2 (Appendix A, SFig 5.1D). To test the effect of palmitic acid, the cells received a 24-hour treatment with either 250μM vehicle control BSA or palmitic acid conjugated to BSA (PAL) in complete glucose containing media.

A total of 101 metabolites were measured with GC-MS (TCA cycle, glycolysis, fatty acids) and 41 metabolites with LC-MS (CoA profile, most energy, and redox metabolites). Partial least squares – discriminant analysis (PLS-DL) performed with Metaboanalyst 5.0 on the GC-MS data demonstrate group difference between control and loss of PANK2 (Fig 3.1) (Pang et al., 2021; Worley & Powers, 2012). The PLS-DL analysis highlighting the effect of PAL on the PANK2 KD in particular (Fig 3.1B).
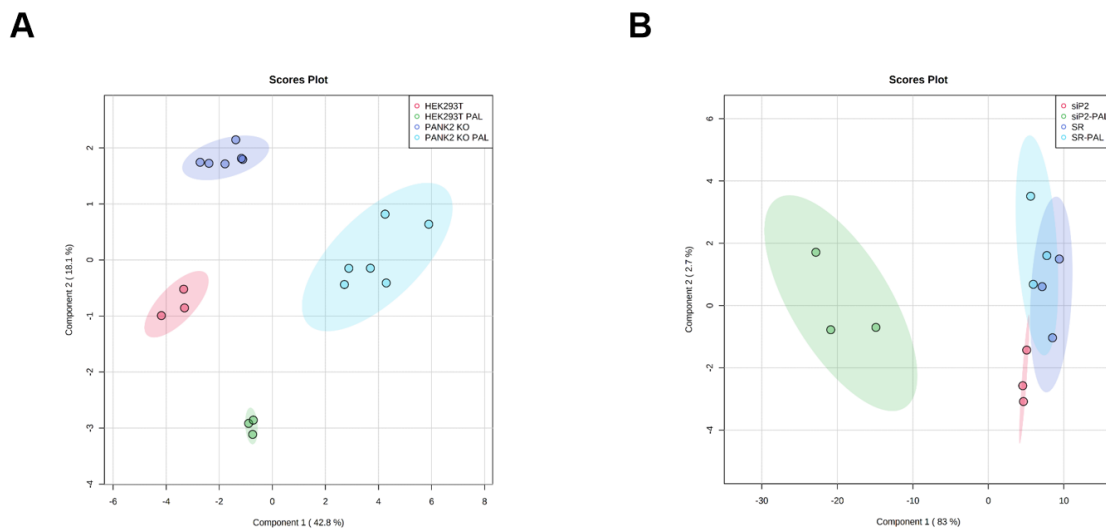
A   **B**

Figure 3.1. Partial least square-discrimination analysis (PLS-DA). PLS-DA show the differences between the groups highlighting the effect of loss of PANK2 and the PAL challenge. PLS-DA for GC-MS metabolites: A) Control: HEK293T-BSA (n=3), PANK2 KO-BSA (n=6), HEK293T-PAL (n=3), PANK2 KO-PAL (n=6), principle component 1 (42.8%), principle component 2 (18.1%). B) Scrambled control: SR-BSA (n=3), siPANK2: siP2-BSA (n=3), scrambled control PAL: SR-PAL (n=3), siPANK2: siP2-PAL (n=3) principle component 1 (83%), principle component 2 (2.7%).

CoA profile show low succinyl-CoA and butyryl-CoA in PANK2 KO cells.

Considering the role of PANK2 as a CoASH synthesizing enzyme the absence of changes to whole-cell CoASH is surprising, but comparable to what others have found (Lambrechts et al., 2019; Mignani et al., 2021). Studies have focused on CoASH and acetyl-CoA, but impaired CoASH synthesis could affect the cells short chain CoA levels. Interestingly, the PANK2 KO cells, which have permanent PANK2 loss, show both significantly lower butyryl-CoA (p= 0.009) and succinyl-CoA (p= 0.04) then the control in the BSA condition (Fig 3.2A). PAL treatment removed this difference, showing how metabolism rearrange in response to PAL. As far as we know this is the first measurement to indicate a CoA species deficiency in whole-cell measurements in PANK2 null cells. The PANK2 KD cells did not show decreased short chain CoA levels

(Fig 3.2B-C). Low butyryl-CoA and succinyl-CoA may only become apparent with time during PANK2 loss.

A surprise was to find an increase in acetyl-CoA across the PANK2 KD models, especially in the PIβ siPANK2 cells compared to PIβ SR control. In siPANK2 cells, the elevation is slight and not significant in the PAL condition with a mean fold change of 1.97 in siPANK2 compared to 1.08 in SR control (Fig 3.2B). In the PIβ cells, acetyl-CoA has a mean of 12.8 in PIβ SR control, which is significantly elevated to a mean of 33.0 for PIβ siPANK2 (p=0.008) in the BSA condition. Although not significantly elevated (p=0.058), acetyl-CoA is increased in the PAL condition in PIβ siPANK2 at a mean of 103.6 compared to PIβ SR control mean of 49.8 (Fig 3.2C).
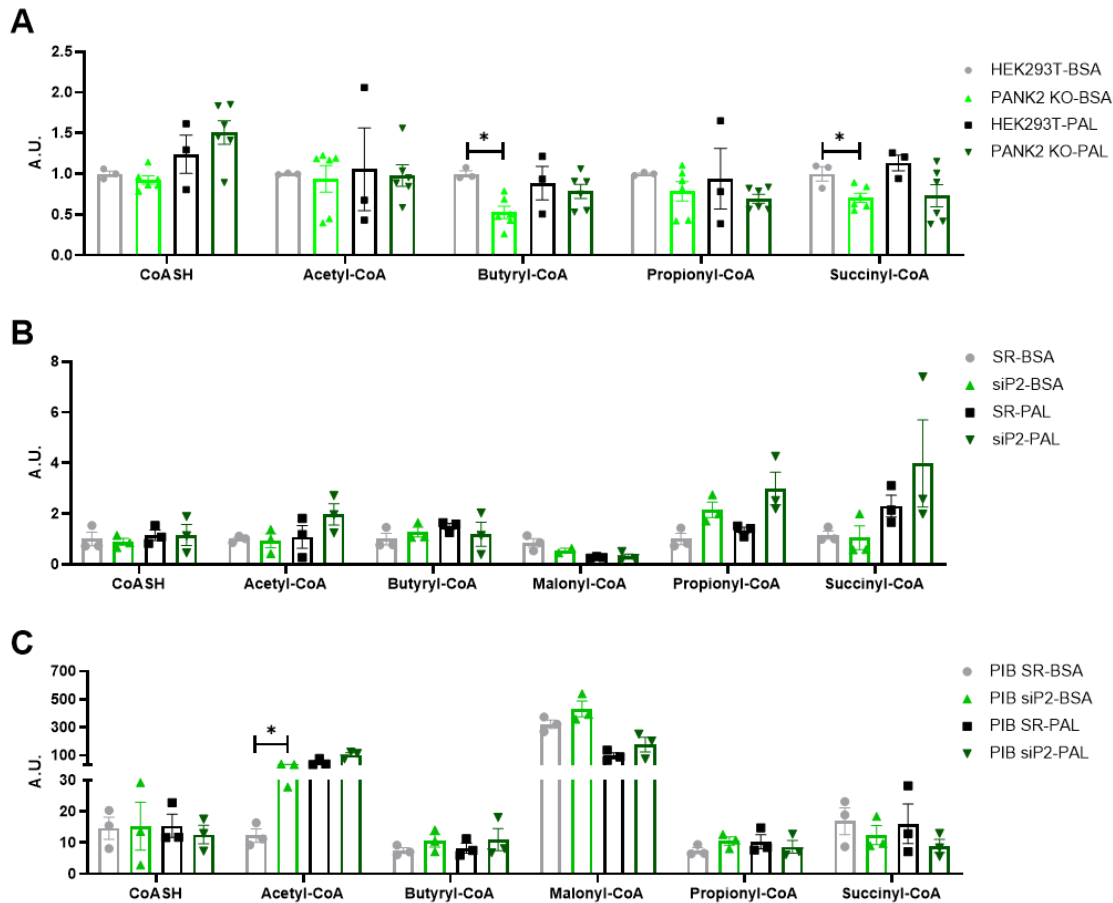
Figure 3.2. Effect of loss of PANK2 and PAL-supplementation to complete media on cellular CoASH and short chain CoA profile. LC-MS measurements for: A) Control-HEK293T-BSA (n=3), PANK2 KO-BSA (n=6), HEK293T-PAL (n=3), PANK2 KO-PAL (n=6) expressed as fold change to Control-HEK293T-BSA in arbitrary units (A.U.). B) Scrambled control: SR-BSA (n=3), siPANK2: siP2-BSA (n=3), scrambled control PAL: SR-PAL (n=3), siPANK2: siP2-PAL (n=3). C) PANK1β scrambled Control: PIβ SR (n=3), PANK1β siPANK2: PIβ siP2 (n=3), PANK1β scrambled control PAL: PIβ SR-PAL (n=3), PANK1β siPANK2 PAL: PIβ siP2-PAL (n=3). B-C) Expressed as fold change and normalized to scrambled control BSA (SR-BSA) allowing for comparison between all siRNA knockdown values, expressed in arbitrary units (A.U.). Statistical significance determined via multiple t-test corrected for multiple comparison with Holm-Sidak. The * indicates statistically significant at $P < 0.05$. For all conditions error bars are SEM.

Disrupted succinyl-CoA metabolism in PANK2-deficient cells.

Mitochondria generate succinyl-CoA via conversion of α-ketogluatarate by α-KGDH in the TCA cycle or via propionyl-CoA derived from amino acid, odd chain fatty acid, and cholesterol metabolism (Fig 3.3) (Trefely et al., 2020). In the PANK2 KD cells, TCA cycle intermediates from citrate to succinyl-CoA are low (Fig 3.4.A-E). Citrate ($p=0.04$) and aconitate ($p=0.006$) (the intermediate between citrate and isocitrate) are significantly lower in siPANK2 cells in the BSA condition (Fig 3.4A-B). Succinate on the other hand was increased in PANK2 KD cells, significantly in the siPANK2 PAL condition ($p=0.0003$) but not in PIβ siPANK2 cells (Fig 3.4F). Low succinyl-CoA, but increased succinate generation, could be an attempt by the cell to free up CoASH, especially in the PAL condition were the CoASH might be needed for fatty acid oxidation. In PANK2 KO cells, only succinyl-CoA is affected in the TCA cycle (Appendix B, SFig 6.1A-H).
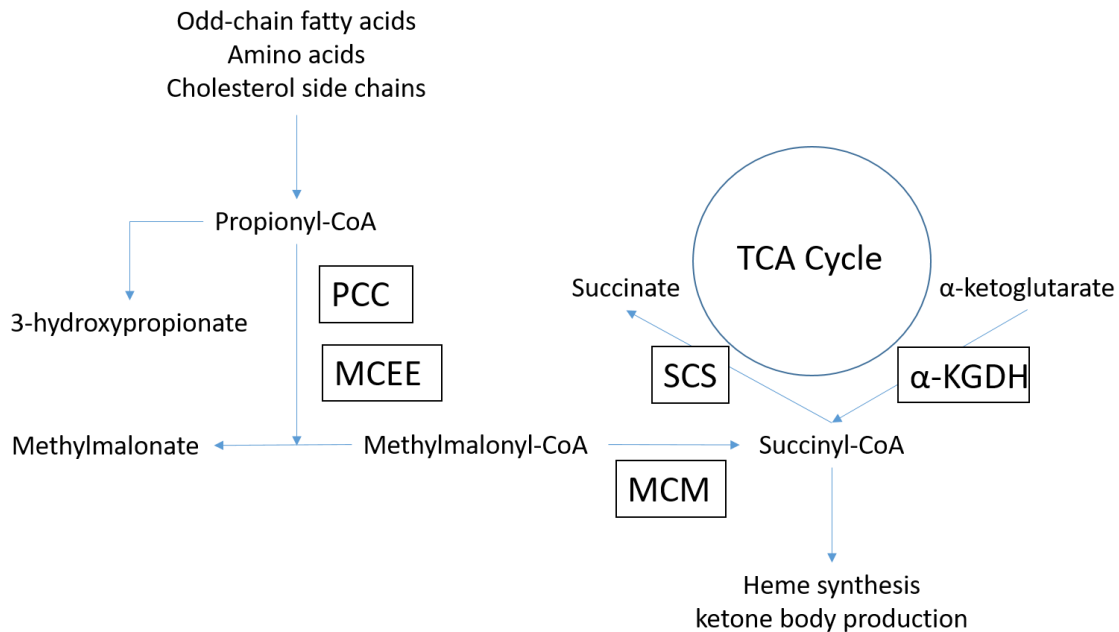

Figure 3.3. Mitochondria succinyl-CoA producing pathways. Odd chain fatty acids, some amino acids, and cholesterol side chains are broken down to propionyl-CoA. Propionyl-CoA is converted to methylmalonyl-CoA by the action of PCC and MCEE.

Methylmalonyl-CoA is converted to succinyl-CoA by MCM. Alternatively if the pathway is disrupted propionyl-CoA can be converted to 3-hydroxypropionate or methylmalonyl-CoA can be converted to methylmalonate. Abbrevations: PCC - Propionyl-CoA carboxylase; α-KGDH - Alpha-ketoglutarate dehydrogenase; SCS - Succinyl-CoA ligase. MCEE - methylmalonyl CoA epimerase; MCM - Methylmalonyl-CoA mutase.
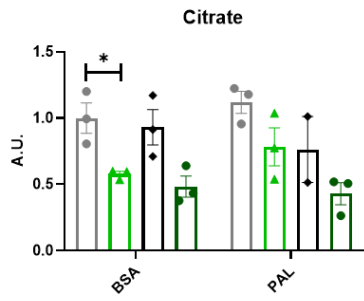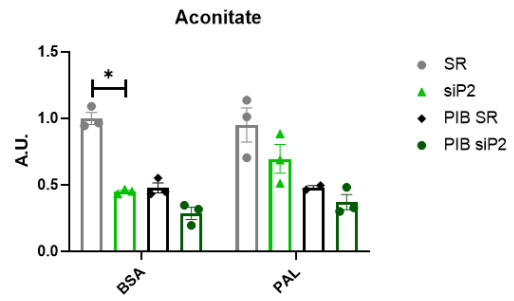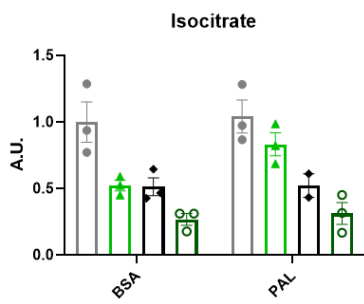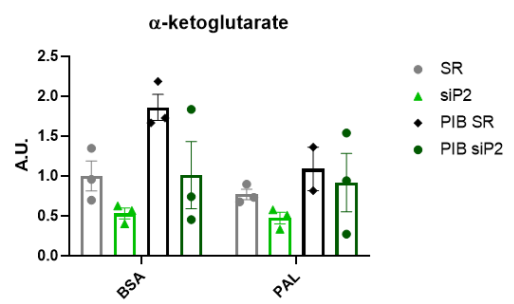
59
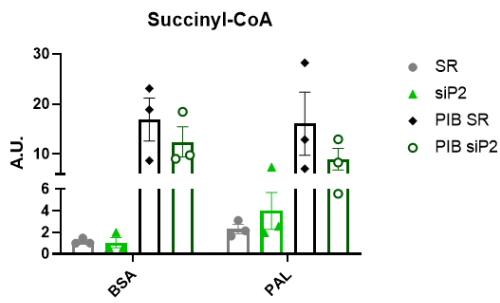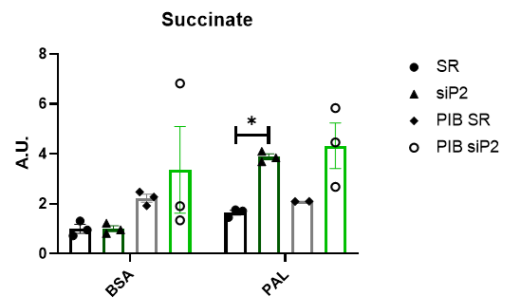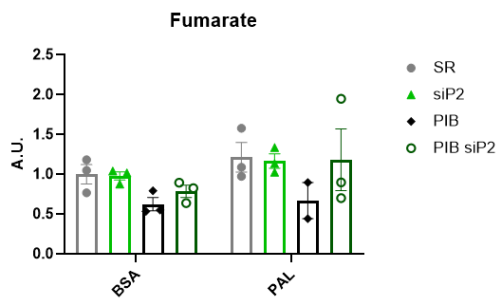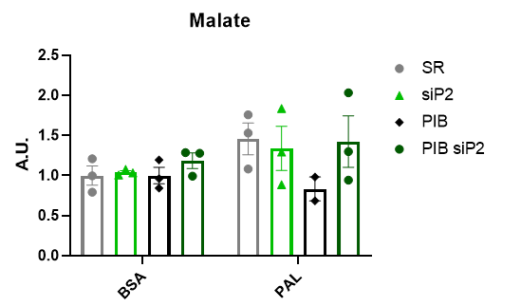
Figure 3.4. Levels of TCA cycle intermediates in PANK2 KD cells. A-D,F-H) Measured with GC-MS, scrambled control: SR-BSA (n=3), siPANK2: siP2-BSA (n=3), scrambled control PAL: SR-PAL (n=3), siPANK2: siP2-PAL (n=3), PANK1β scrambled Control: PIβ SR (n=3), PANK1β siPANK2: PIβ siP2 (n=3), PANK1β scrambled control PAL: PIβ SR-PAL (n=2), PANK1β siPANK2 PAL: PIβ siP2-PAL (n=3) normalized to SR and expressed as fold change. E) The same succinyl-CoA data measurement as reported in figure 3.1B-C. Statistical significance determined via multiple t-test corrected for multiple comparison with Holm-Sidak. The * indicates statistically significant at P < 0.05 for all conditions error bars are SEM.

Defects in the enzymes propionyl-CoA carboxylase (PCC) and L-methylmalonyl-CoA mutase (MCM) in the propionyl-CoA to succinyl-CoA pathway can cause accumulation of 3-hydroxypropionate and methylmalonate (Baumgartner et al., 2014). In PANK2 KO there was a significant accumulation of methylmalonate (p=0.03). Whereas the PANK2 KD cells had a significant accumulation in 3-hydroxypropionate (p=0.04) in the PAL condition of both siPANK2 and PIβ siPANK2 cells (Fig 3.5), hypothetically in order to conserve CoASH utilization.

The difference in acute (PANK2 KD) and chronic (PANK2 KO) metabolite disruption could be due to PANK2 KD cells attempting to find a new homeostatic balance while PANK2 KO cells have adapted. For example in PANK2 KD cells, there is a robust increase in autophagy as measured by LC3II/LC3I ratio and p62 accumulation with the lysosomal inhibitor chloroquine (Chapter 2), while in PANK2 KO cells autophagy is only slightly elevated (Appendix B, SFig 6.2).
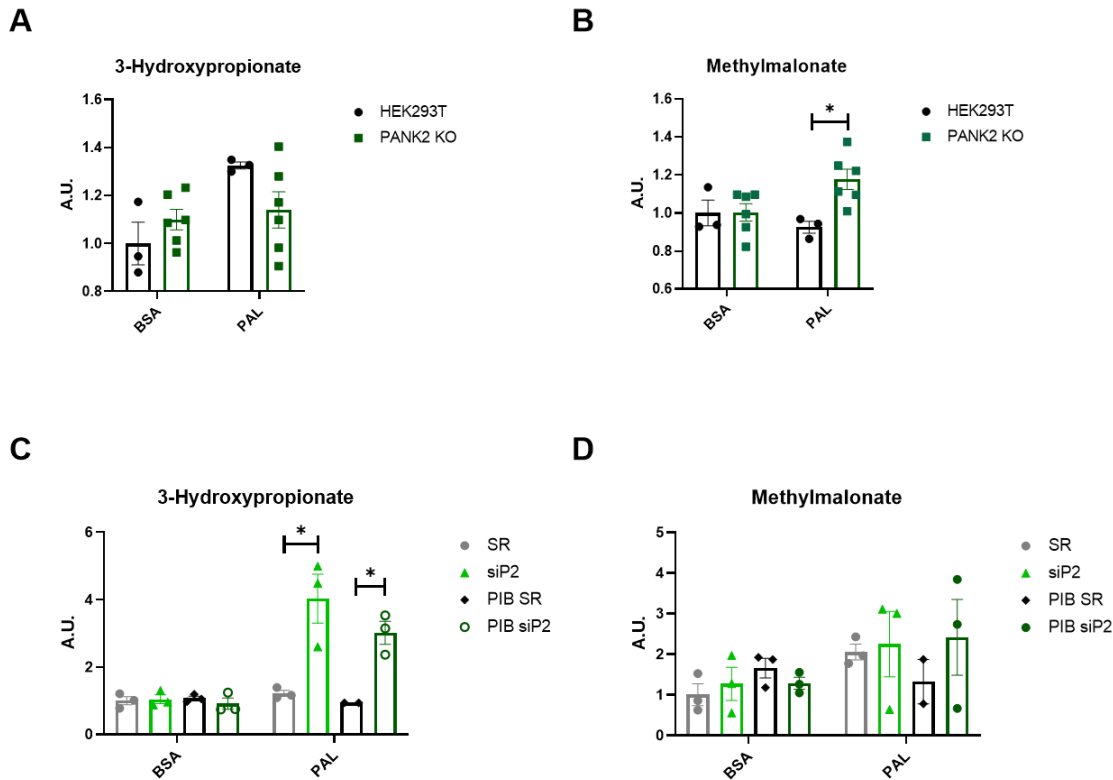
Figure 3.5. Levels of CoASH releasing byproducts of the propionyl-CoA to succinyl-CoA pathway. Measured with GC-MS: A-B) Control: HEK293T-BSA (n=3), PANK2 KO-BSA (n=6), HEK293T-PAL (n=3), PANK2 KO-PAL (n=6) expressed as fold change to HEK293T-BSA. C-D) Scrambled control: SR-BSA (n=3), siPANK2: siP2-BSA (n=3), scrambled control PAL: SR-PAL (n=3), siPANK2: siP2-PAL (n=3), PANK1β scrambled Control: PIβ SR (n=3), PANK1β siPANK2: PIβ siP2 (n=3), PANK1β scrambled control PAL: PIβ SR-PAL (n=2), PANK1β siPANK2 PAL: PIβ siP2-PAL (n=3). Data expressed as fold change to SR (C-D). Statistical significance determined via multiple t-test corrected for multiple comparison with Holm-Sidak. The * indicates statistically significant at $P < 0.05$ for all conditions error bars are SEM expressed as arbitrary units (A.U).

Increased cytosolic acetylation.

When one might expect that dysfunctional CoASH synthesis would cause a decrease in CoA-species, PANK2 KD cells have a paradoxical increase in acetyl-CoA levels (Fig 3.2B-C). In addition to increased acetyl-CoA levels, the siPANK2 cells have elevated global acetylation (Fig 3.6A-B). Global acetylation was almost increased 2-fold

in both the BSA (p=0.01) and in the PAL (p=0.03) condition in siPANK2 cells. In PIβ

cells with high CoASH and acetyl-CoA levels, the increase in acetylation with PANK2

KD was even more evident in the PAL condition increasing approximately 4-fold

(p=0.003) for PIβ siPANK2 cells (Fig 3.6B).

The PANKs show differential subcellular distribution with PANK1β and PANK3

in the cytosol and PANK2 in the mitochondria, cytosol, and nucleus (Alfonso-Pecchio et

al., 2012). During PANK2 knockdown, the mRNA expression of PANK1 and PANK3

increase (Chapter 2). If PANK2 is responsible for mitochondria CoASH species and

PANK1β/PANK3 is mainly responsible for cytosolic CoASH, exporting acetyl-CoA

from the mitochondria would free up mitochondria CoASH. Alternatively, in conditions

were there is a block in the generation of succinyl-CoA in the TCA cycle i.e. during

hypoxia or enzymatic aconitase dysfunction, there can be an increase in citrate export to

the cytosol (Crooks et al., 2018; Trefely et al., 2022). In this case low mitochondria

CoASH availability could limit succinyl-CoA generation (Fig 3.2A).

To determine if the increase in acetylation was cytosolic, we analyzed the

acetylation of the cytosolic protein tubulin at Lys-40 in PANK2 KD cells. In whole-cell

lysate, PANK2 KD increased tubulin acetylation 2.5-fold (p=0.02) and 3-fold (p=0.007)

in siPANK2 cells and PIβ siPANK2 respectively demonstrating an increase in cytosolic

acetylation (Fig 3.6C-D). Acetylated tubulin is not present in the mitochondria and to

exclude increased mitochondria acetylation we performed fractionation on WT

HEK293T and PANK2 KD cells. Checking global acetylation in total (TF), mitochondria

(mito), and cytosolic fractions (cytosol) showed no change to the mitochondria fraction

(Fig 3.7C), but increased cytosolic acetylation (Fig 3.7B) in the PAL condition. Tubulin

acetylation increased in the cytosolic fraction (Fig 3.7A), although not significantly

(p=0.059) in the PAL condition. These results indicate that the increase in acetylation

was predominantly due to cytosolic protein.
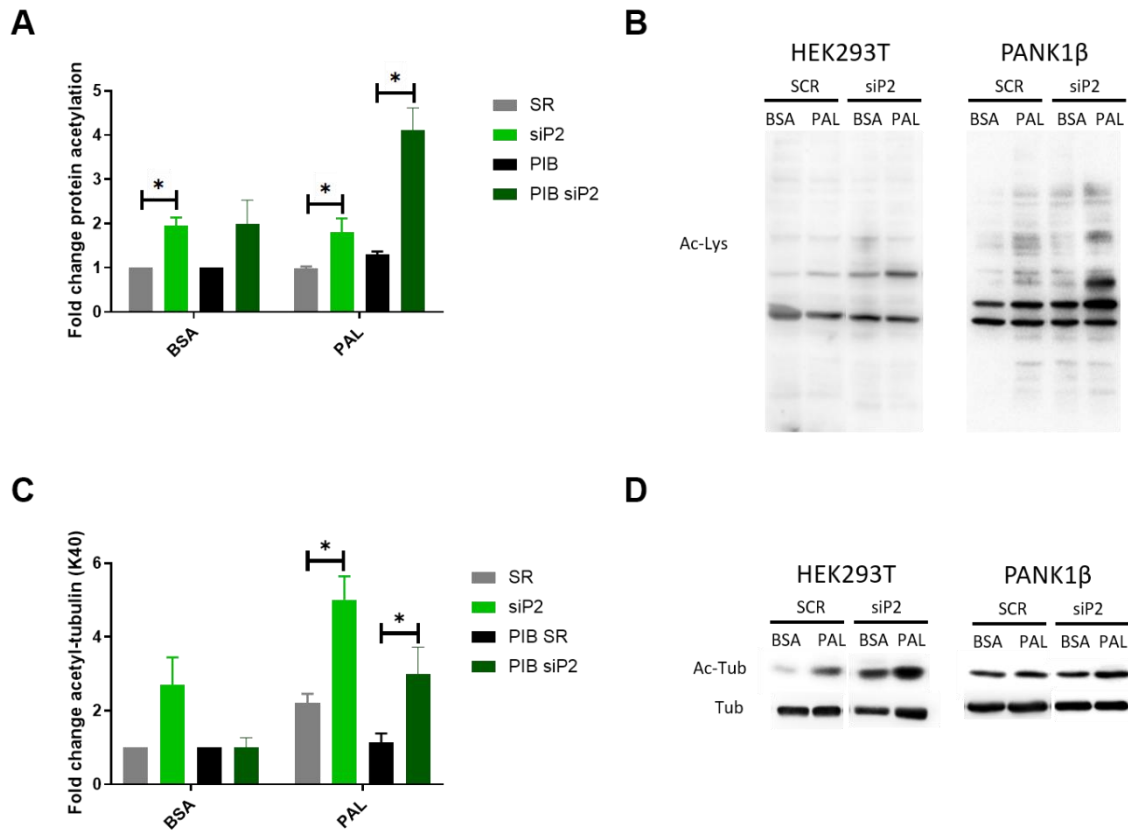
Figure 3.6. Global acetylation and cytosolic acetylation of tubulin increase in PANK2 KD cells. A-B) Quantification of global acetylation in samples SR (n=4), siP2 (n=4), PIβ (n=3), and PIβ siP2 (n=3) with and without PAL-treatment. SR/siP2 expressed as fold change to SR BSA condition, PIβ and PIβ siP2 expressed as fold change to PIβ SR BSA condition. All data normalized to tubulin levels with representative western blot of global acetylation. C-D) Quantification of acetylated tubulin (Lys-40) SR (n=4), siP2 (n=4), PIβ (n=3), and PIβ siP2 (n=3) with and without palmitic acid PAL-treatment. SR/siP2 expressed as fold change to SR BSA condition, PIβ and PIβ siP2 expressed as fold change to PIβ SR BSA condition, normalized to tubulin levels with representative western blot of acetylated tubulin and tubulin. Statistical significance determined with a two-way ANOVA. The * indicates statistically significant at P < 0.05 and for all conditions error bars are SEM.

Figure 3.7. Acetylation is enriched in the cytosol in PANK2 PAL KD cells. A) Quantification of tubulin acetylation normalized to tubuli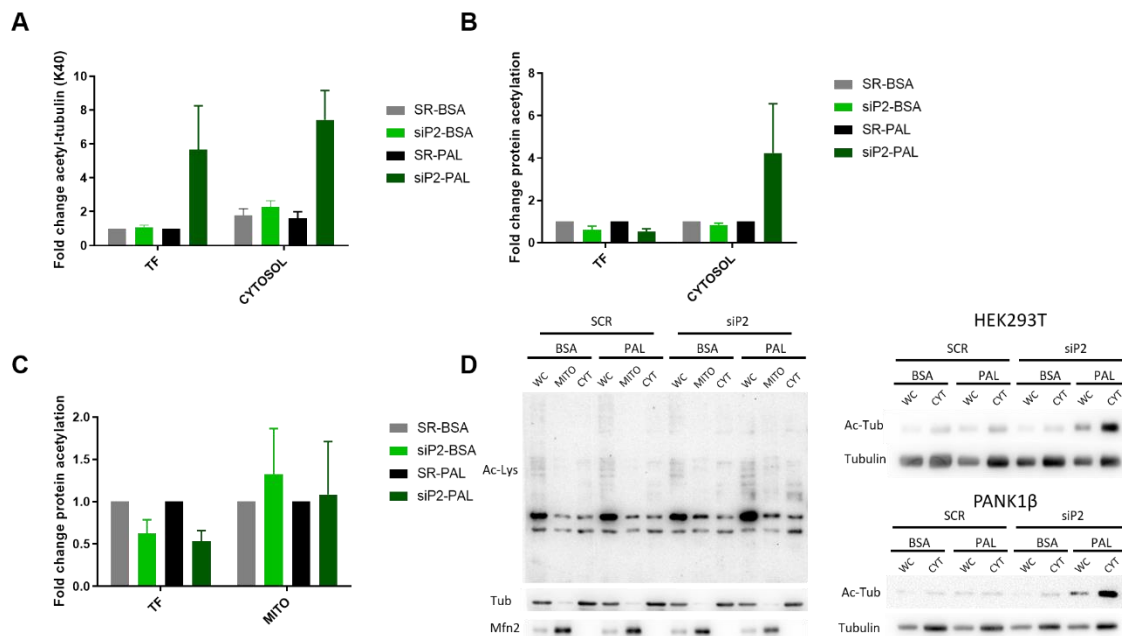n in TF (total fraction) and cytosol expressed as fold change to SR-BSA TF or SR-PAL TF. B) Quantification of global protein acetylation in TF and cytosol normalized to tubulin and expressed as fold change to SR-BSA TF or SR-PAL. C) Quantification of global acetylation in TF and mitochondria (mito) normalized to MFN2 expressed as fold change to SR-BSA TF or SR-PAL. D) Representative western blot for A-C. Left is showing global acetylation, tubulin, MFN2. Top right is showing acetylated tubulin in HEK293T cells. Bottom right is showing acetylated tubulin and tubulin in PANK1β.

Fatty acids increase cytosolic tubulin acetylation in PANK2 KD cells.

Next, we were curious if we could find the source of the increased acetylation by testing inhibitors or by removing nutrients while tracking changes to acetylated tubulin. Previously we demonstrated impaired respiration of palmitoylcarnitine and reduced ATP levels in PANK2-deficient cells treated with PAL (Chapter 2). Surprisingly, when we use a fatty acid oxidation (FAO) inhibitor, trimetazidine (Triz), which inhibit the activity of the FAO enzyme 3-ketoacyl CoA thiolase, we see a decrease in ATP levels in PANK2 KD cells both in the BSA and PAL condition (Fig 3.8A). This experiment indicate that

64

the PANK2 KD cells are attempting to use fatty acid oxidation to generate acetyl-CoA, but failing to generate ATP (Lee et al., 2020).

Therefore, we decided to see if trimetazidine inhibition of FAO would reduce the tubulin acetylation that we have had seen increase in PANK2 KD cells, especially during the PAL-challenge. When fatty acid oxidation is inhibited with trimetazidine in PAL treated cells, the tubulin acetylation is drastically decreased in PANK2 KD cells (p=0.02) compared to PANK2 KD cells with the PAL-challenge only. These experiments show that the increase in tubulin acetylation comes from fatty acid oxidation and that PANK2 KD cells do generate some ATP from fatty acid oxidation. However, their ability to generate ATP from PAL is reduced and instead acetyl-CoA appears to be funneled towards cytosolic protein acetylation i.e. increased tubulin acetylation (Fig 3.8B).
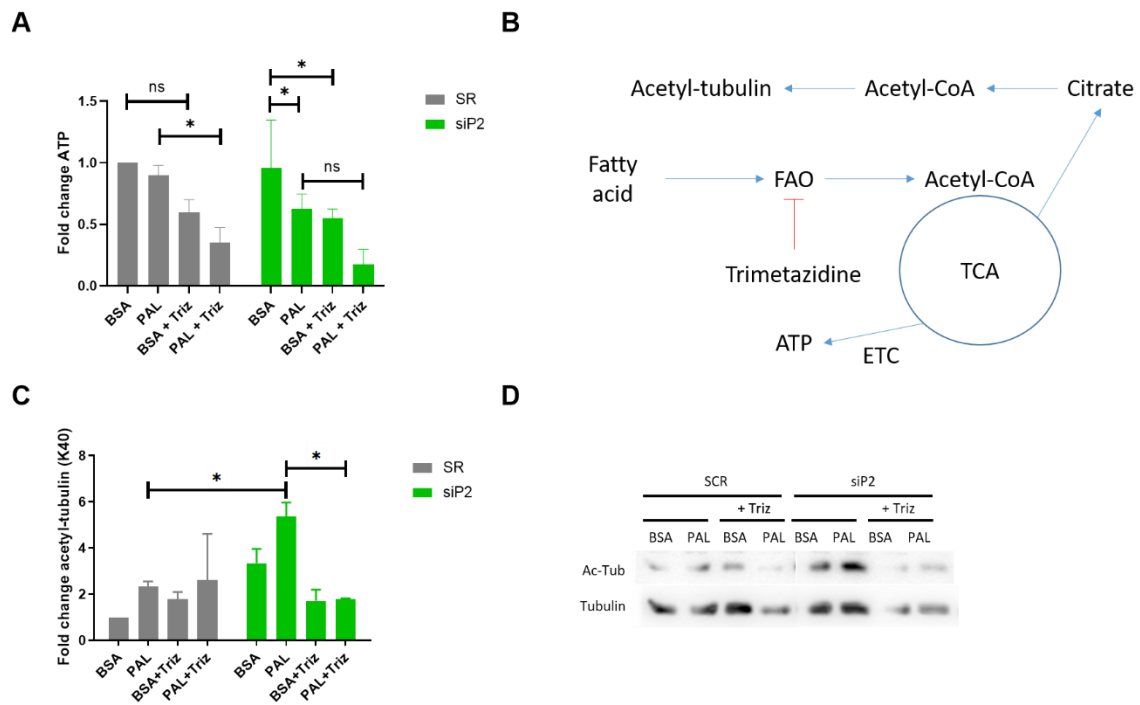

Figure 3.8. PANK2 KD cells export palmitic acid derived acetyl-CoA for cytosolic tubulin acetylation. A) ATP measurements from cells treated with BSA (n=3), PAL

(n=3), BSA+Triz (trimetazidine) (n=3), PAL+Triz (n=3). B) Diagram of how fatty acid derived acetyl-CoA is used for either tubulin acetylation or in the TCA cycle for ATP generation. C) Quantification of acetyl-tubulin with BSA (n=5), PAL (n=5), BSA+Triz (n=2), PAL+Triz (n=2). D) Representative western blot of acetyl-tubulin and tubulin quantified in C. Statistical significance determined with a two-way ANOVA. The * indicates statistically significant at $P < 0.05$, for all conditions error bars are SEM.

Proposed model for how reduced mitochondria CoASH due to lack of PANK2 impairs the TCA cycle causing fatty acid utilization impairment.

Oxidation of fatty acids cause an increase in mitochondria acetyl-CoA generation, which blocks pyruvate utilization as described by the Randle cycle (Hue & Taegtmeyer, 2009; Randle et al., 1963). Our graphical representation in figure 3.9 show how the influx of fatty acids strains a mitochondria CoASH pool reduced due to the absence of PANK2 (Fig 3.9). This forces the cell to respond by freeing up CoASH by: 1) exporting citrate to the cytosol where there is more CoASH to generate cytosolic acetyl-CoA and acetylation (data supporting Fig 3.2A-B, Fig 3.7, and Fig 3.8). 2) Generating waste products such as 3-hydroxypropionate/methylmalonate (data supporting Fig 3.5). 3) Rearranging a strained TCA cycle i.e. succinyl-CoA/citrate reducing ATP generation activating AMPK (data supporting Chapter 2 Fig 2.5G-H, Fig 2A, Fig 2.4). 4) Fatty acids accumulate due to reduced capability to generate acetyl-CoA via fatty acid oxidation and activating AMPK in response to low ATP (data supporting Chapter 2 Fig 2.1D, 2.7D, 2.9).
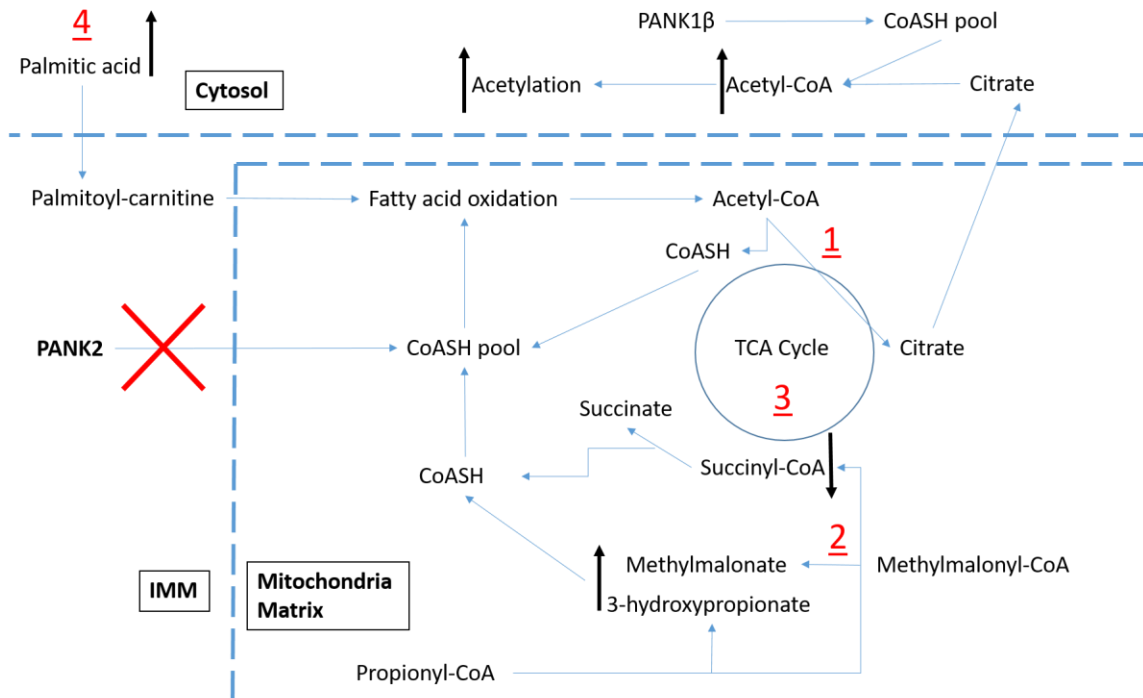
Figure 3.9. Proposed model explaining the fatty acid utilization impairment seen in PANK2-deficient cells. Palmitic acid is converted to palmitoyl-carnitine entering the mitochondria where it is reconverted to palmitoyl-CoA. Palmitoyl-CoA enters fatty acid oxidation (FAO). Fatty acid oxidation generate acetyl-CoA, but due to reduced CoASH availability more citrate is exported to the cytosol (1) then in control cells. To respond to the increased CoASH demand less succinyl-CoA is produced (2) and (3) generating more CoASH availability, but also waste products such as methylmalonate and 3-hydroxypropionate. Reduced TCA cycle output leads to less ATP production. A slowdown of the TCA cycle and reduced ability to generate acetyl-CoA from fatty acid oxidation cause an increase in fatty acids (4).

Altered purine metabolite levels.

Besides the direct effect on mitochondria metabolism we also observed alterations in purine metabolism, which can be affected in mitochondrial disorders (Van Hove et al., 2010). Inosine is elevated in plasma from individuals affected with PKAN (Leoni et al., 2012). The purine degradation pathway and alterations to levels caused by loss of PANK2 is modeled in figure 3.10 (Fig 3.10). PANK2 KO cells had significantly increased inosine ($p=0.005$) and hypoxanthine ($p=0.0002$) levels, while PANK2 KD cells

had elevated inosine and significantly increased hypoxanthine (p=0.0003) levels (Fig

3.11B-C, 3.12B-C). Guanine and guanosine accumulated in the PAL condition of all cells

(Fig 3.11, Fig 3.12). Guanine was significantly elevated for both PANK2 KO (p=0.0008)

and PANK2 KD (p=0.000017) (Fig 3.11E-F) in the PAL condition. Guanosine

accumulation was only significant in the PANK2 KO PAL condition (p=0.01) (Fig

3.12F).
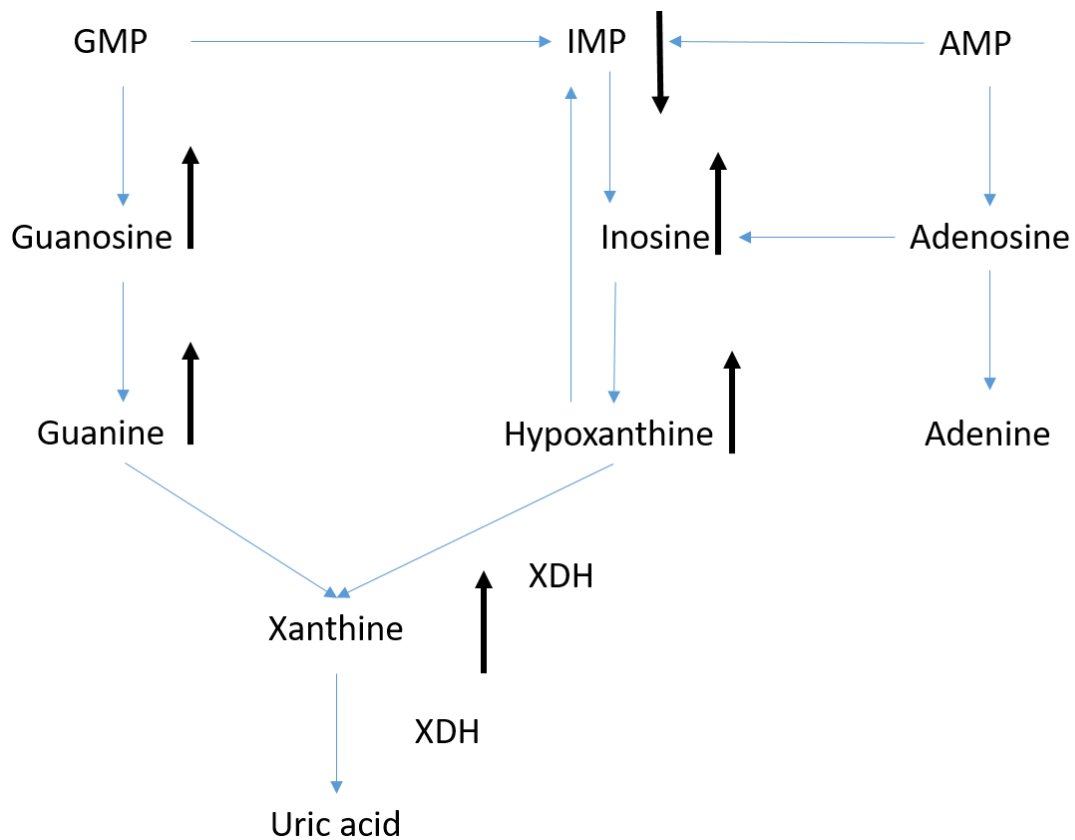
Figure 3.10. Pathways of purine metabolism. Arrows indicate the direction and
interconversion between purine derivatives. Abbreviations: XDH - Xanthine
dehydrogenase.
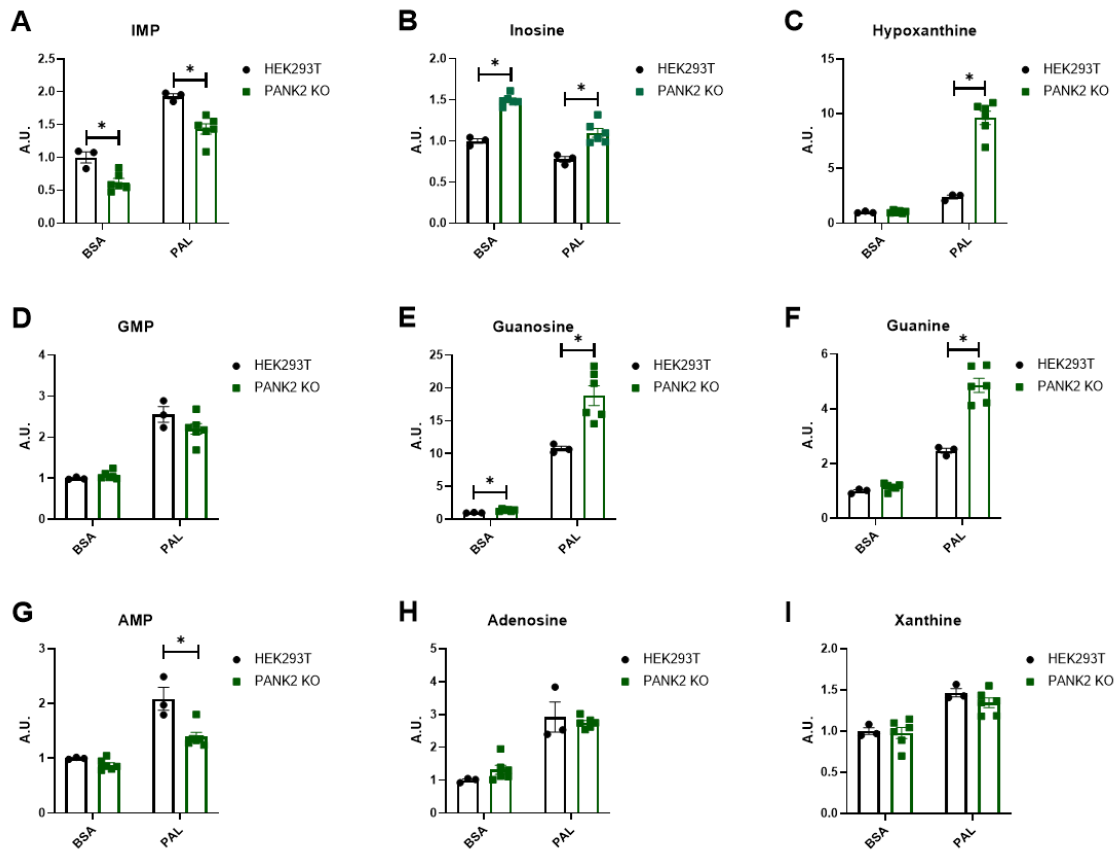
Figure 3.11. Levels of purine metabolites in PANK2 KO cells. A-F) Control-HEK293T-BSA (n=3), PANK2 KO-BSA (n=6), HEK293T-PAL (n=3), PANK2 KO-PAL (n=6) expressed as fold change to Control-HEK293T-BSA. A, D, E) Metabolites measured with LC-MS. B, C, F, H, I) Metabolites measured with GC-MS. Statistical significance determined via multiple t-test corrected for multiple comparison with Holm-Sidak. The * indicates statistically significant at $P < 0.05$ for all conditions error bars are SEM. Expressed in arbitrary units (A.U.).
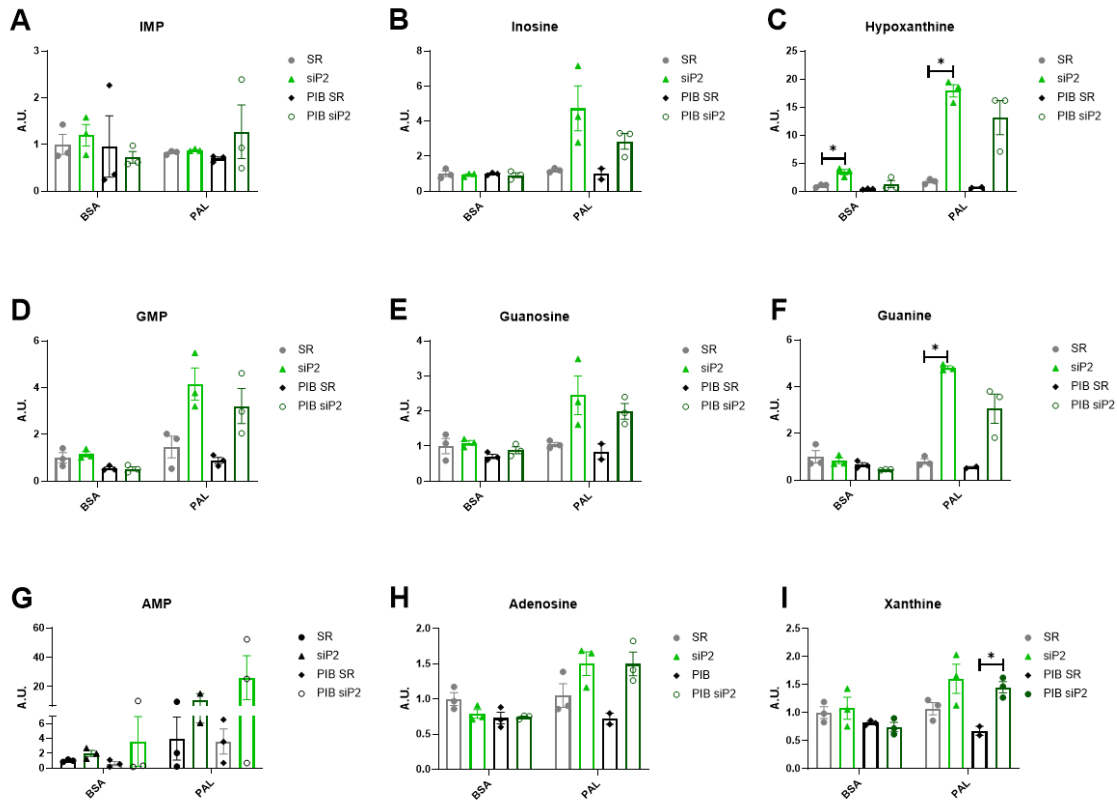
Figure 3.12. Levels of purine metabolites in PANK2 KD cells. A-I) Scrambled control: SR-BSA (n=3), siPANK2: siP2-BSA (n=3), scrambled control PAL: SR-PAL (n=3), siPANK2: siP2-PAL (n=3), PANK1β scrambled Control: PIβ SR (n=3), PANK1β siPANK2: PIβ siP2 (n=3), PANK1β scrambled control PAL: PIβ SR-PAL (n=2 for B, C, F, H, I; n=3 for A, D, E) , PANK1β siPANK2 PAL: PIβ siP2-PAL (n=3) normalized to SR and expressed as fold change. A, D, E) Metabolites measured with LC-MS. B, C, F, H, I) Meatbolites measured with GC-MS. Statistical significance determined via multiple t-test corrected for multiple comparison with Holm-Sidak. The * indicates statistically significant at P < 0.05 for all conditions error bars are SEM. Expressed in arbitrary units (A.U.).

This data show a serious imbalance in purine levels extending beyond elevated inosine levels present in the BSA condition, but exacerbated by the PAL-challenge in PANK2-deficient cells, possibly due to the increased CoASH demand usually met by PANK2. Interestingly, succinyl-CoA synthase (SCS), which converts succinyl-CoA to succinate is known to interact with nucleoside diphosphate kinase (NDPK), and disruptions to this interaction is thought to cause an imbalance in the nucleoside pool

(Elpeleg et al., 2005; Van Hove et al., 2010). Although, speculative one could hypothesis that low succinyl-CoA, the substrate for SCS could have an impact on this interaction also.

Additional metabolites.

In this study, we did not detect elevated pantothenic acid levels or lactate (Appendix B, SFig 6.3), in contrast to what has been detected in plasma from PKAN individuals. We previously reported fatty acid accumulation in PANK2 KD cells in the PAL-condition (Chapter 2). In PANK2 KO cells, there was a significant increase in four fatty acids: heptanoic, heptadecanoic, steric, and oleic acid in both the BSA and PAL condition, while there was a significant decrease in myristic, lauric, and tridecanoic acid in the PAL condition only (Fig 3.13). The mechanism behind the mixed fatty acid profile in PANK2 KO cells is currently unclear. Previous fatty acid measurements in fibroblast showed low oleic, myristic and palmitic acid in standard glucose culturing conditions attributed to impaired fatty acid synthesis (Leoni et al., 2012).
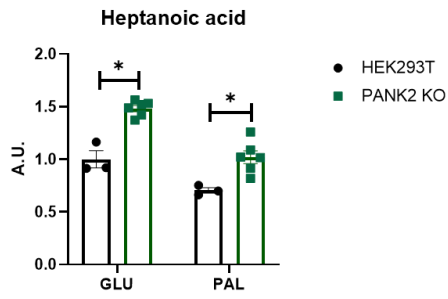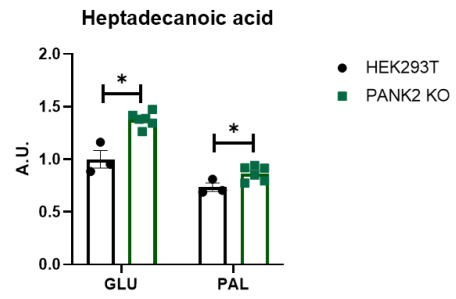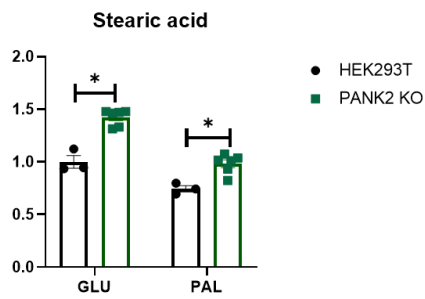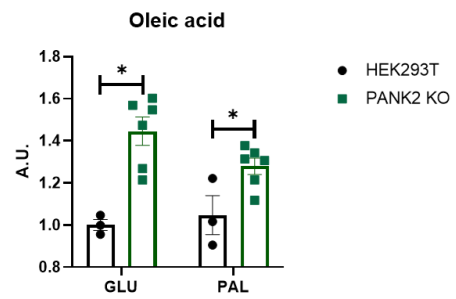
A Heptanoic acid

B Heptadecanoic acid

C Stearic acid

D Oleic acid

E Myristic acid

F Lauric acid

G Tridecanoic acid
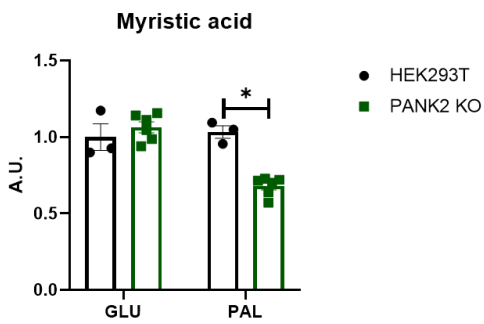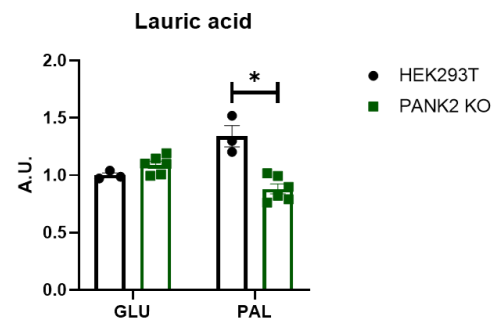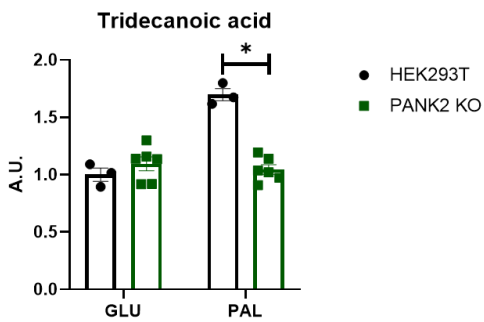
Figure 3.13. Altered fatty acid levels in PANK2 KO cells. A-G) Control: HEK293T-BSA (n=3), PANK2 KO-BSA (n=6), HEK293T-PAL (n=3), PANK2 KO-PAL (n=6) expressed as fold change to Control-HEK293T-BSA. Metabolites measured with GC-MS. Statistical significance determined via multiple t-test corrected for multiple comparison with Holm-Sidak. The * indicates statistically significant at P < 0.05 for all conditions error bars are SEM. Expressed in arbitrary units (A.U.).

Discussion

In this study, we report low succinyl-CoA and butyryl-CoA in whole-cell PANK2 KO cells. One proposed function for PANK2 is to regulate mitochondria CoASH levels. This fits well with low succinyl-CoA levels in PANK2 KO cells, as succinyl-CoA is the predominant mitochondria CoA-derivative (Trefely et al., 2022). CoA-derivatives were not significantly low in PANK2 KD cells, but there were disruption to succinyl-CoA generating pathways. The difference in CoA derivatives between acute and chronic PANK2 loss could depend on permanent PANK2 KO cells reaching a homeostatic balance that the more acute loss of PANK2 in PANK2 KD cells are still trying to attain.

In PANK2 KD cells, there was a reduction in citrate to succinyl-CoA metabolites, with a significant reduction in citrate and aconitate. PANK2 KD cells had an accumulation of 3-hydroxypropionate while PANK2 KO had an accumulation of methylmalonate. Both 3-hydroxypropionate and methylmalonate accumulate when the propionyl-CoA to succinyl-CoA metabolic pathway is blocked (Baumgartner et al., 2014). No study has reported academies in PKAN individuals and we do not know if the accumulation of 3-hydroxypropionate and methylmalonate are physiologically relevant. We propose that reduced CoASH availability cause the cell to generate more non-CoA waste products, reduce TCA output, and reduce fatty acid oxidation in order to free up mitochondria CoASH to maintain metabolic flexibility (Fig 3.9).

Unexpectedly, we found elevated acetyl-CoA levels and increased acetylation in PANK2 KD cells. This is in contrast to a previous report that show a reduction in acetylated tubulin, histone H3, and histone H4 after PANK2 knockdown in HEK293 cells (Siudeja et al., 2011). We propose based on our preliminary data that this increase in acetylation was mainly in the cytosolic compartment in siPANK2 cells. This is based on the increase in acetylated tubulin (a cytosolic protein) and fractionation studies showing increase in acetylation in the cytosolic fraction, while the mitochondria fraction was unchanged. The mechanism for increased cytosolic acetylation is unclear. Inhibition of FAO with trimetazidine in PANK2 KD cells point towards the increased acetylation coming from fatty acid oxidation. Combining our current and previously reported data (Chapter 2), we propose that a loss of PANK2 impairs the TCA cycle obstructing fatty acid oxidation causing an increased export of citrate for cytosolic acetyl-CoA generation (Fig 3.9).

Metabolite levels only provide a snapshot of the cell and the direction of the change is often unclear. More follow up studies are required to determine if an impaired TCA cycle, stressed by an increased demand for CoASH from fatty acids is the cause of the phenotypes we observe here and in our previous study (Chapter 2). For example, tracing studies and compartment specific metabolite measurements would be helpful to confirm or refute our proposed model.

During fasting, when glucose is sparse many organs rely on fatty acid oxidation while neurons switch to ketone body utilization to meet energy needs (Jensen et al., 2020). Oxidation of β-hydroxybutyrate (βHB), the most abundant ketone body, depend on succinyl-CoA. In neurons, succinyl-CoA:3-ketoacid coenzyme A transferase 1

(OXCT1), use succinyl-CoA as a CoASH donor to synthesis acetoacetyl-CoA. Next a thiolase use acetoacetyl-CoA to generate two molecules of acetyl-CoA, which enter the TCA cycle (Jensen et al., 2020). The mostly healthy PANK2 null mice develop a movement disorder when fed a ketogenic diet. Similarly, to our suggested model of CoASH competition between fatty acid oxidation and the TCA cycle, neuronal ketone utilization may strain a diminished succinyl-CoA pool causing PKAN.

Iron accumulation in the basal ganglia is a hallmark of PKAN disease and some individuals with mutations in *SLC25A42* also present with brain iron accumulation (Almannai et al., 2018). Heme, a major iron-containing complex, require mitochondrial succinyl-CoA for synthesis. Aminolevulinic acid synthase (ALAS) depend on the coenzyme pyridoxal phosphate (PLP) for condensing succinyl-CoA to glycine. We have performed a RNA-seq study, which include fibroblasts from individuals with PKAN and one individual with a mutation in *SLC25A42* (unpublished study). Interestingly, in our RNA-seq study we saw a downregulation of pyridoxal kinase (PDXK), the enzyme that synthesis PLP, in both PKAN and SLC25A42-defective fibroblasts. Further, SLC25A42-defective fibroblasts had downregulated the *HMOX1* gene that codes for heme oxygenase (HO), which degrades heme, while q-PCR data from PANK2 KD cells show an increase in *HMOX1* and its regulator *NFL2E2* (NRF2 protein) (unpublished observations and Appendix B, SFig 6.4). Balancing the production and degradation of heme is vital for intracellular iron homeostasis (Atamna, 2004). We propose that more studies are required to investigate the possible link between PANK2, succinyl-CoA, heme, and iron accumulation.

Overall, overexpressing PANK1β and increasing CoASH and short chain CoA derivatives appeared to have little effect on rescuing the metabolite disruption caused by the loss of PANK2. Although fewer metabolites were significantly elevated in PANK1β PANK2 KD this was more likely due to low statistical power. One of the three PANK1β controls failed during analysis. This means that this study further supports our previous conclusion (chapter 2) that PANK2 and PANK1 are non-redundant, especially during the PAL-challenge.

Lastly, we saw imbalanced purine levels. Inosine levels are elevated in plasma from PKAN individuals (Leoni et al., 2012). We confirm elevated inosine and add to these findings that PANK2-deficient cells have elevated hypoxanthine, guanine, and guanosine. We do not know how CoASH or PANK2 connect to purine metabolism. It would be interesting to see if low succinyl-CoA levels affect succinyl-CoA synthase (SCS) interaction with the nucleoside diphosphate kinase causing an imbalance in purine levels (Elpeleg et al., 2005).

Our unpublished RNA-seq data set again strengthen the case that purine metabolism is imbalanced. The *SLC25A42* RNA-seq data set showed upregulated *IMPDH2*, the enzyme that catalyze the conversion of inosine 5'-phosphate (IMP) to xanthosine 5'-phosphate (XMP) and an upregulation of *SLC29A2*, which codes for a purine transporter (unpublished observation). Both the SLC25A42-defective and the PKAN RNA-seq data set show upregulation of *MOCS1* (unpublished observation). MOCS1 protein isoforms are involved in the synthesis of the molybdenum cofactor required for xanthine dehydrogenase (XDH) function, which convert xanthine to uric acid. It is worth noting that MOCS1 and XDH are iron-sulfur proteins and that the purine

metabolism defects could be related to iron dyshomeostasis. Mitochondria CoASH is required to generate 4-phosphopantetheine for mitochondrial acyl carrier protein (ACP) (Beld et al., 2014; Lambrechts et al., 2019). The mitochondrial acyl carrier protein is an essential subunit for iron-sulfur cluster biosynthesis (Van Vranken et al., 2016). Low mitochondria CoASH could cause low 4-phosphopantetheine availability disrupting iron-sulfur cluster formation (Lambrechts et al., 2019). Even with SLC25A42 being a unique form of inborn error in mitochondria CoASH transport the combined data from this study and the RNA-seq points toward a role for mitochondria CoASH in maintaining the cells purine metabolism.

Over 100 cellular reactions depend on CoASH (Leonardi et al., 2005). Our results highlight the complexity of understanding the impact PANK2 has on cell metabolism. The metabolomics data reinforces the role of PANK2 in mitochondria metabolism (succinyl-CoA, TCA cycle disruptions, increase in cytosolic acetyl-CoA, and the failure of cytosolic PANK1β to rescue). However, if there is no complete mitochondria CoASH synthesis, then how does PANK2 uniquely regulate the mitochondria CoASH pool? More studies on CoASH compartmentalization is vital to understand the nuance behind maintaining subcellular CoASH pools and its impact on cell metabolism.

Acknowledgments.

PANK1β cells were a kind gift from Dr. Ivan Gout.

Methods

Cell culture.

All cell lines were maintained in complete growth media containing DMEM (Life Technologies) supplemented with 10% FBS and 1mM GlutaMAX (Gibco) and 1mM

sodium pyruvate (Sigma) at 37°C under 5% carbon dioxide with a humidified
atmosphere.

siRNA knockdown.

Cells were seeded at 0.3x106 in 6-wells the day before transfection. Two
transfections were performed on sequential days in fresh Opti-MEM (Gibco)
supplemented with 6.5% FBS. Transfections followed the Lipofectamine RNAiMAX
(ThermoFisher) protocol with control scramble siRNA (Origene, SR30004), or human
siRNA oligo duplex against either PANK2 (Origene, SR325087) or PANK1 (Origene,
SR309983).

PAL treatment.

On the fourth day, cells were provided with fresh complete growth media
supplemented with either vehicle BSA or palmitic acid conjugated to BSA at a 250µM
final concentration. Cells were harvested after the 24-hour palmitic acid-bsa exposure.

Autophagic flux measurements.

Autophagy was assessed by tracking the conversion of LC3I to LC3II, p62, and
phosphorylated-p62 with and without the lysosomal inhibitor chloroquine (CQ) (Sigma)
at 100nM final concentration for 4-hours. Rapamyacin was used at 200nM to induce
autophagy.

RIPA buffer protein extraction and western blotting.

Cellular proteins were extracted with RIPA buffer (Thermo Fisher) supplemented
with protease cocktail (Thermo Fisher) and phosphaptase inhibitor cocktail (Sigma) on
ice, centrifuged at 13,000g and supernatant collected. Protein concentration were
measured with the BCA assay and an equal amount of protein separated on SDS-page

and transferred to nitrocellulose membrane 0.2µm (BIO-RAD). Membranes were blocked with 5% BSA. The membranes were incubated with antibodies against anti-LC3B (Abcam; ab51520), anti-p62 Abcam; ab109012, anti-PANK2 (Origene; TA501419), anti-tubulin (Abcam; ab4074), and anti-gapdh (Abcam; ab9485), anti-acetylated tubulin (K40) (Cell signaling; 3971), anti-pan-acetylated lysine (Cell signaling; 9441s). Detected with anti-rabbit or anti-mouse HRP (GE Health Sciences) 1:5,000.

q-PCR measurements.

RNA was extracted using a Direct-zol RNA MiniPrep kit (Zymo Research) according to the manufacturer's instructions, with DNase I (Zymo Research) treatment. Reverse transcription was done with iScript™ Reverse Transcription Supermix for RT-qPCR (BIO-RAD) following manufacturers protocol. The qPCR was performed with SsoAdvanced Universal SYBR Green Supermix (BIO-RAD) following manufacturer's protocol. Primers for GAPDH (IDT; Hs.PT.39a.22214836), HMOX1 (IDT; Hs.PT.58.45340055) and NFE2L2 (IDT; Hs.PT.58.39614837.gs).

Confluence measurements for metabolite normalization.

Growth of cells treated with vehicle BSA or palmitic-bsa were monitored with the Incucyte S3 (Sartorius) at 10X and analyzed with the confluence setting for the 24-hour treatment.

ATP quantification.

ATP from 106 cells was quantified via luminescence using an ATP quantification kit (Abcam; ab113849). The fatty acid inhibitor trimetazidine (Sigma) was used at a final concentration of 2.5mM.

Metabolite measurements for PANK2 KO and siRNA knockdown.

Cells were grown in 6-wells, confluence tracked with the Incucyte for normalization, washed with ice cold PBS followed by H2O. GC-MS and LC-MS measurements performed by the University of Iowa's metabolomics core. The plates were snap frozen in liquid nitrogen. Cell culture plates were lyophilized overnight and then scraped into 1 ml of ice-cold 2:2:1 methanol:acetonitrile:water containing a mixture of internal standards (D4-citric acid, D4-succinic acid, D8-valine, and U13C-labeled glutamine, glutamic acid, lysine, methionine, serine, and tryptophan; Cambridge Isotope Laboratories) to extract metabolites. The cell extraction mixtures were transferred to a microcentrifuge tube and flash frozen in liquid nitrogen. Frozen extracts were thawed for 10 minutes in a water bath sonicator and then incubated for 1 hour at –20°C. Metabolite extracts were centrifuged for 10 minutes at 21,000 x g and supernatants were transferred to autosampler vials (GC) or microcentrifuge tubes (LC) and dried using a SpeedVac vacuum concentrator (Thermo).

GC-derivatization. Dried metabolite extracts were derivatized using methoxyamine hydrochloride (MOX) and N,O-Bis(trimethylsilyl)trifluoroacetamide (TMS). Briefly, dried extracts were reconstituted in 30 μl of 11.4 mg/ml MOX in anhydrous pyridine, vortexed for 5 minutes, and heated for 1 hour at 60°C. Next, 20 μl of TMS was added to each sample, samples were vortexed for 1 minute, and heated for 30 minutes at 60°C.

GC-MS method. Derivatized samples were analyzed using GC-MS. GC was conducted using a Trace 1300 GC (Thermo) fitted with a TraceGold TG-5SilMS column (Thermo). 1 μl of derivatized sample was injected into the GC operating under the following conditions: split ratio = 20-1, split flow = 24 μl/minute, purge flow = 5

ml/minute, carrier mode = Constant Flow, and carrier flow rate = 1.2 ml/minute. The GC

oven temperature gradient was as follows: 80°C for 3 minutes, increasing at a rate of

20°C/minute to 280°C, and holding at a temperature at 280°C for 8 minutes. Ion

detection was performed by an ISQ 7000 mass spectrometer (Thermo) operated from

3.90 to 21.00 minutes in EI mode (-70eV) using select ion monitoring (SIM).

LC-sample preparation. Dried metabolite extracts were reconstituted in a 1/10th volume

of 1:1 acetonitrile:water and vortexed for 10 minutes (200 µl of metabolite extract was

resuspended in 20 µl). Reconstituted extracts were maintained at -20°C overnight and

centrifuged at 21,000 x g for 10 minutes. Supernatants were transferred to autosampler

vials for LC-MS analysis.

LC-MS method. 2 µL of the prepared samples were separated using a Millipore

SeQuant ZIC-pHILIC (2.1 X 150 mm, 5 µm particle size) column with a ZIC-pHILIC

guard column (20 x 2.1 mm) attached to a Thermo Vanquish Flex UHPLC. Mobile phase

was comprised of Buffer A [20 mM $(NH_4)_2CO_3$, 0.1% NH_4OH (v/v)] and Buffer B

[acetonitrile]. The chromatographic gradient was run at a flow rate of 0.150 mL/min as

follows: 0–21 min-linear gradient from 80 to 20% Buffer B; 20-20.5 min-linear gradient

from 20 to 80% Buffer B; and 20.5–28 min-hold at 80% Buffer B. Data was acquired

using a Thermo Q Exactive MS operated in polarity-switching fullscan mode from 70-

1000 m/z with a spray voltage set to 3.0 kV, the heated capillary held at 275°C, and the

HESI probe held at 350°C. The sheath gas flow was set to 40 units, the auxiliary gas flow

was set to 15 units, and the sweep gas flow was set to 1 unit. MS data resolution was set

at 70,000, the AGC target at 10e6, and the maximum injection time at 200 ms.

Data analysis. Raw data were analyzed using TraceFinder 4.1 (Thermo). For GC-MS data, metabolite identification and annotation required at least two ions (target + confirming) and a unique retention time per metabolite that corresponded to the ions and retention times of reference standards previously determined in-house. For LC-MS data, metabolite identification and annotation required ion accurate mass ± 5 mmu and retention time per metabolite to correspond to the ions and retentions times of reference standards previously determined in-house. A pooled-sample generated from metabolite extracts was analyzed before, at a set interval, and after the analytical run to correct peak intensities using the NOREVA tool (Li et al., 2017).

Mitochondria and cytosol fractionation.

Cells were grown in two T25 flasks each, washed with PBS and pelleted at 500g. The cell pellet was washed with hypoosmotic buffer (2mM HEPES, 0.15mM MgCl2, 10mM KCl, 0.5mM EGTA, 0.25M sucrose, pH 7.4) and centrifuged for 5min at 1500g. The pellet was resuspended in hypoosmotic buffer supplemented with 20uM PMSF (Sigma) and 10μg/ml protease inhibitor cocktail (Fisher Scientific), followed by homogenization with the Dounce homogenizer. Whole-cell fraction samples were collected from the homogenate and sucrose was added to the remaining cell suspension to a final concentration of 0.32M and centrifuged for 5min at 1000g. The supernatant was centrifuged for 10min at 20,000g. The mitochondria pellet was resuspended in resuspension buffer (2mM HEPES, 0.32M sucrose, pH 7.4) and supernatant spun for 1hr at 100,000g to collect the cytosolic and membrane fractions. Protein content was quantified with the Bradford assay and fractions stored at -80 for either western blotting or metabolic analysis.

CHAPTER 4

DISCUSSION AND CONCLUSION

Discussion

How the mitochondria obtain CoASH is an over 40-year old debate. The first

published study show that isolated rat heart mitochondria can use 4-phosphopantetheine

to generate CoASH (Skrede & Halvorsen, 1979). Although this study does not show a

complete mitochondria CoASH biosynthesis pathway, we cannot exclude the possibility

that mitochondria can perform complete *de novo* CoASH synthesis, partially because the

conditions tested did not include PANK2 activating conditions i.e. fatty acid oxidation.

In figure 4.1, we show possible routes of how mitochondria obtain CoASH (Fig

4.1). SLC25A42 is a mitochondria inner membrane protein transporter that in

reconstituted liposomes can transport CoASH, dephospho-CoA, ADP, and adenosine

3′,5′-diphosphate (Fiermonte et al., 2009). In a yeast knockout model with low

mitochondria CoASH, *SLC25A42* complementation is shown to rescue growth defects

and mitochondria CoASH levels (Fiermonte et al., 2009). As such, it appears likely that

SLC25A42 is a *bona fide* mitochondria CoASH or dephospho-CoASH transporter.

Research has also shown that 4-phosphopanteheine (the precursor for COASY) can

diffuse across membranes (Srinivasan et al., 2015), but it is unknown if 4-

phosphopanteheine can diffuse across mitochondria inner membranes that have a unique

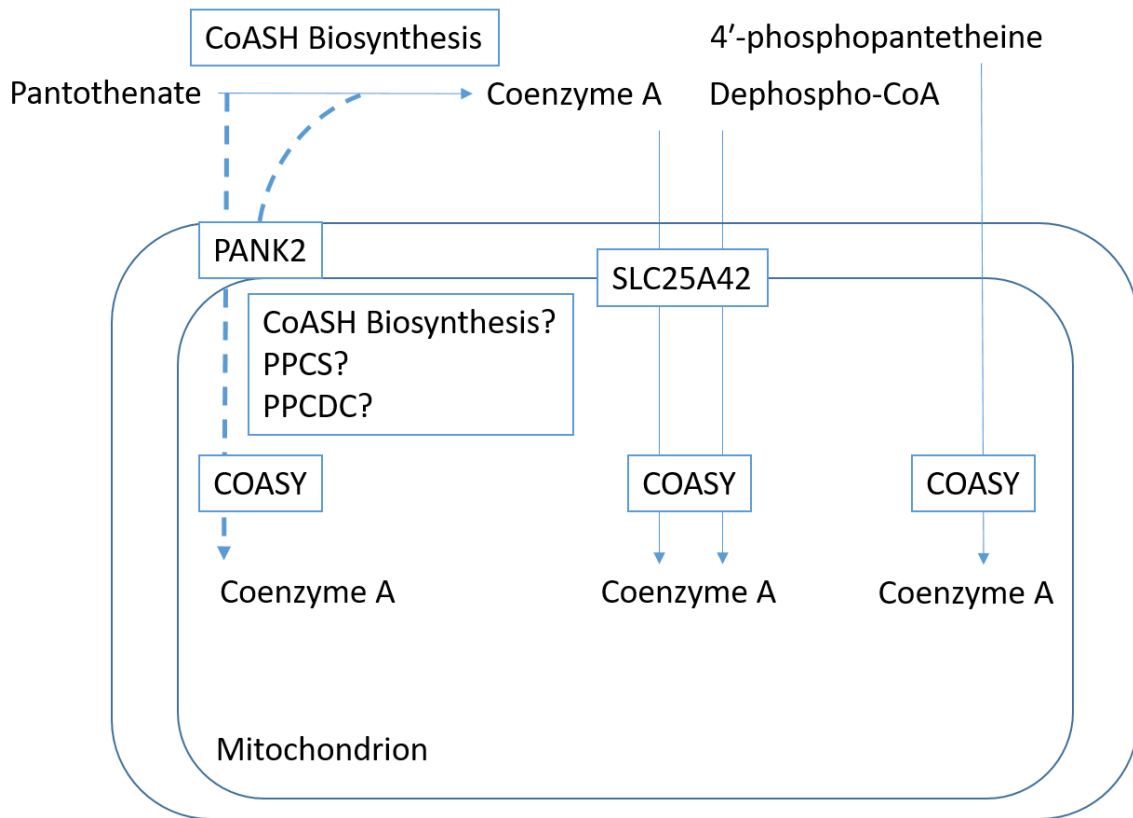composition (Schenkel & Bakovic, 2014).

Figure 4.1. Proposed routes for mitochondria to obtain CoASH. The mitochondria contain PANK2, COASY, and SLC25A42. SLC25A42 is a mitochondria transporter that can transport coenzyme A and depshosho-CoA into the mitochondria matrix. 4-phosphopantetheine is an intermediate in coenzyme A biosynthesis and also a substrate for COASY. 4-phosphopantetheine can passively diffuse across membranes, but it is not known if 4-phosphopantetheine can diffuse across the mitochondria membrane. PANK2 is localized to the mitochondria, but it is unclear if PANK2 iniates complete mitochondria coenzyme A synthesis or if PANK2 catalyze the first step and the following coenzyme A biosynthesis steps are cytosolic.

In the field of PKAN, how mitochondria obtain CoASH is an important outstanding question. PANK2 is a mitochondrial protein, but it is unclear why PANK2 is localized to the mitochondria, especially if there is not complete mitochondria synthesis (Alfonso-Pecchio et al., 2012; Hortnagel, 2003; Kotzbauer et al., 2005). One study show that mitochondria isolated from fibroblasts from individuals affected with PKAN have a mitochondria CoASH deficiency (Álvarez-Córdoba et al., 2019). This is promising evidence for PANK2 controlling mitochondria CoASH, but taking into account the

heterogeneity and possible individual variations in fibroblast CoASH samples, it needs further validation. In our studies, PANK1β could not rescue the loss of PANK2, hypothetically because PANK2 is unique in controlling mitochondria CoASH. Nonetheless, the inability of PANK1β to affect mitochondria CoASH is difficult to reconcile with SLC25A42 as a mitochondria CoASH transporter. If SLC25A42 is a dephospho-CoA transporter *in vivo* then it is possible that elevated cytosolic CoASH does not affect the mitochondria. However, then PANK2 initiated CoASH synthesis has to be coupled to SLC25A42 transport before completed CoASH synthesis.

The question of mitochondria CoASH synthesis and PANK2s role in the mitochondria remains to be answered. The NAD+ field has made progress in compartmentalized NAD+ synthesis by using an intracellular fluorescence biosensor (Ryu et al., 2018). Developing a CoASH biosensor would be useful in tackling compartmentalized CoASH and acetyl-CoA synthesis. Another technique would be to use SILEC-SF to label CoASH in PANK knockout models tracing compartmentalized CoASH synthesis (Basu & Blair, 2012; Trefely et al., 2022). High-resolution microscopy combined with co-localization and or interaction studies would further help in determining if a PANK2 mitochondria CoASH synthesizing complex exists. A combination of these approaches might be necessary to determine how the mitochondria obtain CoASH.

Conclusion

In conclusion, we have uncovered a key role for PANK2 in fatty acid metabolism that is non-redundant with PANK1 and independent of whole-cell CoASH concentrations. Cellular conditions wherein fatty acids are preferentially oxidized over

glucose provoke a remarkable cellular starvation phenotype in PANK2-deficient cells despite a nutrient-replete milieu. This cellular phenotype exposes a unique vulnerability of PANK2-deficient cells to metabolic switching. Although further studies will be required to more completely understand this phenomenon, these findings suggest that there may be a therapeutic benefit for PKAN (and perhaps COPAN) patients to avoid fasting conditions. Our observations are compatible with the observation that a ketogenic diet (widely-considered to be "neuroprotective") provokes a neurodegenerative phenotype in PKAN mice.

Based on the metabolomics data, diminished succinyl-CoA levels appear to be a consequence of PANK2 deficiency and could serve as a potential biomarker for PANK2 deficient states. Succinyl CoA:3-oxoacid CoA transferase 1 (OXCT1) serves as a key enzyme in ketone body utilization and catalyzes the transfer of CoA from succinyl-CoA to acetoacetate. This process could be disrupted under succinyl-CoA depleted conditions, providing an additional explanation for the negative consequences observed when PANK2 knockout mice are challenged with a ketogenic diet.

Future studies are needed to directly measure mitochondrial CoASH levels and determine if mitochondrial CoASH levels are truly diminished as anticipated. If a diminished mitochondrial CoASH pool was confirmed in PANK2-deficient states, low succinyl-CoA could occur as a result of substrate competition as acyl species siphon an already limited mitochondria pool of CoASH and strain an already tenuous TCA cycle. Low succinyl-CoA could in turn disrupt heme synthesis by limiting substrate availability for the rate-limiting step of this process, aminolevulinate synthase.

86

Intriguingly, the acyl carrier protein (ACP) also serves an evolutionarily conserved role in both fatty acid synthesis (utilizing both malonyl-CoA and acetyl-CoA) and iron-sulfur cluster biosynthesis (Van Vranken et al., 2016). ACP function depends on 4-phosphopantetheinylation, a CoASH-coupled post-translational modification (Beld et al., 2014). A diminished mitochondrial CoASH pool could thus both disrupt heme and iron-sulfur cluster biosynthesis, linking a loss of PANK2 to disrupted iron homeostasis.

In summary, my studies have uncovered an essential role for PANK2 in fatty acid metabolism and indicated that PANK1 and PANK2 function are non-redundant. This has important implications for the development of PKAN therapeutics, as our findings suggest that therapeutic strategies that seek to augment PANK1/PANK3 activity are unlikely to be successful. Our findings suggest that diminished succinyl-CoA may play an important role in PKAN pathobiology, not only serving as a potential biomarker for PKAN-deficient states, but potentially contributing to some of the abnormalities of iron homeostasis that characterize the disease via disruption of heme and/or iron-sulfur cluster biosynthesis. Finally, our experiments have raised important questions about cellular CoASH pools, synthesis, compartmentalization and transport that will require additional studies to answer. Nevertheless, the findings suggest a rich, complex, and finely-regulated network of CoASH dynamics that integrate cellular growth, metabolism, and stress signaling in previously unappreciated ways.

REFERNCES

Albaugh, B. N., Arnold, K. M., & Denu, J. M. (2011). KAT(ching) Metabolism by the Tail: Insight into the Links between Lysine Acetyltransferases and Metabolism. *ChemBioChem*, *12*(2), 290-298. https://doi.org/10.1002/cbic.201000438

Alfonso-Pecchio, A., Garcia, M., Leonardi, R., & Jackowski, S. (2012). Compartmentalization of Mammalian Pantothenate Kinases. *PLoS ONE*, *7*(11), e49509. https://doi.org/10.1371/journal.pone.0049509

Almannai, M., Alasmari, A., Alqasmi, A., Faqeih, E., Al Mutairi, F., Alotaibi, M., Samman, M. M., Eyaid, W., Aljadhai, Y. I., Shamseldin, H. E., Craigen, W., & Alkuraya, F. S. (2018). Expanding the phenotype of SLC25A42 -associated mitochondrial encephalomyopathy. *Clinical Genetics*, *93*(5), 1097-1102. https://doi.org/10.1111/cge.13210

Álvarez-Córdoba, M., Fernández Khoury, A., Villanueva-Paz, M., Gómez-Navarro, C., Villalón-García, I., Suárez-Rivero, J. M., Povea-Cabello, S., De La Mata, M., Cotán, D., Talaverón-Rey, M., Pérez-Pulido, A. J., Salas, J. J., Pérez-Villegas, E. M., Díaz-Quintana, A., Armengol, J. A., & Sánchez-Alcázar, J. A. (2019). Pantothenate Rescues Iron Accumulation in Pantothenate Kinase-Associated Neurodegeneration Depending on the Type of Mutation. *Molecular Neurobiology*, *56*(5), 3638-3656. https://doi.org/10.1007/s12035-018-1333-0

Arber, C. E., Li, A., Houlden, H., & Wray, S. (2016). Review: Insights into molecular mechanisms of disease in neurodegeneration with brain iron accumulation: unifying theories. *Neuropathology and Applied Neurobiology*, *42*(3), 220-241. https://doi.org/10.1111/nan.12242

Atamna, H. (2004). Heme, iron, and the mitochondrial decay of ageing. *Ageing research reviews*, *3*(3), 303-318.

Basu, S. S., & Blair, I. A. (2012). SILEC: a protocol for generating and using isotopically labeled coenzyme A mass spectrometry standards. *Nature protocols*, *7*(1), 1-11.

Baumgartner, M. R., Hörster, F., Dionisi-Vici, C., Haliloglu, G., Karall, D., Chapman, K. A., Huemer, M., Hochuli, M., Assoun, M., Ballhausen, D., Burlina, A., Fowler, B., Grünert, S. C., Grünewald, S., Honzik, T., Merinero, B., Pérez-Cerdá, C., Scholl-Bürgi, S., Skovby, F., . . . Chakrapani, A. (2014). Proposed guidelines for the diagnosis and management of methylmalonic and propionic acidemia. *Orphanet Journal of Rare Diseases*, *9*(1), 130. https://doi.org/10.1186/s13023-014-0130-8

Beld, J., Sonnenschein, E. C., Vickery, C. R., Noel, J. P., & Burkart, M. D. (2014). The phosphopantetheinyl transferases: catalysis of a post-translational modification crucial for life. *Nat. Prod. Rep.*, *31*(1), 61-108. https://doi.org/10.1039/c3np70054b

Berge, R. K., Hosøy, L. H., & Farstad, M. N. (1984). Influence of dietary status on liver palmitoyl-coa hydrolase, peroxisomal enzymes, coash and long-chain acyl-coa in rats. *International Journal of Biochemistry*, *16*(4), 403-410. https://doi.org/10.1016/0020-711x(84)90139-3

Bjørkøy, G., Lamark, T., Pankiv, S., Øvervatn, A., Brech, A., & Johansen, T. (2009). Monitoring autophagic degradation of p62/SQSTM1. *Methods in enzymology*, *452*, 181-197.

Brunetti, D., Dusi, S., Giordano, C., Lamperti, C., Morbin, M., Fugnanesi, V., Marchet, S., Fagiolari, G., Sibon, O., Moggio, M., D'Amati, G., & Tiranti, V. (2014). Pantethine treatment is effective in recovering the disease phenotype induced by ketogenic diet in a pantothenate kinase-associated neurodegeneration mouse model. *Brain*, *137*(1), 57-68. https://doi.org/10.1093/brain/awt325

Crewe, C., Schafer, C., Lee, I., Kinter, M., & Szweda, L. I. (2017). Regulation of pyruvate dehydrogenase kinase 4 in the heart through degradation by the Lon protease in response to mitochondrial substrate availability. *Journal of Biological Chemistry*, *292*(1), 305-312.

Crooks, D. R., Maio, N., Lane, A. N., Jarnik, M., Higashi, R. M., Haller, R. G., Yang, Y., Fan, T. W. M., Linehan, W. M., & Rouault, T. A. (2018). Acute loss of iron–sulfur clusters results in metabolic reprogramming and generation of lipid droplets in mammalian cells. *Journal of Biological Chemistry*, *293*(21), 8297-8311. https://doi.org/10.1074/jbc.ra118.001885

Dansie, L. E., Reeves, S., Miller, K., Zano, S. P., Frank, M., Pate, C., Wang, J., & Jackowski, S. (2014). Physiological roles of the pantothenate kinases. *Biochemical Society Transactions*, *42*(4), 1033.

Daugherty, M., Polanuyer, B., Farrell, M., Scholle, M., Lykidis, A., de Crécy-Lagard, V., & Osterman, A. (2002). Complete reconstitution of the human coenzyme A biosynthetic pathway via comparative genomics. *Journal of Biological Chemistry*, *277*(24), 21431-21439.

Dusi, S., Valletta, L., Tobias, Tsuchiya, Y., Venco, P., Pasqualato, S., Goffrini, P., Tigano, M., Demchenko, N., Wieland, T., Schwarzmayr, T., Tim, Invernizzi, F., Garavaglia, B., Gregory, A., Sanford, L., Hamada, J., Bettencourt, C., Houlden, H., . . . Tiranti, V. (2014). Exome Sequence Reveals Mutations in CoA Synthase as a Cause of Neurodegeneration with Brain Iron Accumulation. *The American Journal of Human Genetics*, *94*(1), 11-22. https://doi.org/10.1016/j.ajhg.2013.11.008

Elpeleg, O., Miller, C., Hershkovitz, E., Bitner-Glindzicz, M., Bondi-Rubinstein, G., Rahman, S., Pagnamenta, A., Eshhar, S., & Saada, A. (2005). Deficiency of the ADP-Forming Succinyl-CoA Synthase Activity Is Associated with Encephalomyopathy and Mitochondrial DNA Depletion. *The American Journal of Human Genetics*, *76*(6), 1081-1086. https://doi.org/10.1086/430843

Fiermonte, G., Paradies, E., Todisco, S., Marobbio, C. M. T., & Palmieri, F. (2009). A Novel Member of Solute Carrier Family 25 (SLC25A42) Is a Transporter of Coenzyme A and Adenosine 3′,5′-Diphosphate in Human Mitochondria. *Journal of Biological Chemistry*, *284*(27), 18152-18159. https://doi.org/10.1074/jbc.m109.014118

Gout, I. (2018). Coenzyme A, protein CoAlation and redox regulation in mammalian cells. *Biochemical Society Transactions*, *46*(3), 721-728. https://doi.org/10.1042/bst20170506

Herzig, S., & Shaw, R. J. (2018). AMPK: guardian of metabolism and mitochondrial homeostasis. *Nature Reviews Molecular Cell Biology*, *19*(2), 121-135. https://doi.org/10.1038/nrm.2017.95

HORIE, S., ISOBE, M., & SUGA, T. (1986). Changes in CoA pools in hepatic peroxisomes of the rat, under various conditions. *The Journal of Biochemistry*, *99*(5), 1345-1352.

Hortnagel, K. (2003). An isoform of hPANK2, deficient in pantothenate kinase-associated neurodegeneration, localizes to mitochondria. *Human molecular genetics*, *12*(3), 321-327. https://doi.org/10.1093/hmg/ddg026

Hue, L., & Taegtmeyer, H. (2009). The Randle cycle revisited: a new head for an old hat. *American Journal of Physiology-Endocrinology and Metabolism*, *297*(3), E578-E591.

HumanProteinAtlas. (2022a). *PPCDC*. Retrieved 3/22 from https://www.proteinatlas.org/ENSG00000138621-PPCDC/subcellular

HumanProteinAtlas. (2022b). *PPCS*. The human protein atlas. Retrieved 3/16/2022 from https://www.proteinatlas.org/ENSG00000127125-PPCS/subcellular

Iankova, V., Karin, I., Klopstock, T., & Schneider, S. A. (2021). Emerging disease-modifying therapies in Neurodegeneration with Brain Iron Accumulation (NBIA) disorders. *Frontiers in Neurology*, *12*.

Iuso, A., Wiersma, M., Schüller, H.-J., Pode-Shakked, B., Marek-Yagel, D., Grigat, M., Schwarzmayr, T., Berutti, R., Alhaddad, B., Kanon, B., Grzeschik, N. A., Okun, J. G., Perles, Z., Salem, Y., Barel, O., Vardi, A., Rubinshtein, M., Tirosh, T., Dubnov-Raz, G., . . . Anikster, Y. (2018). Mutations in PPCS, Encoding Phosphopantothenoylcysteine Synthetase, Cause Autosomal-Recessive Dilated Cardiomyopathy. *The American Journal of Human Genetics*, *102*(6), 1018-1030. https://doi.org/10.1016/j.ajhg.2018.03.022

Jensen, N. J., Wodschow, H. Z., Nilsson, M., & Rungby, J. (2020). Effects of ketone bodies on brain metabolism and function in neurodegenerative diseases. *International Journal of Molecular Sciences*, *21*(22), 8767.

Jeong, S. Y., Hogarth, P., Placzek, A., Gregory, A. M., Fox, R., Zhen, D., Hamada, J., van der Zwaag, M., Lambrechts, R., & Jin, H. (2019). 4′-Phosphopantetheine

corrects CoA, iron, and dopamine metabolic defects in mammalian models of PKAN. *EMBO molecular medicine*, *11*(12), e10489.

Johnson, M. A., Kuo, Y. M., Westaway, S. K., Parker, S. M., Ching, K. H. L., Gitschier, J., & Hayflick, S. J. (2004). Mitochondrial Localization of Human PANK2 and Hypotheses of Secondary Iron Accumulation in Pantothenate Kinase-Associated Neurodegeneration. *Annals of the New York Academy of Sciences*, *1012*(1), 282-298. https://doi.org/10.1196/annals.1306.023

Kotzbauer, P. T., Truax, A. C., Trojanowski, J. Q., & Lee, V. M.-Y. (2005). Altered neuronal mitochondrial coenzyme A synthesis in neurodegeneration with brain iron accumulation caused by abnormal processing, stability, and catalytic activity of mutant pantothenate kinase 2. *Journal of Neuroscience*, *25*(3), 689-698.

Kruer, M. C., Hiken, M., Gregory, A., Malandrini, A., Clark, D., Hogarth, P., Grafe, M., Hayflick, S. J., & Woltjer, R. L. (2011). Novel histopathologic findings in molecularly-confirmed pantothenate kinase-associated neurodegeneration. *Brain*, *134*(4), 947-958. https://doi.org/10.1093/brain/awr042

Kuo, Y.-M., Duncan, J. L., Westaway, S. K., Yang, H., Nune, G., Xu, E. Y., Hayflick, S. J., & Gitschier, J. (2005). Deficiency of pantothenate kinase 2 (Pank2) in mice leads to retinal degeneration and azoospermia. *Human molecular genetics*, *14*(1), 49-57.

Lambrechts, R. A., Schepers, H., Yu, Y., van der Zwaag, M., Autio, K. J., Vieira-Lara, M. A., Bakker, B. M., Tijssen, M. A., Hayflick, S. J., & Grzeschik, N. A. (2019). CoA-dependent activation of mitochondrial acyl carrier protein links four neurodegenerative diseases. *EMBO molecular medicine*, *11*(12), e10488.

Lee, J.-S., Oh, S.-J., Choi, H.-J., Kang, J. H., Lee, S.-H., Ha, J. S., Woo, S. M., Jang, H., Lee, H., & Kim, S.-Y. (2020). ATP Production Relies on Fatty Acid Oxidation Rather than Glycolysis in Pancreatic Ductal Adenocarcinoma. *Cancers*, *12*(9), 2477. https://doi.org/10.3390/cancers12092477

Leonardi, R., Rehg, J. E., Rock, C. O., & Jackowski, S. (2010). Pantothenate Kinase 1 Is Required to Support the Metabolic Transition from the Fed to the Fasted State. *PLoS ONE*, *5*(6), e11107. https://doi.org/10.1371/journal.pone.0011107

Leonardi, R., Rock, C. O., Jackowski, S., & Zhang, Y.-M. (2007). Activation of human mitochondrial pantothenate kinase 2 by palmitoylcarnitine. *Proceedings of the National Academy of Sciences*, *104*(5), 1494-1499.

Leonardi, R., Rock, C. O., Jackowski, S., & Zhang, Y. M. (2007). Activation of human mitochondrial pantothenate kinase 2 by palmitoylcarnitine. *Proceedings of the National Academy of Sciences*, *104*(5), 1494-1499. https://doi.org/10.1073/pnas.0607621104

Leonardi, R., Zhang, Y., Rock, C., & Jackowski, S. (2005). Coenzyme A: Back in action. *Progress in lipid research.*, *44*(2-3), 125-153. https://doi.org/10.1016/j.plipres.2005.04.001

info:doi/10.1016/j.plipres.2005.04.001

Leoni, V., Strittmatter, L., Zorzi, G., Zibordi, F., Dusi, S., Garavaglia, B., Venco, P., Caccia, C., Souza, A. L., & Deik, A. (2012). Metabolic consequences of mitochondrial coenzyme A deficiency in patients with PANK2 mutations. *Molecular Genetics and Metabolism*, *105*(3), 463-471.

Li, B., Tang, J., Yang, Q., Li, S., Cui, X., Li, Y., Chen, Y., Xue, W., Li, X., & Zhu, F. (2017). NOREVA: normalization and evaluation of MS-based metabolomics data. *Nucleic acids research*, *45*(W1), W162-W170.

Lin, C.-C., Kitagawa, M., Tang, X., Hou, M.-H., Wu, J., Qu, D. C., Srinivas, V., Liu, X., Thompson, J. W., Mathey-Prevot, B., Yao, T.-P., Lee, S. H., & Chi, J.-T. (2018). CoA synthase regulates mitotic fidelity via CBP-mediated acetylation. *Nature Communications*, *9*(1). https://doi.org/10.1038/s41467-018-03422-6

Madiraju, P., Pande, S. V., Prentki, M., & Madiraju, S. R. M. (2009). Mitochondrial acetylcarnitine provides acetyl groups for nuclear histone acetylation. *Epigenetics*, *4*(6), 399-403. https://doi.org/10.4161/epi.4.6.9767

Mariño, G., Pietrocola, F., Eisenberg, T., Kong, Y., Shoaib, Andryushkova, A., Schroeder, S., Pendl, T., Harger, A., Niso-Santano, M., Zamzami, N., Scoazec, M., Durand, S., David, Álvaro, Martins, I., Kepp, O., Senovilla, L., Bauvy, C., . . . Kroemer, G. (2014). Regulation of Autophagy by Cytosolic Acetyl-Coenzyme A. *Molecular Cell*, *53*(5), 710-725. https://doi.org/10.1016/j.molcel.2014.01.016

McDonnell, E., Crown, S. B., Fox, D. B., Kitir, B., Ilkayeva, O. R., Olsen, C. A., Grimsrud, P. A., & Hirschey, M. D. (2016). Lipids reprogram metabolism to become a major carbon source for histone acetylation. *Cell reports*, *17*(6), 1463-1472.

Mignani, L., Gnutti, B., Zizioli, D., & Finazzi, D. (2021). Coenzyme a Biochemistry: From Neurodevelopment to Neurodegeneration. *Brain Sciences*, *11*(8), 1031. https://doi.org/10.3390/brainsci11081031

Morais, V. A., Verstreken, P., Roethig, A., Smet, J., Snellinx, A., Vanbrabant, M., Haddad, D., Frezza, C., Mandemakers, W., Vogt-Weisenhorn, D., Van Coster, R., Wurst, W., Scorrano, L., & De Strooper, B. (2009). Parkinson's disease mutations in PINK1 result in decreased Complex I activity and deficient synaptic function. *EMBO molecular medicine*, *1*(2), 99-111. https://doi.org/10.1002/emmm.200900006

Naquet, P., Kerr, E. W., Vickers, S. D., & Leonardi, R. (2020). Regulation of coenzyme A levels by degradation: the 'Ins and Outs'. *Progress in lipid research*, *78*, 101028.

Nemazanyy, I., Panasyuk, G., Zhyvoloup, A., Panayotou, G., Gout, I. T., & Filonenko, V. (2004). Specific interaction between S6K1 and CoA synthase: a potential link between the mTOR/S6K pathway, CoA biosynthesis and energy metabolism. *FEBS Letters*, *578*(3), 357-362. https://doi.org/10.1016/j.febslet.2004.10.091

Orellana, D. I., Santambrogio, P., Rubio, A., Yekhlef, L., Cancellieri, C., Dusi, S., Giannelli, S. G., Venco, P., Mazzara, P. G., Cozzi, A., Ferrari, M., Garavaglia, B., Taverna, S., Tiranti, V., Broccoli, V., & Levi, S. (2016). Coenzyme A corrects pathological defects in human neurons of PANK 2-associated neurodegeneration. *EMBO molecular medicine*, *8*(10), 1197-1211. https://doi.org/10.15252/emmm.201606391

Pang, Z., Chong, J., Zhou, G., David, A., Chang, L., Barrette, M., Gauthier, C., Jacques, P.-É., Li, S., & Xia, J. (2021). MetaboAnalyst 5.0: narrowing the gap between raw spectra and functional insights. *Nucleic acids research*, *49*(W1), W388-W396. https://doi.org/10.1093/nar/gkab382

Pettersen, I. K. N., Tusubira, D., Ashrafi, H., Dyrstad, S. E., Hansen, L., Liu, X.-Z., Nilsson, L. I. H., Løvsletten, N. G., Berge, K., & Wergedahl, H. (2019). Upregulated PDK4 expression is a sensitive marker of increased fatty acid oxidation. *Mitochondrion*, *49*, 97-110.

Randle, P. J., Garland, P. B., Hales, C. N., & Newsholme, E. A. (1963). THE GLUCOSE FATTY-ACID CYCLE ITS ROLE IN INSULIN SENSITIVITY AND THE METABOLIC DISTURBANCES OF DIABETES MELLITUS. *The Lancet*, *281*(7285), 785-789. https://doi.org/10.1016/s0140-6736(63)91500-9

Rath, S., Sharma, R., Gupta, R., Ast, T., Chan, C., Durham, T. J., Goodman, R. P., Grabarek, Z., Haas, M. E., Hung, W. H. W., Joshi, P. R., Jourdain, A. A., Kim, S. H., Kotrys, A. V., Lam, S. S., McCoy, J. G., Meisel, J. D., Miranda, M., Panda, A., . . . Mootha, V. K. (2021). MitoCarta3.0: an updated mitochondrial proteome now with sub-organelle localization and pathway annotations. *Nucleic acids research*, *49*(D1), D1541-D1547. https://doi.org/10.1093/nar/gkaa1011

Redmann, M., Benavides, G. A., Berryhill, T. F., Wani, W. Y., Ouyang, X., Johnson, M. S., Ravi, S., Barnes, S., Darley-Usmar, V. M., & Zhang, J. (2017). Inhibition of autophagy with bafilomycin and chloroquine decreases mitochondrial quality and bioenergetic function in primary neurons. *Redox Biology*, *11*, 73-81.

Rhee, H.-W., Zou, P., Udeshi, N. D., Martell, J. D., Mootha, V. K., Carr, S. A., & Ting, A. Y. (2013). Proteomic Mapping of Mitochondria in Living Cells via Spatially Restricted Enzymatic Tagging. *Science*, *339*(6125), 1328-1331. https://doi.org/10.1126/science.1230593

Robishaw, J. D., Berkich, D., & Neely, J. R. (1982). Rate-limiting step and control of coenzyme A synthesis in cardiac muscle. *Journal of Biological Chemistry*, *257*(18), 10967-10972.

Rock, C. O., Karim, M. A., Zhang, Y.-M., & Jackowski, S. (2002). The murine pantothenate kinase (Pank1) gene encodes two differentially regulated pantothenate kinase isozymes. *Gene*, *291*(1-2), 35-43. https://doi.org/10.1016/s0378-1119(02)00564-4

Rowland, E. A., Snowden, C. K., & Cristea, I. M. (2018). Protein lipoylation: an evolutionarily conserved metabolic regulator of health and disease. *Current Opinion in Chemical Biology*, *42*, 76-85. https://doi.org/10.1016/j.cbpa.2017.11.003

Ryu, K. W., Nandu, T., Kim, J., Challa, S., DeBerardinis, R. J., & Kraus, W. L. (2018). Metabolic regulation of transcription through compartmentalized NAD+ biosynthesis. *Science*, *360*(6389), eaan5780.

Schafer, C., Young, Z. T., Makarewich, C. A., Elnwasany, A., Kinter, C., Kinter, M., & Szweda, L. I. (2018). Coenzyme A–mediated degradation of pyruvate dehydrogenase kinase 4 promotes cardiac metabolic flexibility after high-fat feeding in mice. *Journal of Biological Chemistry*, *293*(18), 6915-6924. https://doi.org/10.1074/jbc.ra117.000268

Schenkel, L. C., & Bakovic, M. (2014). Formation and Regulation of Mitochondrial Membranes. *International Journal of Cell Biology*, *2014*, 1-13. https://doi.org/10.1155/2014/709828

Shi, L., & Tu, B. P. (2015). Acetyl-CoA and the regulation of metabolism: mechanisms and consequences. *Current Opinion in Cell Biology*, *33*, 125-131. https://doi.org/10.1016/j.ceb.2015.02.003

Siudeja, K., Srinivasan, B., Xu, L., Rana, A., De Jong, J., Nollen, E. A. A., Jackowski, S., Sanford, L., Hayflick, S., & Sibon, O. C. M. (2011). Impaired Coenzyme A metabolism affects histone and tubulin acetylation in Drosophila and human cell models of pantothenate kinase associated neurodegeneration. *EMBO molecular medicine*, *3*(12), 755-766. https://doi.org/10.1002/emmm.201100180

Skrede, S., & Halvorsen, O. (1979). Mitochondrial biosynthesis of coenzyme A. *Biochemical and Biophysical Research Communications*, *91*(4), 1536-1542. https://doi.org/10.1016/0006-291x(79)91239-7

Srinivasan, B., Baratashvili, M., Van Der Zwaag, M., Kanon, B., Colombelli, C., Lambrechts, R. A., Schaap, O., Nollen, E. A., Podgoršek, A., Kosec, G., Petković, H., Hayflick, S., Tiranti, V., Reijngoud, D.-J., Grzeschik, N. A., & Sibon, O. C. M. (2015). Extracellular 4′-phosphopantetheine is a source for intracellular coenzyme A synthesis. *Nature Chemical Biology*, *11*(10), 784-792. https://doi.org/10.1038/nchembio.1906

Sutendra, G., Kinnaird, A., Dromparis, P., Paulin, R., Trevor, Haromy, A., Hashimoto, K., Zhang, N., Flaim, E., & Evangelos. (2014). A Nuclear Pyruvate Dehydrogenase Complex Is Important for the Generation of Acetyl-CoA and Histone Acetylation. *Cell*, *158*(1), 84-97. https://doi.org/10.1016/j.cell.2014.04.046

Tahiliani, A. G. (1991). Evidence for net uptake and efflux of mitochondrial coenzyme A. *Biochimica et Biophysica Acta (BBA) - Biomembranes*, *1067*(1), 29-37. https://doi.org/10.1016/0005-2736(91)90022-z

Tahiliani, A. G., & Beinlich, C. J. (1991). Pantothenic Acid in Health and Disease. In (pp. 165-228). Elsevier. https://doi.org/10.1016/s0083-6729(08)60684-6

Tanji, K., Miki, Y., Ozaki, T., Maruyama, A., Yoshida, H., Mimura, J., Matsumiya, T., Mori, F., Imaizumi, T., Itoh, K., Kakita, A., Takahashi, H., & Wakabayashi, K. (2014). Phosphorylation of serine 349 of p62 in Alzheimer's disease brain. *Acta Neuropathologica Communications*, *2*(1), 50. https://doi.org/10.1186/2051-5960-2-50

Theodoulou, F. L., Sibon, O. C., Jackowski, S., & Gout, I. (2014). Coenzyme A and its derivatives: renaissance of a textbook classic. *Biochemical Society Transactions*, *42*(4), 1025-1032.

Thul, P. J., Åkesson, L., Wiking, M., Mahdessian, D., Geladaki, A., Ait Blal, H., Alm, T., Asplund, A., Björk, L., & Breckels, L. M. (2017). A subcellular map of the human proteome. *Science*, *356*(6340), eaal3321.

Trefely, S., Huber, K., Liu, J., Noji, M., Stransky, S., Singh, J., Doan, M. T., Lovell, C. D., von Krusenstiern, E., & Jiang, H. (2022). Quantitative subcellular acyl-CoA analysis reveals distinct nuclear metabolism and isoleucine-dependent histone propionylation. *Molecular Cell*, *82*(2), 447-462. e446.

Trefely, S., Lovell, C. D., Snyder, N. W., & Wellen, K. E. (2020). Compartmentalised acyl-CoA metabolism and roles in chromatin regulation. *Molecular metabolism*, *38*, 100941.

Tsuchiya, Y., Peak-Chew, S. Y., Newell, C., Miller-Aidoo, S., Mangal, S., Zhyvoloup, A., Bakovic´, J., Malanchuk, O., Pereira, G. C., Kotiadis, V., Szabadkai, G., Duchen, M. R., Campbell, M., Cuenca, S. R., Vidal-Puig, A., James, A. M., Murphy, M. P., Filonenko, V., Skehel, M., & Gout, I. (2017). Protein CoAlation: a redox-regulated protein modification by coenzyme A in mammalian cells. *Biochemical Journal*, *474*(14), 2489-2508. https://doi.org/10.1042/bcj20170129

Van Hove, J. L. K., Saenz, M. S., Thomas, J. A., Gallagher, R. C., Lovell, M. A., Fenton, L. Z., Shanske, S., Myers, S. M., Wanders, R. J. A., Ruiter, J., Turkenburg, M., & Waterham, H. R. (2010). Succinyl-CoA Ligase Deficiency: A Mitochondrial Hepatoencephalomyopathy. *Pediatric Research*, *68*(2), 159-164. https://doi.org/10.1203/pdr.0b013e3181e5c3a4

Van Vranken, J. G., Jeong, M.-Y., Wei, P., Chen, Y.-C., Gygi, S. P., Winge, D. R., & Rutter, J. (2016). The mitochondrial acyl carrier protein (ACP) coordinates mitochondrial fatty acid synthesis with iron sulfur cluster biogenesis. *eLife*, *5*. https://doi.org/10.7554/elife.17828

Wagner, G. R., & Payne, R. M. (2013). Widespread and Enzyme-independent Nϵ-Acetylation and Nϵ-Succinylation of Proteins in the Chemical Conditions of the Mitochondrial Matrix*♦. *Journal of Biological Chemistry*, *288*(40), 29036-29045.

Wellen, K. E., Hatzivassiliou, G., Sachdeva, U. M., Bui, T. V., Cross, J. R., & Thompson, C. B. (2009). ATP-Citrate Lyase Links Cellular Metabolism to

Histone Acetylation. *Science*, *324*(5930), 1076-1080. https://doi.org/10.1126/science.1164097

Williams, S., Gregory, A., Hogarth, P., Hayflick, S. J., & Gillingham, M. B. (2013). Metabolism and energy requirements in pantothenate kinase-associated neurodegeneration. *Molecular Genetics and Metabolism*, *110*(3), 336-341.

Woolbright, B. L., & Harris, R. A. (2021). PDK2: An Underappreciated Regulator of Liver Metabolism. *Livers*, *1*(2), 82-97.

Worley, B., & Powers, R. (2012). Multivariate Analysis in Metabolomics. *Current Metabolomics*, *1*(1), 92-107. https://doi.org/10.2174/2213235x11301010092

Yu, Y., Moretti, I. F., Grzeschik, N. A., Sibon, O. C., & Schepers, H. (2021). Coenzyme A levels influence protein acetylation, CoAlation and 4′-phosphopantetheinylation: Expanding the impact of a metabolic nexus molecule. *Biochimica et Biophysica Acta (BBA)-Molecular Cell Research*, *1868*(4), 118965.

Zhang, Y.-M., Rock, C. O., & Jackowski, S. (2005). Feedback regulation of murine pantothenate kinase 3 by coenzyme A and coenzyme A thioesters. *Journal of Biological Chemistry*, *280*(38), 32594-32601.

Zhang, Y.-M., Rock, C. O., & Jackowski, S. (2006). Biochemical properties of human pantothenate kinase 2 isoforms and mutations linked to pantothenate kinase-associated neurodegeneration. *Journal of Biological Chemistry*, *281*(1), 107-114.

Zhou, B., Westaway, S. K., Levinson, B., Johnson, M. A., Gitschier, J., & Hayflick, S. J. (2001). A novel pantothenate kinase gene (PANK2) is defective in Hallervorden-Spatz syndrome. *Nature Genetics*, *28*(4), 345-349. https://doi.org/10.1038/ng572

Zhyvoloup, A., Nemazanyy, I., Panasyuk, G., Valovka, T., Fenton, T., Rebholz, H., Wang, M.-L., Foxon, R., Lyzogubov, V., Usenko, V., Kyyamova, R., Gorbenko, O., Matsuka, G., Filonenko, V., & Gout, I. T. (2003). Subcellular Localization and Regulation of Coenzyme A Synthase. *Journal of Biological Chemistry*, *278*(50), 50316-50321. https://doi.org/10.1074/jbc.m307763200

APPENDIX A

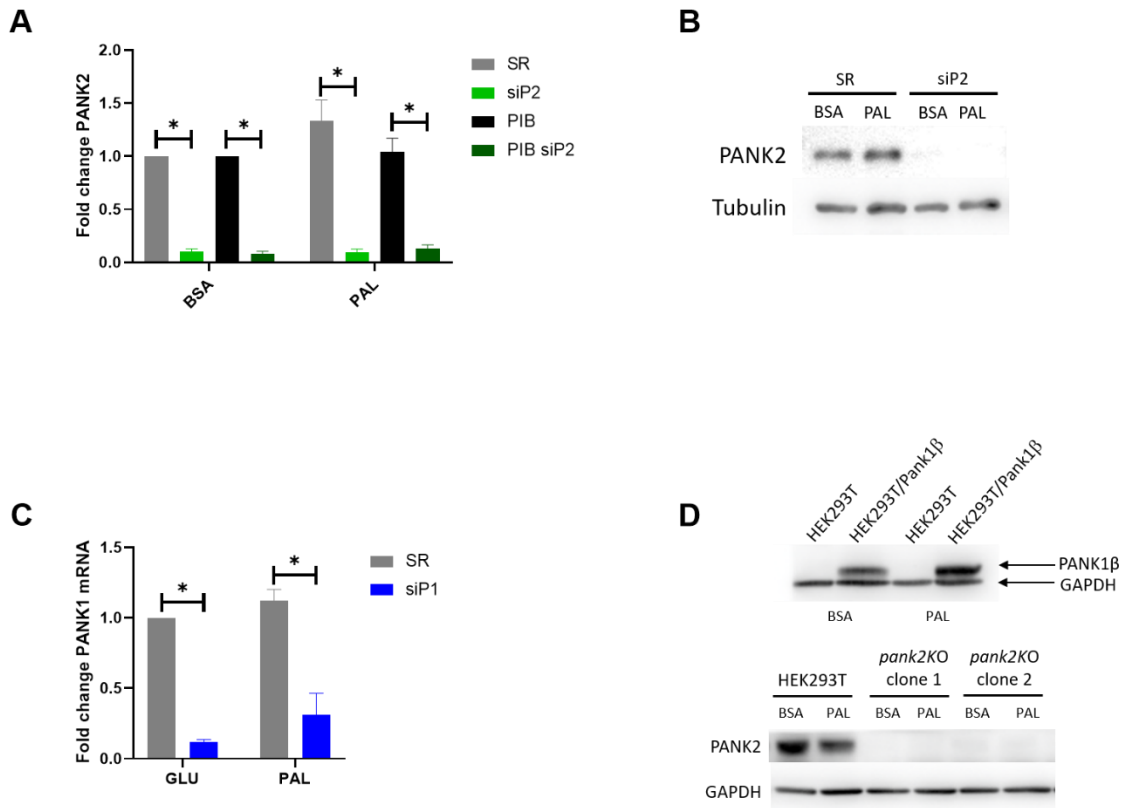SUPPLEMENTAL FIGURES CHAPTER 2

Figure 5.1. Assessment of PANK1 and PANK2 KD, PANK2 KO, and PANK1β overexpression. A) Quantification of PANK2 in HEK293T and PANK1β overexpressing cells normalized to tubulin and expressed as fold change to SR BSA for each cell line. B) Representative western blot for PANK2 KD in HEK293T. C) Quantification of PANK1 mRNA expression following PANK1 KD in HEK293T cells expressed as fold change to SR BSA. D) Top: representative western blot of PANK1β overexpression, probing for PANK1β and tubulin loading control. Bottom: representative western blot of PANK2 knockout clones probing for PANK2 and GAPDH loading control.
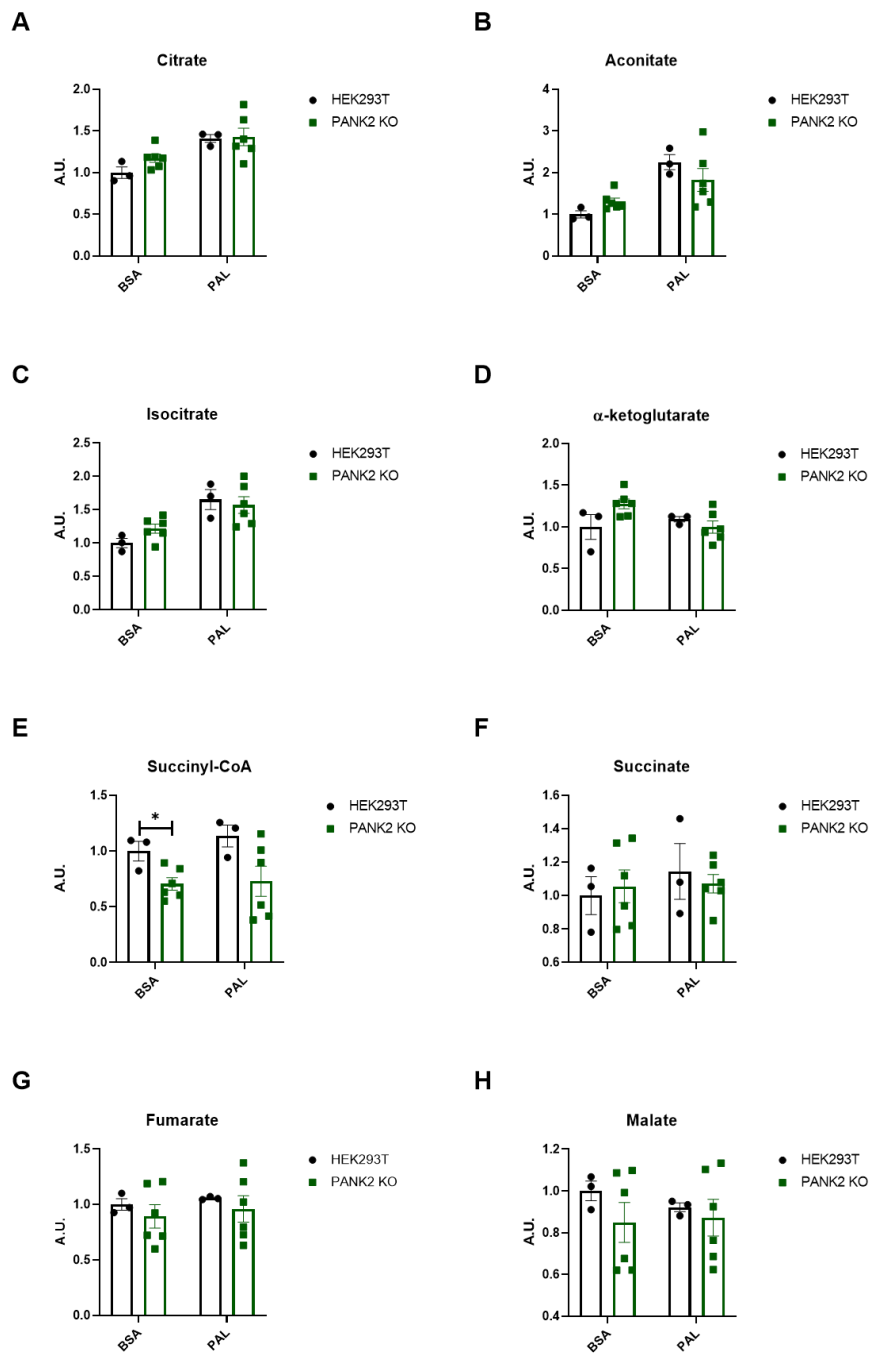
APPENDIX B

SUPPLEMENTAL FIGURES CHAPTER 3

Figure 6.1. Levels of TCA cycle intermediates in PANK2 KO cells. A-H) Control: HEK293T-BSA (n=3), PANK2 KO-BSA (n=6), HEK293T-PAL (n=3), PANK2 KO-PAL (n=6) expressed as fold change to HEK293T-BSA. A-D, F-H) Metabolites measured with GC-MS, E) Succinyl-CoA same as in figure 3.2 in chapter 3 measured

with LC-MS. Statistical significance determined via multiple t-test corrected for multiple comparison with Holm-Sidak. The * indicates statistically significant at $P < 0.05$ for all conditions error bars are SEM. All data is expressed in arbitrary units (A.U.).
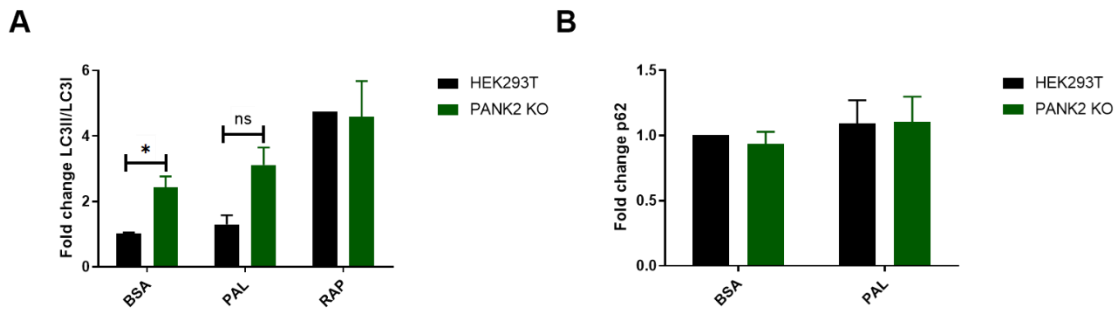

Figure 6.2. Autophagy measurement in PANK2 KO cells. Measuring the change in LC3II/LCR3I ratio and p62 accumulation with chloroquine inhibition. A) Quantification of LC3II/LC3I ratio during chloroquine inhibition with rapamycin as a positive control. HEK293T (n=7), PANK2 KO (n=14) expressed as fold change to HEK293T control normalized to GAPDH. B) Quantification of p62 accumulation during chloroquine inhibition, HEK293T (n=7), PANK2 KO (n=16) expressed as fold change to HEK293T BSA normalized to GAPDH. The * indicates statistically significant at $P<0.05$ determined with two-way ANOVA with Tukey's multiple comparisons test. All error bars are SEM.
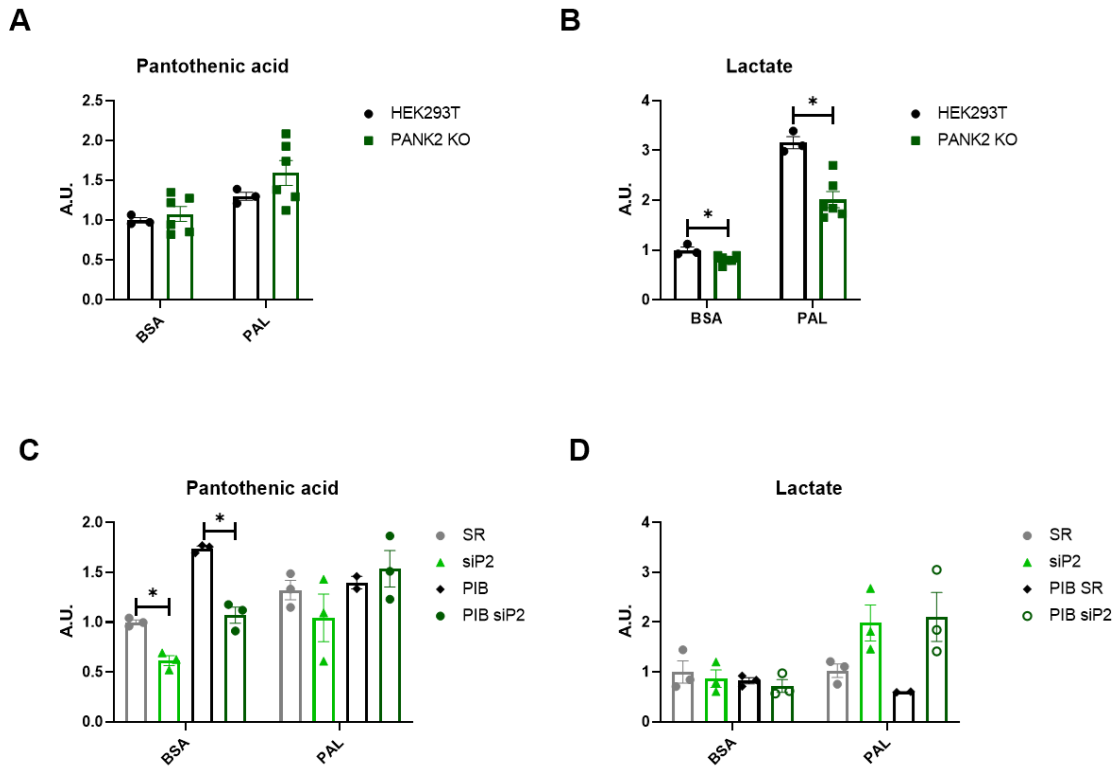
Figure 6.3. Pantothenic acid and lactate measurements in PANK2 KO and PANK2 KD cells. A-B) Pantothenic acid and lactate in HEK293T (n=3), PANK2 KO (n=6) expressed as fold change to HEK293T KO. C-D) Pantothenic acid and lactate in scrambled control: SR-BSA (n=3), siPANK2: siP2-BSA (n=3), scrambled control PAL: SR-PAL (n=3), siPANK2: siP2-PAL (n=3), PANK1β scrambled Control: PIβ SR (n=3), PANK1β siPANK2: PIβ siP2 (n=3), PANK1β scrambled control PAL: PIβ SR-PAL (n=2), PANK1β siPANK2 PAL: PIβ siP2-PAL (n=3) normalized to SR and expressed as fold change. Statistical significance determined via multiple t-test corrected for multiple comparison with Holm-Sidak. The * indicates statistically significant at $P < 0.05$ for all conditions error bars are SEM. All data expressed in arbitrary units (A.U.).

Figure 6.4. Quantification of *HMOX1* and *NFE2L2 mRNA* expression in PANK2 KD cells. A-B) Quantification of mRNA expression of *HMOX1* and *NFE2L2* in PANK2 KD cells data from two independent experiments normalized to SR-BSA.